7 Insights into Magma Genesis at Convergent Margins from U-series Isotopes

Simon Turner

Department of Earth Sciences
Wills Memorial Building
University of Bristol
Bristol, BS8 1RJ, United Kingdom

Bernard Bourdon

Laboratoire de Géochimie et Cosmochimie
IPGP-CNRS UMR7579
4, Place Jussieu, 75252
Paris cedex 05 France

Jim Gill

Department of Earth Sciences
University of California
Santa Cruz, California, 95064, USA

1. INTRODUCTION

Convergent margins (oceanic and continental arcs) form one of the Earth's key mass transfer locations, being sites where melting and transfer of new material to the Earth's crust occurs and also where crustal materials, including water, are recycled back into the mantle. Volcanism in this tectonic setting constitutes ~15% (0.4-0.6 km^3/yr) of the total global output (Crisp 1984) and the composition of the erupted magmas is, on average, similar to that of the continental crust (Taylor and McLennan 1981). Moreover, many arc volcanoes have been responsible for the most hazardous, historic volcanic eruptions. Yet, despite their importance, many fundamental aspects of convergent margin magmatism remain poorly understood. Key among these are the rates of processes of fluid addition from the subducting plate. Furthermore, in stark contrast to the ocean ridges, where adiabatic decompression provides a simple and robust physical model for partial melting, no consensus has yet been reached about the physics of the partial melting process and the mechanism of melt extraction beneath arcs.

Preceding chapters concerned with partial melting in this volume (Lundstrom 2003; Bourdon and Sims 2003) have discussed how the differing half-lives and distribution coefficients of the various U-series nuclides result in disequilibria through in-growth. This provides important information on the nature and timing of mantle partial melting processes. In convergent margin settings the differential fluid mobility of U and Ra relative to Th and Pa provides an additional source of fractionation leading to in-growth and this is crucial to understanding the timing and mechanisms of fluid addition. Here we review the role that the proliferation of high quality U-series isotope data, over the last decade, have had in obtaining precise information on time scales and the development of quantitative physical models for convergent margin magmatism. Our approach is to use trace element and isotope data to determine the nature of the contributing source components and then to use the U-series isotopes to constrain processes and time scales. We begin with a brief review of the evidence for multiple source component contributions to most arc magmas and then summarize the empirical and experimental evidence for the behavior of the U-series nuclides of interest in aqueous fluids. Subsequent sections look in turn at the U-series

1529-6466/00/0052-0007$10.00

evidence for the timing and mechanisms of sediment and fluid addition and the important new constraints that U-series disequilibria are beginning to place on partial melting and melt extraction processes beneath arc volcanoes. These are followed by brief discussions of the few data available from rear arc lavas, the processes which might modify source-derived U-series signals and finally some of the implications of U-Th isotopes as long term tracers of the evolution of the terrestrial reservoirs.

2. CONVERGENT MARGIN MAGMATISM

Convergent margin magmatism is widely regarded to reflect partial melting that is in some way linked to the lowering of the peridotite solidus through addition of fluids released by dehydration reactions in the subducting plate (e.g., Tatsumi et al. 1986; Davies and Bickle 1991). For example, the relatively constant ~110 km depth to Benioff zone was, for a long time, taken as evidence that an isobaric dehydration reaction in the subducting plate is responsible for melting (Gill 1981; Tatsumi et al. 1986). Stolper and Newman (1994) noted a strong positive correlation between H_2O content and inferred degree of melting in lavas from back arc spreading centers behind the Marianas. A strong dependence on fluid addition is also consistent with the apparent positive correlation between volcanic output and rate of subduction from east to west along the Aleutian arc (Marsh 1987; George et al. 2003). Conversely, there is an absence of volcanism in South America above the area of subduction of the Chile ridge. This will be the hottest part of the wedge but also the driest, again suggesting that partial melting is linked to fluid addition. Exceptions can occur when the subducting plate is sufficiently young to be hot enough for the altered oceanic crust to undergo hydrous partial melting (Peacock et al. 1994). However, these distinctive, adakitic lavas (Defant and Drummond 1990) appear to be volumetrically minor in the present day convergent margins (but see also Kelemen et al. 2003) and their U-series systematics will be considered separately under the section on partial melting. Finally, amphibole-rich sub arc mantle xenoliths provide direct evidence for hydration of the mantle wedge (e.g., Maury et al. 1992; Blatter and Carmichael 1998).

2.1. Geochemical signatures of source components

A distinctive geochemical signature of island arc lavas is that, compared to mid-ocean ridge and ocean island basalts (MORB and OIB), they are enriched in large ion lithophile elements (LILE), such as Rb, Ba, K, Sr and Pb, and depleted in high field strength elements (HFSE), such as Ta, Nb and Ti, relative to the rare earth elements (REE) (e.g., Gill 1981; Hawkesworth et al. 1997a). Similar trace element signatures are observed in sub arc mantle xenoliths (Maury et al. 1992). Furthermore, Nb and often Zr, Hf, and Ti abundances in arc lavas are usually depleted with respect to MORB, at a given MgO content. Consequently, the arc mantle source is often thought to be even more depleted than the MORB source. Note that with an ionic charge of +4 and ionic radius of ~1 Å, Th has an ionic potential (or field strength) <2 and is classified as a HFSE and whilst U has a similar ionic radius, the fluid mobility of U^{6+} (see Section 4) has lead to U being considered as similar to a LILE element. If the mantle wedge peridotite is similar to that of the MORB source, then the incompatible trace element data from arc lavas appear to require contributions from two additional components. Figure 1a emphasizes this by showing that the compositions of arc lavas extend well beyond those of MORB and OIB and demonstrates the need for both an enriched component with elevated La/Sm and a component with high Ba/Th.

2.2. The enriched component—sediment or OIB?

The upper portions of the subducting plate are comprised of hydrothermally altered oceanic crust and an overlying layer of sediments, sometime jointly referred to as “the

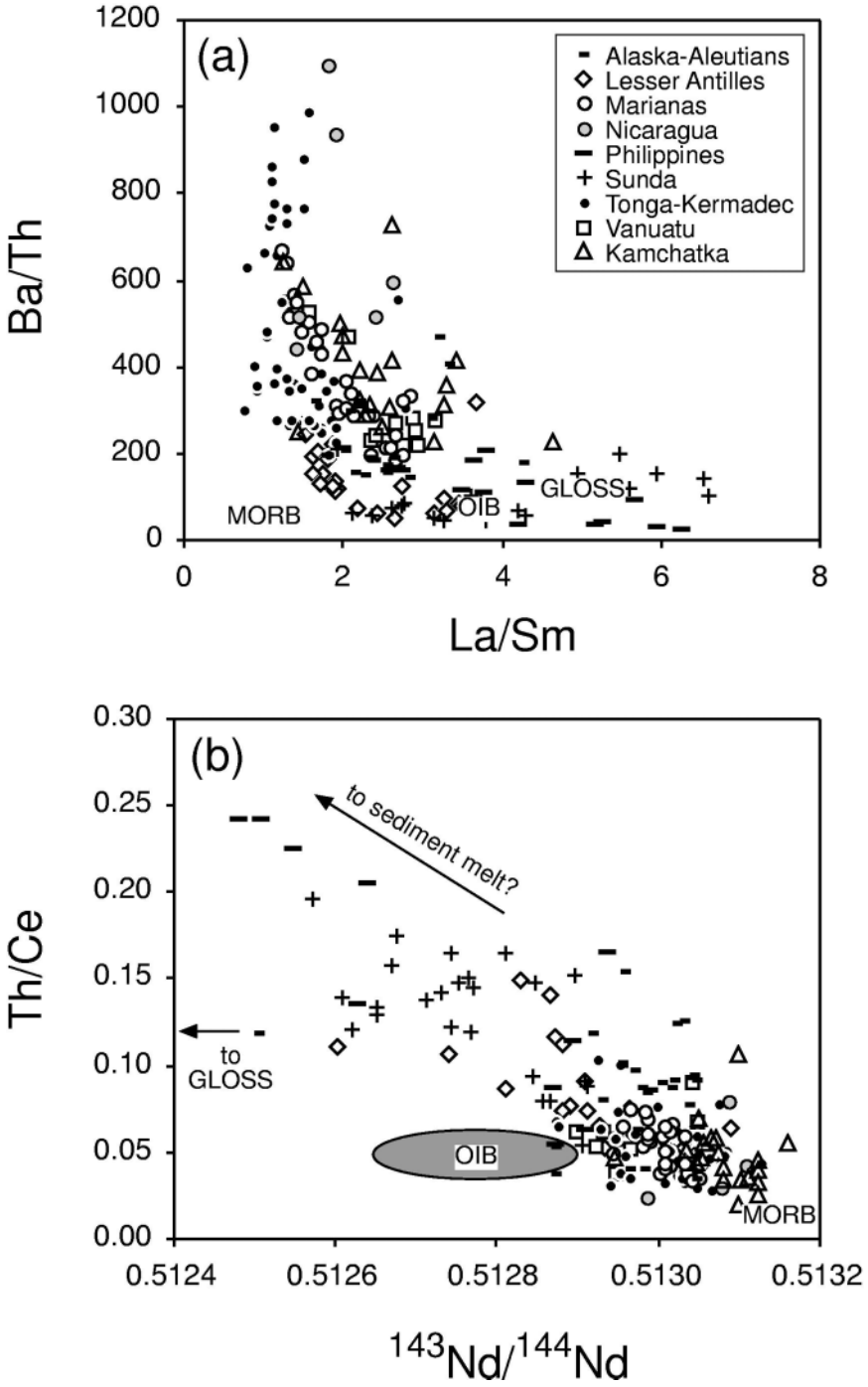

Figure 1. (a) Ba/Th versus La/Sm for all published along-arc suites of arc rocks for which both mass spectrometric U-Th isotope data and a comprehensive range of accompanying trace element and radiogenic isotope data are available (see Table 1 for data sources). For clarity on this and most subsequent diagrams only samples with SiO_2 < 60 wt. % are plotted. Also plotted are typical compositions for MORB and OIB (Sun and McDonough 1989) and GLOSS (Plank and Langmuir 1998). The array demonstrates the need for contributions from two components in addition to MORB-source type mantle wedge—an enriched component with elevated La/Sm (sediment) and a component with high Ba/Th (fluid). (b) Th/Ce versus $^{143}Nd/^{144}Nd$ illustrating that the low $^{143}Nd/^{144}Nd$ component in arc lavas is subducted sediment not OIB-type mantle. The trajectory toward higher Th/Ce ratios than GLOSS provides one line of evidence that the sediment component is added as a partial melt.

slab." The presence of ^{10}Be and negative Ce anomalies in many arc lavas can be taken as unambiguous evidence for a contribution from the subducted sediments (e.g., Hole et al. 1984; Morris et al. 1990), although neither are universal features of arc lavas. Nevertheless, at first glance, OIB-type mantle, which also has elevated La/Sm and thus low time-integrated ^{143}Nd/^{144}Nd relative to MORB, might be considered as a candidate for the enriched component (e.g., Morris and Hart 1983). However, OIB are also characterized by Nb ≥ La and low Th/Ce ratios whereas the enriched component in arc lavas has low Nb/La and high Th/Ce at low ^{143}Nd/^{144}Nd (Fig. 1b) and so the enriched component is unlikely to reflect OIB material trapped within the mantle wedge (Hawkesworth et al. 1997a). Sediments have high Th/Ce and Figure 1b shows that the arc lavas form an array toward high Th/Ce and low ^{143}Nd/^{144}Nd which is broadly characteristic of average global subducted sediment GLOSS (Plank and Langmuir 1998). The significance of the array projecting towards higher Th/Ce than GLOSS will be discussed later. Many oceanic arc lavas are congested in the lower right corner of Figure 1b where there is a range in ^{143}Nd/^{144}Nd and low Th/Ce and broad overlap with MORB and OIB. For these lavas, it is primarily the observation of low Nb/La (and the presence of ^{10}Be and negative Ce anomalies in some instances) which argues for the presence of a sediment component and an absence of an OIB component (e.g., Elliott et al. 1997).Thus, on a plot of Th/Nb versus ^{143}Nd/^{144}Nd (not shown) the different arcs form steep arrays rather than shallow trends toward a low Th/Nb, low ^{143}Nd/^{144}Nd OIB component. An exception to this is the northernmost islands of the Tonga arc where decreases in ^{143}Nd/^{144}Nd are accompanied by increases in Ta/Nd (Regelous et al. 1997; Turner et al. 1997; Wendt et al. 1997). However, Turner and Hawkesworth (1998) have argued that this OIB signal was introduced into the sub arc mantle in the form of volcaniclastic sediments carried on the subducting plate rather than requiring the presence of OIB mantle in the wedge.

2.3. The fluid component

Undegassed, primitive arc lavas are uncommon but available analyses generally show elevated volatile contents relative to MORB (e.g., Harris and Anderson 1984; Sisson and Layne 1993), although some exceptions do occur (Sisson and Bronto 1998). Phase relations indicate that the amount of H_2O available in the subducting plate at ~ 100 km depth beneath arc front volcanoes will be in the range 1-5% (Poli and Schmidt 1995). Experimental data suggest that the high LIL/HFSE ratios in arc lavas reflect the relative mobility and immobility (respectively) of these elements in aqueous fluids (Section 4.3) and empirical evidence supports this. For example elements like Cl, Ba and U all correlate positively with H_2O content in the Mariana back arc lavas (Stolper and Newman 1994). Consequently, the high Ba/Th component in Figures 1 and 2 is inferred to reflect fluid addition. Importantly, the highest LIL/HFSE ratios (e.g., Ba/Th) are usually found in those rocks with the highest ^{143}Nd/^{144}Nd (and lowest ^{87}Sr/^{86}Sr ± ^{206}Pb/^{204}Pb) ratios (Fig. 2a) from which it has been inferred that the fluid end-member is most typically derived more from the subducting altered basaltic crust rather than the overlying sediments (Miller et al. 1994; Turner et al. 1996; Turner and Hawkesworth 1997). This is consistent with flux calculations by Staudigel et al. (1996) which showed that the altered oceanic crust potentially can contribute ~ 70% of the U recycled into the arc crust. However, we also note that several studies have provided evidence for transport of some of the sediment components in a fluid (Morris et al. 1990; Class et al. 2000; Hochstaedter et al., 2001; Sigmarsson et al. 2002) and so the relative role of altered oceanic crust versus sediment as source of the fluid apparently varies substantially between and even within arcs.

In summary, many recent studies have argued for three components in most arc lavas: depleted mantle, basalt-derived fluid, and sediment (in bulk, via fluid, or via melt)

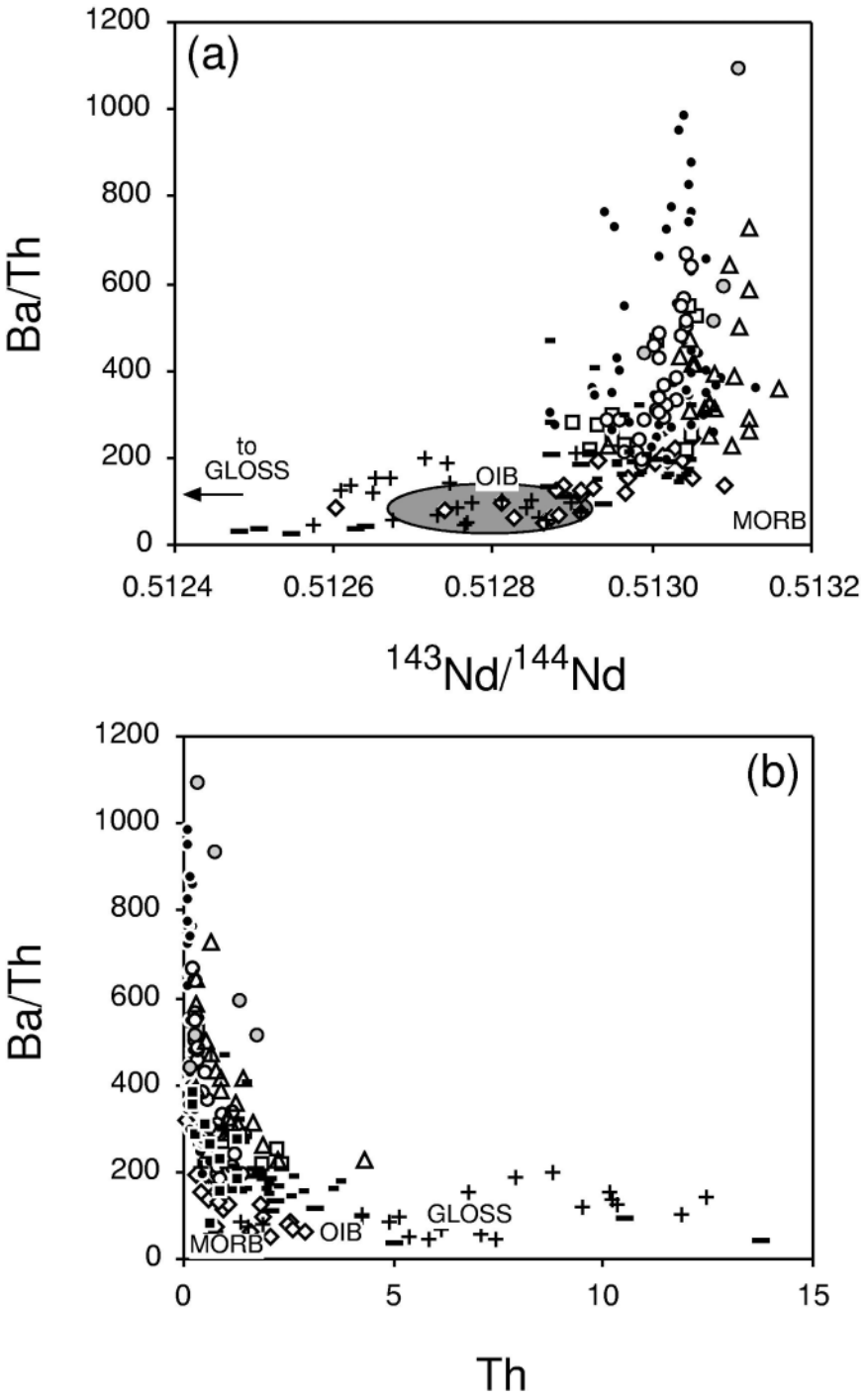

Figure 2. (a) Ba/Th versus $^{143}Nd/^{144}Nd$ for arc lavas illustrating that the fluid component (elevated Ba/Th) has high $^{143}Nd/^{144}Nd$ and must therefore generally be derived from the subducting altered oceanic crust. (b) Ba/Th ratio versus Th content from which is can be inferred that Th is less mobilized in the fluid component and that the relative effect of the fluid component is more pronounced in the more depleted lavas with the lowest Th contents. Symbols and data sources as in Figure 1.

(e.g., Kay 1980; Ellam and Hawkesworth 1988; Miller et al. 1994; Turner et al. 1996, 1997; Elliott et al. 1997; Hawkesworth et al. 1997a). Debate continues about whether and where enriched mantle (e.g., Morris and Hart 1983) and basalt melts (adakites) are involved (e.g., Kelemen et al. 2003; George et al. 2003).

2.4. Relative depletion of the mantle wedge

A final and most important point to emphasize before turning to the implications of U-series isotope data is that the nature of the arc lava array in Figure 2a requires that the relative contributions of the fluid and sediment components vary both within individual arcs as well as from arc to arc. Figure 2b shows that Ba/Th ratio varies inversely with Th content and thus the largest fluid signals are found in those lavas with the lowest Th contents (Condomines and Sigmarsson 1993; McDermott and Hawkesworth 1991). This provides one line of evidence that Th is not strongly mobilized in the fluid (see Section 4) and it is argued that much of the Th abundances in arc lavas are controlled by the competing effects of prior melt depletion of the mantle wedge (Ewart and Hawkesworth 1987; Woodhead et al. 1993; Stolper and Newman 1994), which acts to lower the Th contents, and addition of sediment which has a high Th/U ratio relative to MORB (Fig. 3) and thus has the opposite effect of enriching Th (see Section 5.1). For this reason, sediment-rich arc lavas with high Th contents are often referred to as "enriched" and the nature of the arrays in Figures 2a and b are consistent with a mass balance model in which a broadly similar fluid flux is added to sources containing a variable sediment component (Condomines and Sigmarsson 1993; Turner et al. 1996, 1997; Elliott et al. 1997; Hawkesworth et al. 1997a, b). Note that flux melting models (e.g., Stolper and Newman 1994; Eiler et al. 2000; Thomas et al. 2002) in which the decreases in Th content on Fig. 2b are thought to reflect increasing degrees of partial melting due to a higher fluid flux (i.e., and thus higher Ba/Th) do not predict the broad associated change in $^{143}Nd/^{144}Nd$ observed in Fig. 2a.

3. U-SERIES ISOTOPES IN ARC LAVAS

Since publication of the second edition of Ivanovich and Harmon (1992) there has been a proliferation of high quality U-series isotope data, the majority of which have been analyzed by thermal- and, more recently, plasma-source mass spectrometry. Table 1 represents an updated version of Table 7.1 from Gill et al. (1992) and summarizes (to the best of our knowledge) specific arc studies which have been divided into a three-tier hierarchy of global surveys, along-arc studies and studies of individual volcanoes. For the purposes of much of the discussion in this chapter and for most of the figures we concentrate on the data sets from along-arc suites of arc rocks for which both mass spectrometric U-series isotope data and a comprehensive range of accompanying trace element and radiogenic isotope data are available. For clarity we have restricted the dataset to only samples with $SiO_2 < 60$ wt. % unless otherwise specified. The data from numerous studies of individual volcanoes have also been omitted since the variations in recent lavas from individual volcanoes are likely to dominantly reflect the effects of magma chamber processes which are less relevant to this chapter and are discussed separately by Condomines et al. (2003).

In Figure 3 we have plotted histograms of U/Th, ($^{230}Th/^{238}U$), ($^{231}Pa/^{235}U$) and ($^{226}Ra/^{230}Th$) in arc lavas and compared these with MORB (data sources from Lundstrom 2003). This shows that the majority of arc lavas have higher U/Th ratios and the opposite sense of fractionation of ($^{230}Th/^{238}U$) to MORB with the majority being characterized by excesses of ^{238}U over ^{230}Th, though many are close to ^{230}Th-^{238}U equilibrium and some have ^{230}Th-excesses (e.g., Reagan and Gill 1989; Reagan et al. 1994; George et al. 2003). This observation has not changed significantly since the early global surveys of Gill and Williams (1990), McDermott and Hawkesworth (1991) and Condomines and Sigmarsson (1993) excepting that the advances in analytical techniques have allowed more highly depleted arc rocks to be analyzed and this has increased the total number analyzed that have large ^{238}U-excesses. Note that the U/Th ratio of GLOSS is lower than most MORB

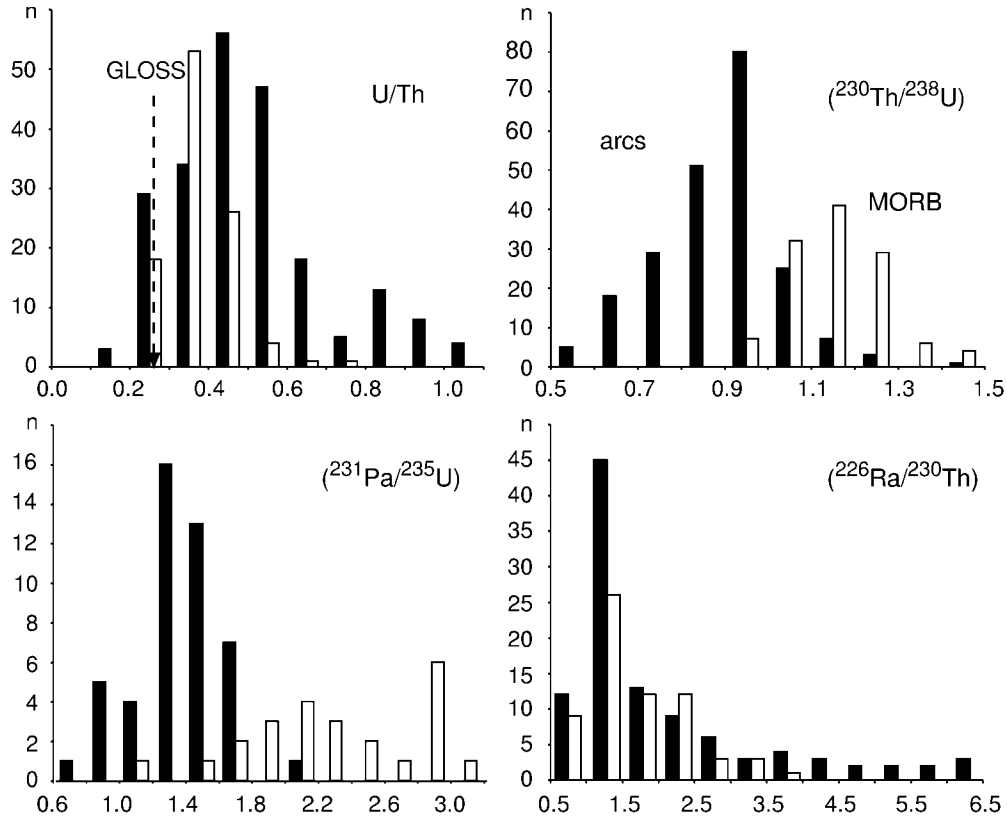

Figure 3. Histograms of U/Th, (^{230}Th/^{238}U), (^{231}Pa/^{235}U) and (^{226}Ra/^{230}Th) for arc lavas (data sources as in Figure 1) compared with MORB (data sources from Lundstrom 2003). Note that the U/Th ratio of GLOSS (Plank and Langmuir 1998) is lower than that in most MORB or arc lavas.

or arc lavas (Fig. 3). Due to analytical difficulties ^{231}Pa-^{235}U data are much scarcer but the histogram shows that arc lavas have the same sense of ^{231}Pa-^{235}U disequilibria to MORB but that the absolute size of the disequilibria is typically less, and similar to OIB. Exceptions to this are the lavas from Tonga which are characterized by excesses of ^{235}U over ^{231}Pa, or (^{231}Pa/^{235}U)< 1 (Bourdon et al. 1999). The third U-series system for which there are appreciable mass spectrometric data is the ^{226}Ra-^{230}Th system and the histogram shows that whilst the sense and median size of fractionation is similar to that observed in MORB, the arc data extend to (^{226}Ra/^{230}Th) ratios > 6 that are far larger than those observed in MORB.

The most important observations about U-series isotopes in arc lavas for this chapter are: (1) the widespread excess of ^{238}U over ^{230}Th but deficit of ^{235}U with respect to ^{231}Pa; and (2) the extreme ^{226}Ra enrichments in some arc lavas. We will explore the profound implications of these for magma genesis and transport at subduction zones. The conclusions apply most convincingly to the oceanic arcs where the observations are most extreme (the volcanic fronts of Tonga, Marianas, and eastern Sunda, and one or two volcanoes in some other arcs). Whether the conclusions apply elsewhere is harder to verify but there is no convincing reason with respect to U-series data to believe that they do not.

4. BEHAVIOUR OF THE U-SERIES NUCLIDES IN AQUEOUS FLUIDS

Most of the differences between arc magmas and those from other tectonic settings result from oxidation (Wood et al. 1990; Blatter and Carmichael 1998; Parkinson and Arculus 1999) and hydration (Blatter and Carmichael 1998) of arc magma sources by

Table 1. Summary of published U-Th-Pa-Ra data from detailed studies of convergent margin rocks.

Global	*Arcs*	*Volcanoes*	*($^{230}Th/^{238}U$)*	*($^{235}U/^{231}Pa$)*	*($^{226}Ra/^{230}Th$)*	*Reference(s)*
Island arcs			α, TIMS	TIMS	α, TIMS	Gill and Williams (1990); McDermott and Hawkesworth (1991); Pickett and Murrell (1997); Hawkesworth et al. (1997a); Turner et al. (2001)
	Aleutians		α, T-, P-IMS	---	TIMS	Newman et al. (1984); Turner et al. (1998); George et al. (2003)
	Eolian		α	---	γ	Capaldi et al. (1983)
		Stromboli	α, TIMS	---	α, TIMS	Capaldi et al. (1978); Gauthier and Condomines (1999)
	Lesser Antilles		α, TIMS	---	γ, TIMS	Turner et al. (1996); Chabaux et al. (1999); Turner et al. (2001)
		Soufriere	TIMS	---	TIMS	Heath et al. (1998); Turner et al. (2001)
	Marianas		α, TIMS	---	TIMS	Newman et al. (1984); Elliott et al. (1997); Turner et al. (2001)
	New Britain		α	---	α	Gill et al. (1993)
	Philippines		TIMS	---	TIMS	McDermott et al. (1993); Turner et al. (2001)
	Sunda		TIMS	---	TIMS	Condomines and Sigmarsson (1993); Turner and Foden (2001)
		Merapi	α, TIMS	---	α, TIMS	Gauthier and Condomines (1999); Turner and Foden (2001)
	Banda		α	---	α	Hoogewerff et al. (1997)
		Batur	α	---	α	Rubin et al. (1989)
		Galunggung	α, TIMS	---	α, TIMS	Gerbe et al. (1992); Turner and Foden (2001)
		Sangeang Api	TIMS	---	TIMS	Turner et al. (2003)
	Tonga-Kermadec		TIMS	TIMS	TIMS	Regelous et al. (1997); Turner et al. (1997, 2000); Bourdon et al. (1999)
	Vanuatu		α, TIMS	---	TIMS	Condomines and Sigmarsson (1993); Turner et al. (1999); Turner et al. (2001)
Continental arcs			α, TIMS	TIMS	α, TIMS	Gill and Williams (1990); McDermott and Hawkesworth (1991); Pickett and Murrell (1997); Hawkesworth et al. (1997a); Turner et al. (2001)
	Aegean					
		Santorini	α, TIMS	---	γ, TIMS	Pyle et al. (1988); Druitt et al. (1999); Zellmer et al. (2000)
	Alaska		TIMS	---	TIMS	George et al. (2002)
	Central Andes					
		Nevado del Ruiz	TIMS	---	α	Schaefer et al. (1993)
		Parinacota	TIMS	---	TIMS	Bourdon et al. (2000)
	Southern Andes		α	---	TIMS	Sigmarsson et al. (1992, 2002)
	Austral Andes		α	---	TIMS	Sigmarsson et al. (1998)
	Cascades		α	---	---	Newman et al. (1986)
		St Helens	α, TIMS	---	α, TIMS	Bennett et al. (1982); Volpe and Hammond (1991)
		Shasta	TIMS	---	TIMS	Newman et al. (1986); Volpe (1992)
	Kamchatka		TIMS	TIMS	TIMS	Turner et al. (1998); Dosseto et al. (2003)
	Nicaragua		α, TIMS	TIMS	TIMS	Condomines and Sigmarsson (1993); Reagan et al. (1994); Herrstrom et al. (1995); Thomas et al. (2002)
	Costa Rica		α, TIMS	TIMS	TIMS	Clark et al. (1998); Thomas et al. (2002)
		Turrialba	α, TIMS	---	α, TIMS	Reagan and Gill (1989); Thomas et al. (2002)
	Italy					
		Vesuvius	α	---	---	Capaldi et al. (1982); Villemant and Flehoc (1989); Black et al. (1998)

α = alpha counting; γ = gamma counting; TIMS = thermal ionization mass spectrometry; PIMS = plasma ionization mass spectrometry

aqueous fluids. The single-most striking U-series observation, that is largely unique to the arc environment, is the tendency towards excesses of ^{238}U over ^{230}Th. This has been attributed for over two decades to the addition of U by fluids from the subducting plate (e.g., Gill, 1981; Allègre and Condomines 1982). The inference that aqueous fluids have a particularly strong effect on partitioning between U and its daughter nuclides dictates that any interpretation requires constraints on their solid/fluid partitioning behavior. As we will see later (Section 8), whether or not small amounts of Th and Pa are mobilized in subduction zone fluids is critical to many of the U-series time scale interpretations. We will now look at the evidence for U-series nuclide solid/fluid partitioning in closer detail.

4.1. General empirical evidence

The behavior of the U-series nuclides at the Earth's surface, in the oceans and in ground waters is discussed at length in chapters 8-14 of this volume and the reader is referred to these for details of the following summary. U is characterized by two main oxidation states (+4 and +6) with the hexavalent state occurring under oxidizing conditions in which the uranyl ion (UO_2^{2+}) is highly fluid mobile. This is manifest at the Earth's surface by elevated U concentrations in surficial and ground waters (Porcelli 2003) and a long residence time in the oceans (Cochran and Masque 2003). Ra, whose closest chemical analogue is Ba, is an alkaline earth element which forms the +2 oxidation state and is also commonly mobile in fluids. Th on the other hand only forms the +4 oxidation state and is generally immobile in aqueous fluids at the Earths surface as evidenced by its insolubility in the laboratory (Goldstein and Stirling 2003), surface and ground waters and its short residence time in the oceans (Cochran and Masque 2003). Less information is available for Pa which adopts the +5 oxidation state and for which the best chemical analogue may be the HFSE Nb or Ta (Lundstrom et al. 1994). Various lines of evidence suggest that Pa is highly fluid immobile (Guillaumont et al. 1968), and certainly Pa is even harder to keep in solution than Th in the laboratory (Goldstein and Stirling 2003). At depths within the crust, the formation of barite and uranium deposits but absence of thorium deposits suggests that U and Ra are still fluid mobile whilst Th is much less so and we infer the same for Pa. More difficult is inferring the behavior of these nuclides at the temperatures and pressures appropriate to the dehydration of subducting oceanic plates beneath arcs and in the likely presence of additional solute species like Na and Cl. For information on relative fluid mobility under these conditions we are restricted to inferences from empirical observations and the few available results from very difficult fluid-mineral partitioning experiments.

4.2. Empirical observations from arc lavas

The fact that the that highest U/Th ratios are found in the arc lavas with the lowest Th contents (Gill and Williams 1990; McDermott and Hawkesworth 1991; Condomines and Sigmarsson 1993; Hawkesworth et al. 1997a,b), that excesses of ^{238}U over ^{230}Th are rare apart from arc lavas, and that ^{238}U-excesses often correlate positively with fluid-mobile elements within arc lavas, provides strong empirical evidence that U is significantly more fluid mobile than Th. Secondly, Stolper and Newman (1994) found a good positive correlation between U and H_2O in the Marianas back arc lavas. Thirdly, Hawkesworth et al. (1997a) showed that Th/Nd ratios in arc lavas converge towards those of MORB at high $^{143}Nd/^{144}Nd$ ratios rather than the opposite correlation for Ba/Th in Figure 2a which would be expected if Th was more mobilized than Ba in the fluid. Finally, Plank and Langmuir (1993) investigated the correlations between sedimentary influx and volcanic output for a range of elements enriched in arc lavas from a number of arcs worldwide. Plots of those elements extrapolated to 6% MgO (to correct for magma differentiation) and normalized to Na at 6% MgO (to correct for relative dilution due to variation in the degree of melting) versus sediment flux yield strong positive correlations

implicating the sediments as the major source of those elements. Importantly, the correlation for Th passes through the origin implying zero Th flux at zero sediment input whereas those for U and Ba intercept at elevated Ba_6/Na_6 and U_6/Na_6 (Fig. 4) which requires a semi-constant flux of U and Ba in addition to that supplied by the subducting sediment and that is inferred to be the fluid contribution. Thus, this approach also suggests that U and Ba are added in the fluid component much more than Th.

An important aspect in the preceding discussion is the need to separate the fluid and sediment components spatially and (as we will see) also temporally. Quantitative mass balance estimates (e.g., McCulloch and Gamble 1991; Stolper and Newman 1994; Ayers 1998) often conclude that there is as much, or even more, Th and U in the bulk "slab component" (i.e., sediment plus fluid from the altered oceanic crust). However, if the sediment component added is in U-Th isotope equilibrium (or returns to this state prior to fluid addition; see Section 5.3), then addition of only 0.02 ppm U in the fluid will result in significant ^{238}U-excesss in the composite source (e.g., Condomines and Sigmarsson 1993; Turner et al. 1997).

4.3. Experimental constraints on mineral/fluid partitioning

Experimental verification of the observational inferences is complicated by the difficulty of performing mineral/fluid partitioning experiments at high temperatures and pressures and their dependence on fO_2 and complexing agents in the fluid (especially CO_3^{2-} and Cl^-). Nevertheless some attempts have been made (e.g., Tatsumi et al. 1986; Brenan et al. 1994, 1995; Keppler 1996; Ayers et al. 1998; Johnson and Plank 1999).

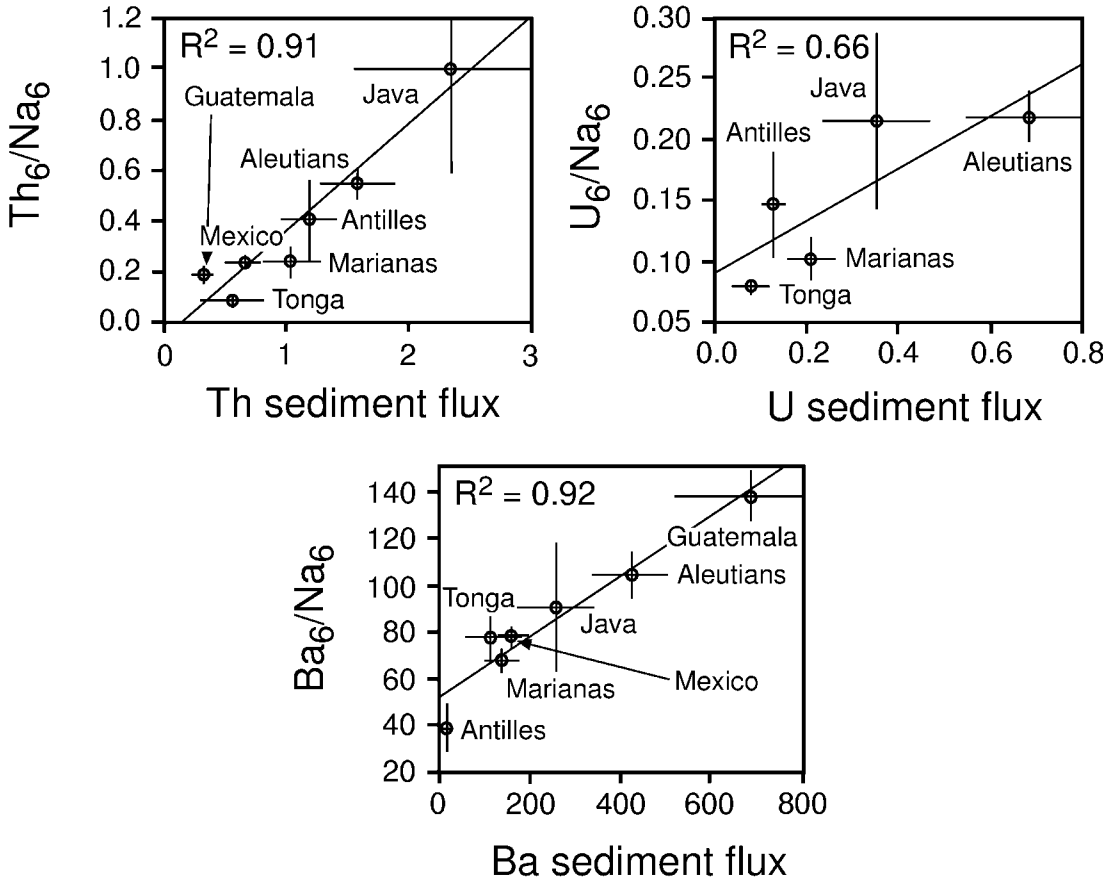

Figure 4. Plots of Th_6/Na_6, U_6/Na_6 and Ba_6/Na_6 versus sediment flux for a number of arcs. Modified from Plank (1993) and Plank and Langmuir (1993).

Tatsumi et al. (1986) noted that the mobility of elements in fluids released during dehydration of serpentinite increased with ionic radius. This correctly predicts the greater mobility of the LILE relative to the HFSE and REE but does not account for the observed U/Th fractionation in arc lavas.

Brenan et al. (1994, 1995) conducted experiments to directly determine mineral/fluid partition coefficients for a range of mantle minerals with incompatible element concentrations similar to those that might occur naturally. In evidence of the difficulty of such experiments, they expressed concern about the attainment of equilibrium and adherence to Henry's law as well as apparatus design and analysis of very low concentration run products (Brenan et al. 1995). These authors also noted the strong influence of oxygen fugacity on U partitioning which decreases by over an order of magnitude on going from log fO_2 = QFM – 4 (Fig. 5a), which might be expected in the MORB source, to QFM + 2 which is likely to be more typical in the mantle wedge beneath arcs (Blatter and Carmichael 1998; Parkinson and Arculus 1999). In order to circumvent some of the experimental difficulties, Keppler (1996) used an indirect approach whereby fluid/andesite-melt partition coefficients were determined and $D^{fluid/clinopyroxene}$ was calculated from $D^{fluid/melt} \div D^{clinopyroxene/melt}$. The results of the Brenan et al. (1995) and Keppler (1996) experiments are summarized in Table 2 along with calculated U/Th and inferred U/Pa and Ra/Th mineral/fluid partition coefficients.

First we compare the results for clinopyroxene which was the only phase common to both of these studies. The results from the pure H_2O experiments are somewhat inconsistent. Keppler (1996) found that Th was more mobile than U, contrary to all observations, whereas Brenan et al. (1995) found the reverse. However, subduction zone fluids are almost certain to contain solutes like Na and Cl derived from seawater and Keppler and Wyllie (1990) showed that the solubility of U, but not Th, is enhanced by the presence of Cl, although the salinities used by Keppler (1996) were very high. Both Brenan et al. (1995) and Keppler (1996) found that U was an order of magnitude more fluid mobile than Th when NaCl was present, although, in the Brenan et al. (1995) experiments, the absolute $D^{clinopyroxene/fluid}$ for Th was lower in the presence of NaCl than in H_2O alone (Table 2), which is inconsistent with the findings of Keppler and Wyllie (1990). However, this may reflect the effects of oxygen fugacity noted above. The results for Nb, taken as an analogue for Pa (Lundstrom et al. 1994), are even more variable. Keppler (1996) found Nb to be fluid immobile whereas Brenan et al. (1995) found it to be quite strongly partitioned into fluids in equilibrium with a range of mantle phases (Table 2) which goes against most observational evidence. It seems likely that most of these inconsistencies reflect the difficulty of the experiments. In contrast, the results for Ba, taken as an analogue for Ra, are entirely consistent with this element being highly fluid mobile with respect to anhydrous phases.

Of the other phases analyzed by Brenan et al. (1994, 1995), neither olivine nor orthopyroxene will contain appreciable incompatible element concentrations. Garnet will be an important residual phase during either dehydration or melting of eclogite and also during mantle melting beneath some rear arc volcanoes (there is little evidence that garnet is a residual phase during mantle melting for most arc front lavas). However, is it important to realize that, like clinopyroxene (Fig. 5a), an order of magnitude decrease in D_U is also expected for garnet with increasing oxygen fugacity (Brenan pers. comm.), so that U is significantly more fluid mobile than Th with respect to garnet at fO_2 = QFM +2. Finally, although rutile will not be stable in the mantle wedge, it may be present as a trace phase in eclogite (Ryerson and Watson 1987).

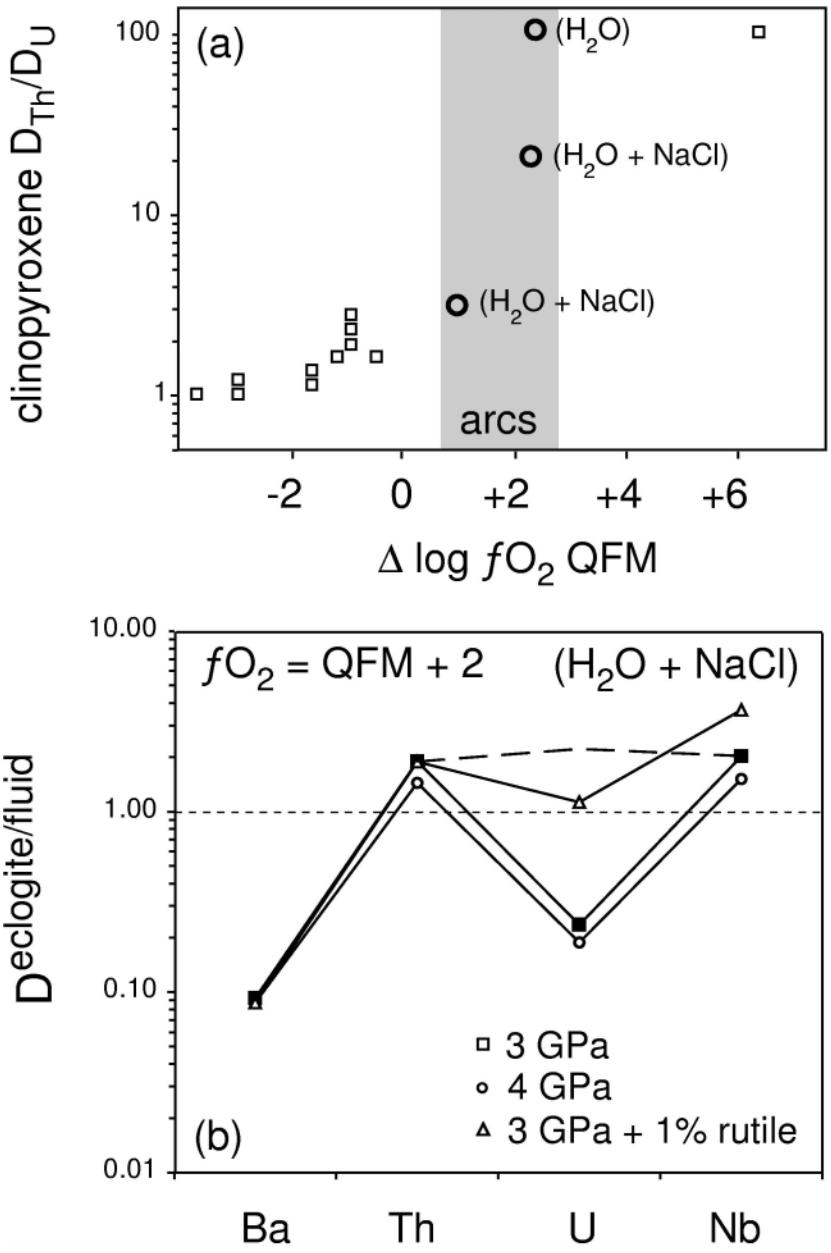

Figure 5. (a) Ratio of D_{Th}/D_U for clinopyroxene/fluid (large circles; Brenan et al. 1995) or clinopyroxene/melt (small squares; Lundstrom et al. 1994) partitioning as a function of oxygen fugacity relative to the QFM buffer. Shaded bar indicated range of oxygen fugacities determined for arcs (Blatter and Carmichael 1998; Parkinson and Arculus 1999). (b) Log-plot of eclogite/fluid (H_2O + NaCl) partition coefficients from Table 2 for Ba, U, Th and Nb based on partition coefficients from Brenan et al. (1994, 1995) and Keppler (1996) and assuming that fO_2 = QFM + 2 from (a). Ba and Nb are assumed to represent reasonable analogies for Ra and Pa. Eclogite mineralogy at 3 and 4 GPa is taken from Schmidt and Poli (1998) with amphibole used to represent the hydrous phases present because mineral-fluid partition coefficients are unavailable for other hydrous minerals (this approximation is likely to have little influence on the results which are strongly controlled by the garnet/clinopyroxene ratio ± rutile). Dashed line is for 3 GPa at fO_2 = QFM – 2 and indicates that there would be little, or even the reverse sense of U/Th and U/Nb (and by implication U/Pa) fractionation at low oxygen fugacity conditions.

Table 2. Experimental mineral/fluid partition coefficients[a]

Mineral	*Fluid*	*Ba*	*Th*	*U*	*Nb*	$D_{U/Th}$	$D_{U/Pa}$[b]	$D_{Ra/Th}$[c]
Clinopyroxene	H_2O[d]	0.02	0.13	3.33	1.75	25.67	1.90	0.17
	H_2O + NaCl[d]	7.88E-04	0.25	0.01	3.33	0.04	2.86E-03	3.15E-03
	H_2O[e]	7.95E-04	3.60	0.24	0.17	0.07	1.41	2.21E-04
	H_2O + NaCl[e]	4.8E-04	3.13	0.26	0.20	0.08	1.33	1.53E-04
Cpx @ fO_2=QFM+2[f]	H_2O + NaCl	4.8E-04	3.13	0.31	3.33	0.10	0.09	1.53E-04
Garnet	H_2O[e]	3.3	0.08	0.88	0.05	10.60	17.25	39.16
	H_2O + NaCl[e]	4.8E-05	0.13	0.72	0.06	5.54	12.63	3.69E-04
Gt @ fO_2=QFM+2[g]	H_2O + NaCl	4.8E-05	0.13	0.01	0.06	0.10	0.23	3.69E-04
Amphibole	H_2O + NaCl[e]	0.51	0.93	0.35	1.10	0.38	0.32	0.55
Olivine	H_2O + NaCl[e]	0.00	0.01	0.01	0.25	1.07	0.03	3.19E-03
Rutile	H_2O[h]	n/a	0.10	89	164	890	0.54	n/a
Eclogite @ 3GPa[i]	H_2O + NaCl	0.092	1.895	0.236	2.014	0.12	0.12	0.049
Eclogite @ 4GPa[j]	H_2O + NaCl	0.087	1.437	0.187	1.512	0.13	0.12	0.060
Eclogite @ 3GPa+ 1% rutile	H_2O + NaCl	0.087	1.887	1.122	3.643	0.59	0.31	0.046

[a] An average is quoted when more than one determination was available
[b] Inferred from $D_{U/Nb}$
[c] Inferred from $D_{Ba/Th}$
[d] Keppler (1996)
[e] Brenan et al. (1995)
[f] Using clinopyroxene-fluid (H_2O + NaCl) D's from Brenan et al. (1995), excepting D_{Nb} from Keppler (1996) and assuming $D_U = D_{Th/10}$
[g] Using garnet-fluid (H_2O + NaCl) D's from Brenan et al. (1995), excepting D_{Nb} from Keppler (1996) and assuming $D_U = D_{Th/10}$
[h] Brenan et al. (1994); n/a = not analyzed
[i] Assuming garnet:clinopyroxene:amphibole[k] = 28:54:18, mineral-fluid D's from Brenan et al. (1995) and fO_2 = QFM + 2
[j] Assuming garnet:clinopyroxene:amphibole[k] = 44:39:17, mineral-fluid D's from Brenan et al. (1995) and fO_2 = QFM + 2
[k] Based on modal proportions given by Schmidt and Poli (1998)

4.4. Composition of fluids released from the subducting plate

During subduction, both the hydrated oceanic crust and over-riding sediments undergo a progressive sequence of up-grade metamorphic reactions, many of which involve dehydration (e.g., Poli and Schmidt 1995; Schmidt and Poli 1998; Johnson and Plank 2000). However, as discussed above, it would appear that the altered oceanic crust is the major source of fluid for most arc lavas. The altered oceanic crust becomes progressively converted to eclogite and the ratio of garnet to clinopyroxene increases rapidly beneath the arc front volcanoes from 34:66 at 3 GPa to 53:47 at 4 GPa (Schmidt and Poli 1998). In Table 2, we give the calculated eclogite/fluid partition coefficients for fO_2 = QFM +2 at both 3 GPa and 4 GPa and for eclogite + 1% rutile at 3 GPa and these values are plotted on Figure 5b. For this oxygen fugacity D_{Th}/D_U for both clinopyroxene and garnet was assumed to be 10 on the basis of the median value on Figure 5a. We have used amphibole as a proxy for the additional phases (phengite and lawsonite) in the eclogite because there are no available mineral/fluid partition coefficients for these minerals. However, phengite is likely to have a very low D_U (Becker et al. 1999) and because clinopyroxene and garnet dominate the mode (Schmidt and Poli 1998) and thus the bulk D's (Table 2) this is unlikely to significantly alter the conclusions. The importance of oxygen fugacity is re-emphasized by the dashed line on Figure 5b which indicates that there will be minimal U/Th and U/Pa fractionation at fO_2 = QFM – 2. Thus, if oxygen fugacity varies significantly between or within subduction zones this could have a major effect on U-series fractionation.

Notwithstanding the complexities discussed above, results are encouragingly consistent with empirical observations in that the relative order of fluid compatibility is Ba (and by inference Ra) > U > Th > Nb (and by inference Pa). In detail, Ba is highly fluid mobile which is consistent with all observations (D < 0.1) and the eclogite/fluid partition coefficient for U averages around 0.2. The eclogite/fluid partition coefficients for Th and Nb range from 1.9 to 1.4 and 1.5 to 2, respectively, from 3 to 4 GPa. Again, this is consistent with the inferred relatively immobile nature of these elements. However, the presence of 1% residual rutile has a significant effect in increasing the eclogite/fluid partition coefficient for U to 1.1 and Nb to 3.6 at 3 GPa. So, although the experimental data predict more U than Th in the fluid under all conditions, neither Th nor Nb are predicted to be completely fluid immobile and the relative fractionation of U/Th decreases in the presence of residual rutile. Thus, it seems likely that the thermal conditions of the subducting plate and the presence or absence of rutile may also play an important role in determining the relative fractionation of the U-series nuclides in subduction zone fluids.

In Table 3 we have calculated the composition of fluids produced by dehydration of subducting altered oceanic crust that has a composition based on that of Staudigel et al. (1996). The model assumes that the altered oceanic crust is in U-series equilibrium, bulk eclogite/fluid D's for a rutile-free mineralogy at 3 GPa from Table 2 in which $D_{Ra} = D_{Ba}$ and $D_{Pa} = D_{Nb}$, and a Rayleigh distillation process with 2, 3 and 5% H_2O release. Taking 3% H_2O as the likely amount of fluid added to the wedge beneath arc front volcanoes (Davies and Bickle 1991; Poli and Schmidt 1995), we calculate that this fluid will have the following composition: U/Th = 35.9, Ba/Th = 6470, $(^{238}U/^{232}Th)$ = 113, $(^{235}U/^{231}Pa)$ = 7.6 and $(^{226}Ra/^{230}Th)$ = 15 and this will be used in the subsequent discussion and figures with the acknowledgement that this composition will vary somewhat if different mineral/fluid partition coefficients and/or a different altered oceanic crust composition was used.

4.5. Chromatographic interaction with the mantle wedge

Several authors have suggested that the composition of subduction zone fluids is likely to change by chromatographic interaction during their passage through the mantle

Table 3. Calculated compositions of fluids produced by dehydration of the altered oceanic crust[a]

% fluid	*AOC*[b]	*2*	*3*	*5*
Ba (ppm)	31	276	249	203
Th (ppm)	0.072	0.038	0.039	0.039
U (ppm)	0.36	1.430	1.383	1.293
Nb (ppm)	1.18	0.592	0.595	0.601
U/Th	5.0	37.3	35.9	33.2
U/Nb	0.31	2.42	2.32	2.15
Ba/Th	431	7193	6470	5217
(^{238}U/^{232}Th)	15.3	117	113	104
(^{238}U/^{230}Th)	1.0[c]	7.9	7.6	7.0
(^{235}U/^{231}Pa)	1.0[c]	7.9	7.6	7.0
(^{226}Ra/^{230}Th)	1.0[c]	16.7	15.0	12.1
apparent U-Th age (kyr)[d]	-	14	15	16
apparent U-Pa/Nb age (kyr)[e]	-	0.040	0.042	0.045

[a] Assuming a Rayleigh distillation process and bulk eclogite/fluid D's for 3 GPa without rutile from Table 2

[b] Altered oceanic crust composition based on Staudigel et al. (1996)

[c] Assuming U-series equilibrium in altered oceanic crust

[d] Two point isochron tied to composition in U-series equilibrium with (^{238}U/^{232}Th) = 1

[e] Two point isochron tied to composition in U-series equilibrium with 0.047 ppm U, 2.33 ppm Nb

wedge (Navon and Stolper 1987; Kelemen et al. 1990; Hawkesworth et al. 1993; Stolper and Newman 1994). In the mantle wedge, clinopyroxene is likely to be the main host of incompatible trace elements and the mineral/fluid partition coefficients for clinopyroxene under oxidizing conditions in Table 2 suggest that the effect of such interaction would be to increase the U/Th, U/Nb and Ba/Th (and by analogy U/Pa and Ra/Th) ratios of the fluids. The magnitude of such effects is unknown and will be lessened if the mantle wedge becomes increasingly reducing with distance away from the subducting plate or if the fluid transport velocities are too fast to allow significant equilibration en route (see sections 6 and 7.2).

In summary, a key aspect to the utility of U-series isotopes in the study of arc lavas is that whereas Th and Pa are observed and predicted to behave as relatively immobile high field strength elements (HFSE), Ra and (under oxidizing conditions) U behave like large ion lithophile elements (LILE) and are significantly mobilized in aqueous fluids. Fluid-wedge interaction will only serve to increase these fractionations. Just how robust the experimental partition coefficients are remains to be established by future experiments.

5. SEDIMENT ADDITION, MASS BALANCE FOR Th AND TIME SCALES

The presence of ^{10}Be or negative Ce anomalies, or both, in some arc lavas provide unambiguous evidence for a contribution from subducted sediments to the source of arc lavas (Morris et al. 1990; Hole et al. 1984). In addition, Pb isotopes commonly are

elevated above the northern hemisphere reference line (NHRL) and arc lavas form arrays pointed toward the isotopic composition of locally subducting sediment (Kay 1980; Gill 1981). Consequently, we look next at the impact of sediment addition on the abundances of U-series nuclides and the resulting implications for the time scale and process of mass transfer of the sediment component beneath arc volcanoes.

5.1. Mass balance for Th content and $^{230}Th/^{232}Th$ ratios

The implication of Figure 1 is that the Th content of arc lavas is dominated by the sediment component and this can be verified by simple mass balance. In N-MORB reflect ~10% partial melting then MORB-source mantle is likely to have ~ 0.01 ppm Th (Sun and McDonough 1989) or lower, if there has been back-arc melt extraction, whereas GLOSS has ~6.9 ppm (Plank and Langmuir 1998). If a primitive arc lava contains 0.5 ppm Th and represents a 15% partial melt then its source had a Th content of ~0.075 ppm, assuming for the purposes of illustration that Th is completely incompatible during melting. By simple mass balance, the sediment contribution required to produce a source with this Th content can be estimated to 100 × (0.075-0.011)/(6.9-0.011) or ~1%. Lower Th in primitive melts or smaller percent melting require less sediment; lower Th in sediments requires more. Regardless, even 1% sediment accounts for 80-98% of the Th in the source of most arc magmas.

This conclusion is supported by the calculations of Plank and Langmuir (1993) who showed that the Th output of arc volcanoes is directly proportional to the sediment flux of Th (Fig. 4). Using an arc growth rate of 1.1 km^3/yr (Reymer and Schubert 1984), a density of 2.8 g/cm^3 and a Th content of 1 ppm, and assuming that the arc mantle source is similar to that of N-MORB, the annual flux of Th from subducted sediment is estimated at ~2.7×10^9 g (Hawkesworth et al. 1997a). From these estimates and an annual flux of Th from subducted sediment of 9×10^9 g/yr (Plank and Langmuir 1998), Hawkesworth et al. (1997a) calculated that ~30% of the Th in subducted sediments is returned to the crust in arc magmas, leaving 70% to be recycled beyond the arc into the deep mantle. Using the fluxes provided by Plank and Langmuir (1998) this equates to ~ 2.7×19^9 g/yr entering the arc crust and 6.3×10^9 g/yr continuing on into the mantle. Because 0.5 ppm Th is a relatively high value for some primitive arc melts (see Fig. 2b), the percent and amount of recycled Th may be even higher in places.

An important consequence of the Th abundance mass balance is that the Th isotopes of the mantle wedge will usually be dictated by that of the subducting sediment. Nicaragua provides a particularly clear example where the distinctive signature of subducted, carbonate-rich sediment with high U/Th and ($^{230}Th/^{232}Th$) also characterizes the adjacent arcs lavas (McDermott and Hawkesworth 1991; Reagan et al., 1994; Thomas et al., 2002). More generally the subducting sediment will be dominantly pelagic, in which case the ($^{230}Th/^{232}Th$) ratio of the sediment modified mantle wedge will typically be significantly lower than MORB mantle. This is illustrated by a MORB-source – sediment mixing curve in Figure 6 which shows that the Th isotopic composition of a sediment-wedge mixture becomes effectively that of the sediment after 1% sediment addition. Thus, so long as the subducting sediments can be assumed to be in secular equilibrium (see Section 5.2) the ($^{230}Th/^{232}Th$) ratio of the sediment-wedge mixture can be estimated directly from the U/Th ratio of the subducting sediments. Moreover, if the composition of the subducting sediments is relatively constant along a given arc and if the sediment contribution is ≥ 1%, the ($^{230}Th/^{232}Th$) ratio of the sediment-wedge mixture will be invariant. As we shall see this not only has fundamental implications for how the time scales of fluid addition are determined (see Section 6), but it also provides one means of determining the rate of transfer, or recycling, of the sediment component back into the crust via the arc lavas.

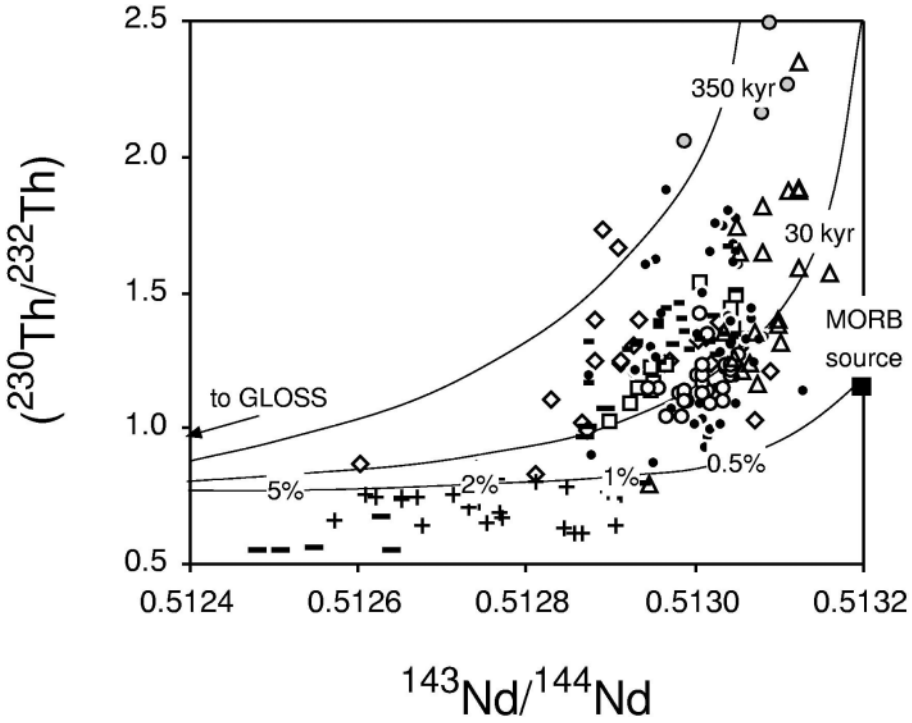

Figure 6. ($^{230}Th/^{232}Th$) versus $^{143}Nd/^{144}Nd$ for arc lavas. The mixing curve between a nominal MORB mantle and subducted sediment illustrates that the Th isotope signature of the mantle wedge will be dictated by as little as 1% subducted sediment (assuming no ^{230}Th in-growth). The model uses a MORB-source with 0.004 ppm U, 0.011 ppm Th, 0.67 ppm Nd and $^{143}Nd/^{144}Nd = 0.51321$ and GLOSS (Plank and Langmuir 1998) and assumes that both are initially in U-Th equilibrium. The upper curves represent the Th isotope ratios which will be reached 30 and 350 kyr after addition of a constant fluid flux of 0.021 ppm U which results in variable ^{238}U-excesses whose magnitude depends on the mass balance between this U addition and the Th content resulting from the sediment- mantle wedge mix. The degree of melting used is 15% and U and Th are assumed to be completely incompatible. Symbols and data sources as in Figure 1.

5.2. Mechanism of sediment transfer—implications for the temperature of the wedge?

Sediment may be added by bulk mixing via imbricate thrusting (Bebout and Barton 2002), dehydration (Class et al. 2000), or melting (Johnson and Plank 1999). The latter two may differ in their P-T conditions and, therefore, residual mineralogy as well as relevant partition coefficients. In general, fluids are less effective transport agents than melts (i.e., trace elements are more soluble in melt than in pure water or even brine), but fluid/solid partitioning can fractionate some elements, notably Ba-Th and U-Th, more than melt/solid. However, as pressure increases, the distinction between "fluid" and "melt" decreases as their mutual solubility increases and they approach a critical end-point.

It is widely thought that melts can transport Th, light REE, and Zr-Hf much more than fluids can (e.g., Johnson and Plank 1999), although this is a relative statement in which the relevant partition coefficients are poorly known and variable. However, lavas from several arcs have Nd/Ta and Th/Ce ratios that are significantly higher than those in their input bulk sediments (see Fig. 1b) and so it has been suggested that the sediment component is transferred as a partial melt formed in the presence of residual accessory phases (Nichols et al. 1994; Johnson and Plank, 1999) which retain HFSE (Elliott et al. 1997; Turner and Hawkesworth 1997; Johnson and Plank, 1999). At the Marianas volcanic front, the lavas with the highest Th contents (highest sediment contribution) lie on or near the U-Th equiline with ($^{230}Th/^{232}Th$) ~1.04 (Elliott et al. 1997). However, the

bulk subducting sediment (Plank and Langmuir 1998) has a much lower ($^{230}Th/^{232}Th$) ratio of 0.58 (see Fig. 7). Because mass balance calculations show that the Th isotope composition of the wedge-sediment mix is controlled by the sediment, the U/Th ratio of the sediment component has been modified. Elliott et al. (1997) concluded that the sediment component was added as a partial melt which had a higher U/Th ratio than that of the bulk sediments. Note that this cannot be due to melting in the presence of residual rutile, as originally suggested by Elliott et al. (1997), because U is much more compatible than Th in rutile (Blundy and Wood 2003). Some other residual phase, such as apatite, may be responsible.

This discussion leads us to perhaps one of the most serious apparent discrepancies between current geochemical and geophysical models. Experimental data demonstrate that partial melting of sediments at shallow levels (3 GPa) requires temperatures ≥ 670 ˚C (Nichols et al. 1994; Johnson and Plank 1999) and thus a thermal structure in the mantle wedge several hundred degrees hotter than that predicted by many numerical thermal models (e.g., Davies and Stevenson 1992; Peacock 1996). However, the viscosity of the mantle wedge may be lower than often assumed (Billen and Gurnis 2001) and numerical models that incorporate a temperature-dependant viscosity predict a component of upward flow beneath arcs and thus a hotter temperature structure (e.g., Furukawa 1993a, b; Kincaid and Sacks 1997). Such models may also help to reconcile the high eruption and equilibration temperatures inferred for some arc lavas (e.g., Sisson and Bronto 1998; Elkins Tanton et al. 2001).

5.3. Time scale of sediment transfer

Three lines of evidence suggest that the sediment component is added to the arc mantle before the principal fluid component that appears in arc magmas. First, the mechanical mixing of sediment and peridotite observed in outcrops of subduction

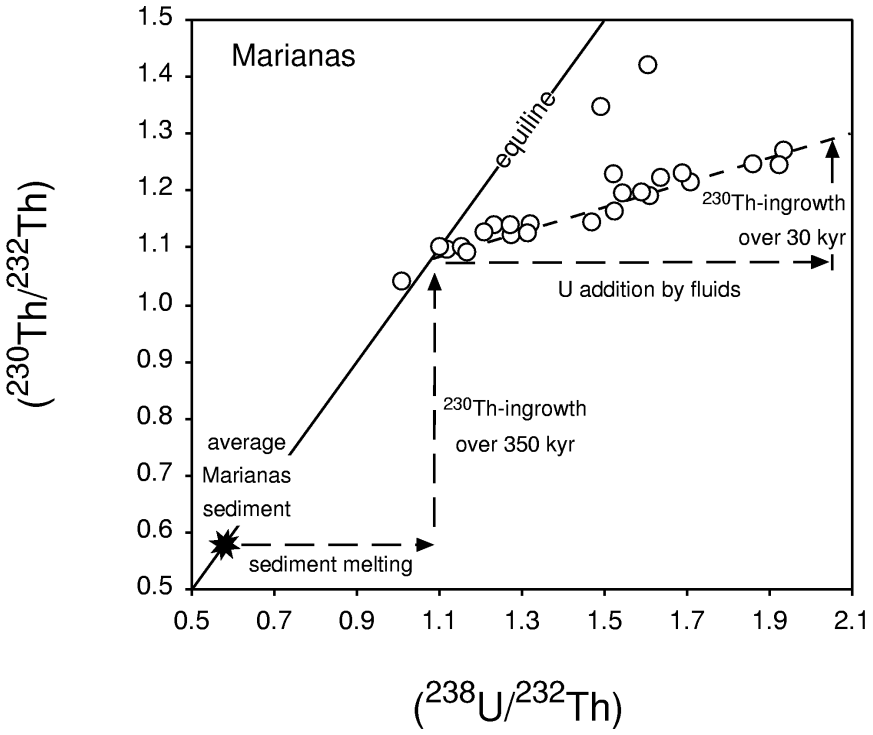

Figure 7. U-Th equiline diagram for lavas from the Marianas with dashed arrows showing the preferred interpretation of the sediment melt and fluid transfer times (after Elliott et al. 1997).

complexes occurs beneath the forearc (Bebout and Barton 2002). Secondly, geochemical observations of arc lavas also suggest addition of sediment prior to events that most affect U-series disequilibria. Returning to the case of the Marianas, the increased U/Th ratio inferred to have been produced from the sediment component by partial melting would result in the sediment melt having ^{238}U-excess. Because the Marianas lava array projects back to the equiline, Elliott et al. (1997) argued that the sediment melt was added sufficiently long ago for it to have decayed back up to the equiline (see Fig. 7) which would require that the transfer time of this component was at least 350 kyr. Of course, this is a minimum estimate because the U/Th isotope system cannot resolve beyond 350 kyr. The Marianas argument applies only if the subducting sediment has a high Th/U ratio (e.g., is dominated by clay more than carbonate or organic-rich components) and it also loses force if some lavas along the (^{230}Th/^{232}Th)-(^{238}U/^{232}Th) correlation line are Th-enriched instead of in equilibrium (e.g., Reagan et al. 1994). Thirdly, in addition to these same arguments applying to Tonga, a Pb isotopic signature there, that occurs only in the northernmost lavas, has been attributed to Louisville volcaniclastic sediments which are presently being subducted some 1000 km further south (Regelous et al. 1997; Turner and Hawkesworth 1997). Because the line of volcaniclastics is being subducted obliquely beneath the arc, the locus of their subduction has migrated southwards over time and from this Turner and Hawkesworth (1997) inferred a sediment transfer time of 2-4 Myr. In the simplest model, such long transfer times require the transfer of sediment into the mantle wedge at shallow levels and decoupling of convection in the wedge from the subducting plate in order to slow the rate of transfer of the sediment component to the site of partial melting (Turner and Hawkesworth 1997). We note in passing that there is some evidence that flow within the mantle wedge may be oriented along the arc parallel to the trench rather than being directly coupled to the subducting plate (Turner and Hawkesworth 1998; Smith et al. 2001).

In summary, there is permissive evidence that the sedimentary component is added to the mantle wedge before the fluid addition and melting that leads to arc magmatism.

6. FLUID ADDITION TIME SCALES

In the following sections we look at the evidence for the timing of fluid addition to the sources of arc magmas from U-series disequilibria data and then discuss the extent to which some apparently conflicting time scale information might be reconciled.

6.1. U addition time scales

Fluids produced by dehydration reactions in the subducting, altered oceanic crust preferentially add U (along with other fluid mobile elements) to the mantle wedge. So long as this is the principal cause of U/Th fractionation (but see sections 7 and 8), U-Th isotopes can be used to estimate the time elapsed since fluid release into the mantle wedge. Firstly, U and Th have similar and small distribution coefficients in most mantle minerals at depths < 80 km (Blundy and Wood 2003) and so neither partial melting or gabbroic crystal fractionation are likely to have much effect on elemental U/Th ratios at the degrees of melting inferred for arcs (>5%). Secondly, continental upper crustal materials generally have low U/Th and so bulk crustal contamination would act to decrease U/Th. Therefore, since the vast majority of arc lavas have U/Th ratios exceeding anything found in MORB or OIB and frequently preserve ^{238}U-excesses (Fig. 3), the high U/Th ratios are generally accepted to reflect U addition to their mantle source by fluids from the subducting plate.

In practice, information on the timing of fluid release can either be obtained from along-arc suites of lavas which form inclined arrays on U-Th equiline diagrams, where the

age = $-1/\lambda^{230} \times \ln(1 - \text{slope})$, or if the initial ($^{230}Th/^{232}Th$) ratio is constrained for an individual sample. For example, Sigmarsson et al. (1990) obtained an inclined U-Th isotope array for lavas from the southern Andes and suggested that the slope of this array reflected the time (20 kyr) since U addition by fluids. Similarly, Elliott et al. (1997) showed that lavas from the Marianas form a 30 kyr U-Th isotope array (Fig. 7). In total about 15 arcs have now been studied for U-Th disequilibria indicating that the time since U addition by fluids from the subducting oceanic crust varies from 10 to 200 kyr prior to eruption (Fig. 8a), if the correlations have strict time significance (see Section 8). All of these arrays show variable degrees of scatter and any chronological interpretation should be viewed as the time-integrated effect of U addition rather than to imply that U addition occurred at a discrete and identical time along the length of an arc. Indeed, variations can occur within the single arc due to the effects of tectonic collisions on the rate of subduction, such as occurs in New Britain (Gill et al. 1993) and Vanuatu (Turner et al. 1999), or possibly even through the life of a single volcano such as Santorini (Zellmer et al. 2000).

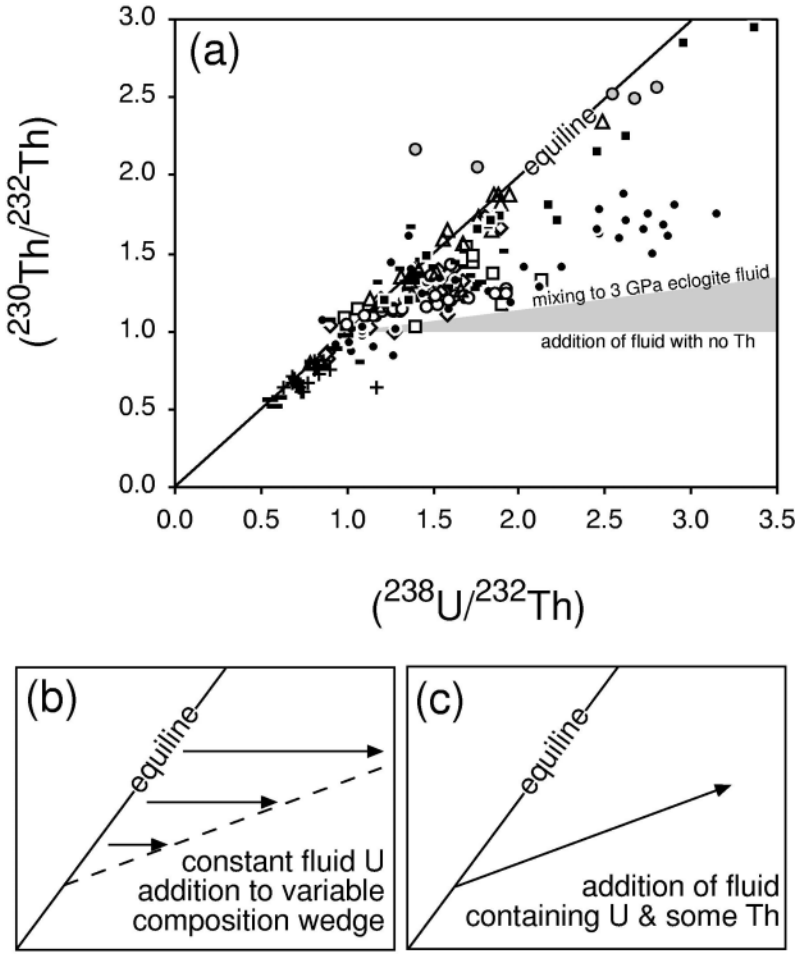

Figure 8. (a) U-Th equiline diagram for arc lavas. Symbols and data sources as in Figure 1. (b) Schematic U-Th equiline diagram showing how addition of a constant U fluid flux to a wedge with variable composition could in principle produce an inclined array. (c) Schematic U-Th equiline diagram showing how addition of a fluid containing some Th could in principle produce an inclined array. Shaded envelope in (a) indicates the range of compositions which could be produced by adding either a fluid containing no Th or the calculated 3 GPa eclogite fluid from Table 3 to a mantle wedge in equilibrium with an arbitrary ($^{238}U/^{232}Th$) ratio of 1. The majority of arc lavas lie above this envelope (even though their arrays often tie back to the equiline around ($^{238}U/^{232}Th$) = 1). The slope of a hypothetical array produced by addition of the latter fluid corresponds to an age of 15 kyr.

An underlying assumption in these interpretations is that U addition by fluids is the only cause of U/Th fractionation (see Fig. 8b,c) and if the same were true of U/Pa ratios then U addition should likewise produce U-Pa arrays which record a similar time to the U-Th arrays. So far the only arc where this may be true is Tonga, where Turner et al. (1997) showed that the combined Tonga and Kermadec lava array scatters around a ~ 50 kyr U-Th isochron (Fig. 9a). Subsequently, Bourdon et al. (1999) showed that the Tonga lavas are characterized by excesses of ^{235}U over ^{231}Pa, and by normalizing to Nb, obtained a U addition age of 60 kyr (Fig. 9b). This result supports the interpretation that the U-Th arrays have time significance (see Section 8). In the original age calculation made by Bourdon et al. (1999) the most depleted sample (26837) was omitted because of its very high (^{235}U)/Nb ratio which was most likely due to imprecision on its very low Nb

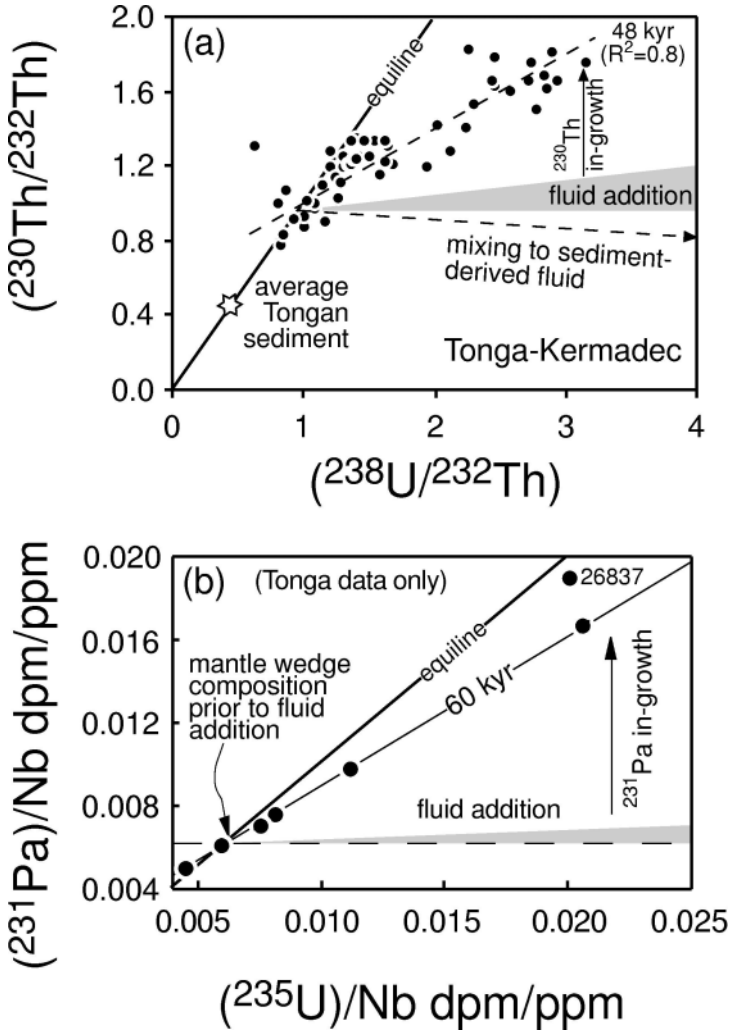

Figure 9. (a) U-Th isotope data from the Tonga-Kermadec island arc (Turner et al. 1997; Regelous et al. 1997). The dashed line indicates that an regression line through the full Tonga-Kermadec data set has an age of 48 kyr. Shaded envelope encompasses likely fluid compositions ranging from Th-free to an fluid in equilibrium with eclogite at 3 GPa (as in Table 3 and Fig. 8). (b) U-Pa isotopes (Bourdon et al. 1999) normalized to Nb on the basis that it behaves as a stable analogue of Pa (see text). Note the addition of the Tofua sample 26837 using the revised Nb concentration (T. Plank pers. comm.). The arrows show that if the fluid contains U but no Pa then the lavas from Tonga record similar U addition times in both the U-Th and U-Pa systems. As in (a) the shaded envelope encompasses the likely range of fluid compositions and illustrates that the Pa content of the fluid is predicted to be so low that the age determined from the isochron requires virtually no correction for the fluid composition (i.e., the assumption of addition of U only is justifiable).

concentration. Using a revised Nb measurement of 0.23 ppm (T. Plank pers. comm.), this point lies closer to, but still slightly above the array defined by the other 6 samples (Fig. 9b). When the 7 Tongan samples analyzed for U-Th-Pa are considered, their U-Th and U-Pa arrays yield apparent ages of 35 +24/−15 kyr and 60 +20/−25 kyr, respectively. Thus, they agree within 1σ analytical error of each other and with a regression through the complete Tonga-Kermadec U-Th dataset which yields 48 kyr (r^2 = 0.8), although the errors are large. Finally, Bourdon et al. (2003) have used a Th/U versus Pa/U concordia diagram to show that the Tonga samples are consistent with addition of U 60 kyr ago. Consequently, it may be that a single U-addition event is recorded in the Tongan lavas, but more such studies are needed to determine where else this may apply.

More typically, arc lavas preserve ^{231}Pa-excesses (Fig. 3) which is inconsistent with *only* fluid addition of U and subsequent in-growth of ^{231}Pa and, instead, suggests additional in-growth of ^{231}Pa during partial melting as well. The balance between addition and in-growth of all U-series nuclides is a substantive issue and we will return to it below.

6.2. Ra addition time scales

^{226}Ra has a much shorter half life (1600 yr) than its parent ^{230}Th (75 kyr) and so provides the opportunity to look at very recent fractionation between Ra and Th. Global surveys by Gill and Williams (1990) and Turner et al. (2001) have shown that most arc lavas are characterized by ^{226}Ra-excesses. Reagan et al. (1994), Chabaux et al. (1999) and Sigmarsson et al. (2002) noted positive correlations between (^{226}Ra/^{230}Th) and (^{238}U/^{230}Th) and, like Gill and Williams (1990), inferred that the ^{226}Ra-excesses may reflect very recent metasomatism of the wedge. Turner et al. (2001) have subsequently shown that ^{226}Ra-excesses is arcs can greatly exceed those in other tectonic settings that the largest ^{226}Ra-excesses are found in those arc lavas with the highest Ba/Th ratios. The latter are usually taken as a good index of fluid addition (Fig. 10a) and these two traits are greatest in Th-poor oceanic arcs but it is important to verify that this is indeed a fluid signal.

Most arc lavas are plagioclase-phyric and because Ba and Ra are mildly compatible in plagioclase (Bundy and Wood 2003) it might be thought that the elevated Ba/Th and ^{226}Ra in arc lavas results from plagioclase accumulation. However, because D_{Plag} for Ra is predicted to be < 0.1 for mafic to intermediate magmatic systems (Bundy and Wood 2003), the Ra concentration in a rock will always be dominated by the groundmass component and the ^{226}Ra-excesses cannot have resulted from plagioclase accumulation. The elevated Ba/Th ratios are also unlikely to reflect gabbroic fractionation or crustal contamination because Ba is more compatible than Th during in gabbroic mineral assemblage and crustal materials have low Ba/Th relative to most arc lavas. In any case, the highest Ba/Th ratios occur in those arc rocks with the lowest SiO_2 and ^{87}Sr/^{86}Sr ratios and so the observed ^{226}Ra-excesses are inferred to be a mantle signature. Because Ba is more incompatible than Th during mantle melting (Blundy and Wood 2003), the ^{226}Ra-excesses in arc lavas might have been developed during partial melting (e.g., Turner and Hawkesworth 1997). However, both elements are highly incompatible, making them hard to fractionate by melting processes and Bourdon et al. (2003) noted that the largest ^{226}Ra-excesses also tend to occur in those arc lavas with the highest Sr/Th ratios (Fig. 10b). This latter correlation cannot be a melting signature because Sr is more compatible than Th during mantle melting.

Therefore, since both Ba and Sr are fluid mobile, the large ^{226}Ra-excesses at high Ba/Th and Sr/Th ratios are inferred to result from fluid addition to the mantle wedge. At the other end of the arrays in Figure 10 it is notable that the intercept for any arc is with the Ba/Th, not (^{226}Ra/^{230}Th) axis. This contrasts strikingly with MORB, for example,

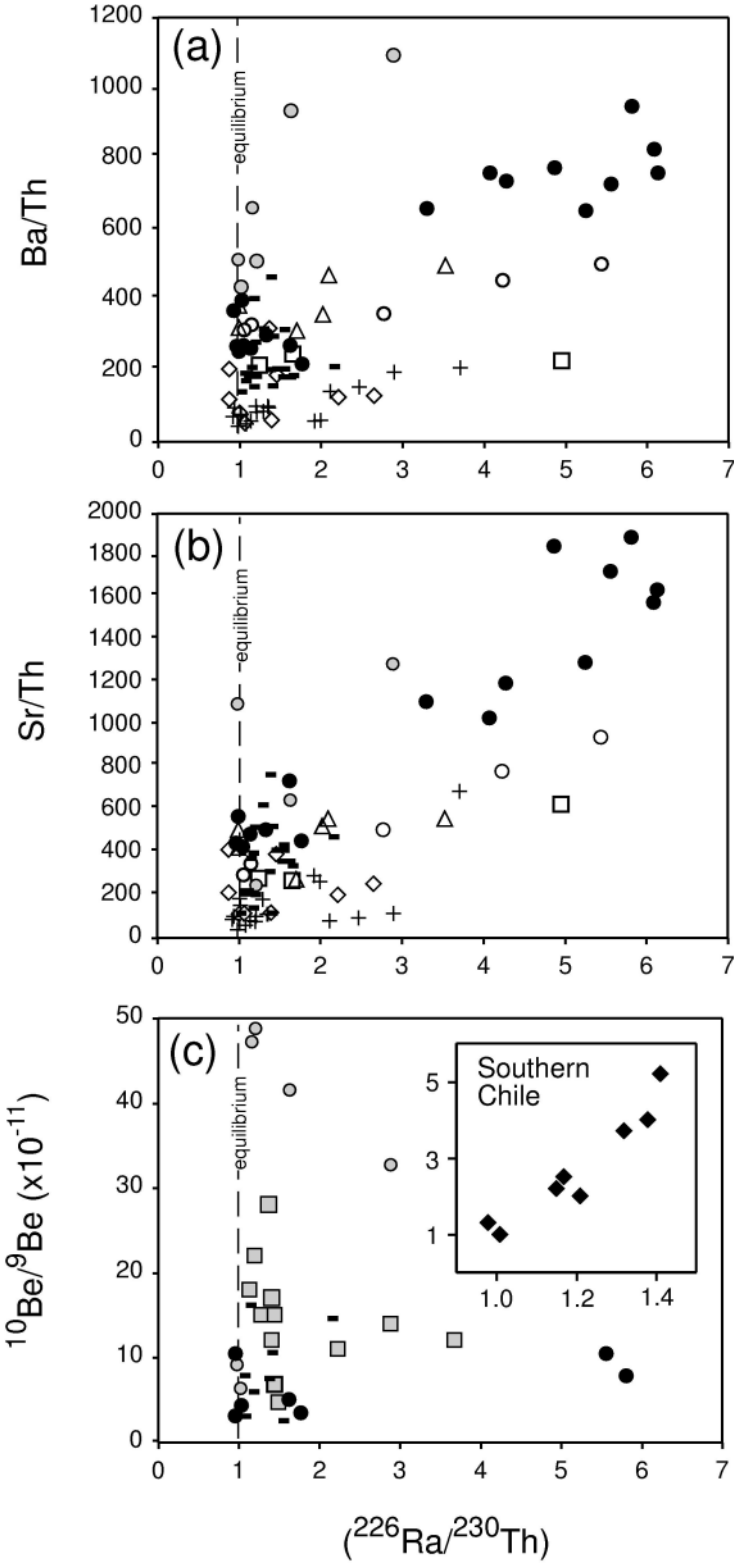

Figure 10. ^{226}Ra-^{230}Th disequilibria plotted against (a) Ba/Th, (b) Sr/Th and (c) ^{10}Be/^{9}Be. The positive correlations with Ba/Th and Sr/Th which are sensitive to fluid additions (cf. Figs. 1 and 2), suggest that the observed ^{226}Ra-excesses result from Ra addition by fluids from the subducting plate. The positive correlation in southern Chile (Sigmarsson et al. 2002) shown in the insert to (c) is also consistent with derivation of the ^{226}Ra-excesses from the subducting plate (see text). Symbols and data sources as in Figure 1. In (c) grey squares are data from New Britain (Gill et al. 1993); Tonga Be isotopes are unpublished data from Turner, George and Morris (in prep.).

where (^{226}Ra/^{230}Th) is high even when Ba/Th is low. This means that the most recent addition of Ba and Ra is superimposed on a mantle previously enriched in Ba, and that whatever excess ^{226}Ra is produced during low-porosity melting in the mantle wedge is overwhelmed by the slab contribution.

Recently, Sigmarsson et al. (2002) showed that there is a good positive correlation between (^{226}Ra/^{230}Th) and ^{10}Be/^{9}Be in lavas from southern Chile. More commonly, (^{226}Ra/^{230}Th) is not well correlated with ^{10}Be/^{9}Be (Fig. 10c) consistent with decoupling between the sediment and fluid signatures. Nevertheless, since ^{10}Be is unambiguously derived from the subducted sediments, the Chile data provides independent evidence that ^{226}Ra-excesses are derived from the subducted plate. It also indicates that, in Chile, fluids from the altered oceanic crust may scavenge ^{10}Be from the overlying sediments as they pass through them from the underlying altered oceanic crust and out into the mantle wedge.

In summary, there is now convincing evidence that ^{226}Ra is added to the mantle wedge source of arcs by fluids and that the most recent of these additions must have occurred less than 8 kyr ago. The evidence depends on the magnitude of (^{226}Ra/^{230}Th) and the quality of its correlation with subduction parameters. The evidence is most robust for oceanic arcs and it usually hinges on data for a few volcanoes, usually the ones with the lowest Th concentrations.

6.3. Reconciling the U and Ra time scales

At face value, the ^{226}Ra evidence for fluid addition in the last few 1000 years appears inconsistent with the interpretation that U/Th disequilibria resulted from fluid addition 10-200 kyr ago and we now discuss some possible models for reconciling these disparate time scales.

6.4. Single-stage fluid addition

Chabaux et al. (1999) noted a good correlation between (^{226}Ra/^{230}Th) and (^{238}U/^{230}Th) in lavas from the Lesser Antilles and, although this correlation is weaker with new mass spectrometric data for Kick 'em Jenny (Turner et al. 2001), (^{226}Ra/^{230}Th) and (^{238}U/^{230}Th) are broadly correlated globally in arc lavas of known eruption age (Fig. 11a). Section A1 of the Appendix provides a method for estimating the range of U-Th-Ra disequilibria in the wedge prior to melting. Sigmarsson et al (2002) also observed a strong correlation between (^{226}Ra/^{230}Th) and (^{238}U/^{230}Th) in lavas from southern Chile. On the basis of this, Chabaux et al. (1999) and Sigmarsson et al (2002) suggested that both U and Ra were added together in a single very recent fluid addition. Such an interpretation requires that the U-Th (and U-Pa in the case of Tonga) arrays do not simply reflect the time elapsed since U addition and, in principle, this could arise in several ways as discussed by Elliott et al. (1997).

Firstly, the slope of the U-Th arrays might reflect addition of a constant U flux to a mantle wedge with variable U-Th concentrations and isotope ratios (Fig. 8b). However, the mass balance calculations show that the Th isotope composition of the mantle wedge will *usually* be dictated by the composition of the subducted sediment so this is generally only likely if the sediment composition varies significantly and U-Th correlates positively with other sediment indicators within the arc. Vanuatu provides an interesting exception to this because in this arc the composition of the wedge (especially as seen with Pb isotope data) does vary, not due to sediment addition, but from to a change from Pacific to Indian mantle in the area of the D'Entrecastreaux collision. Significantly, here the lavas erupted above the Indian and Pacific portions of the wedge define two separate, inclined U-Th arrays which intersect the equiline at the compositions predicted for Indian

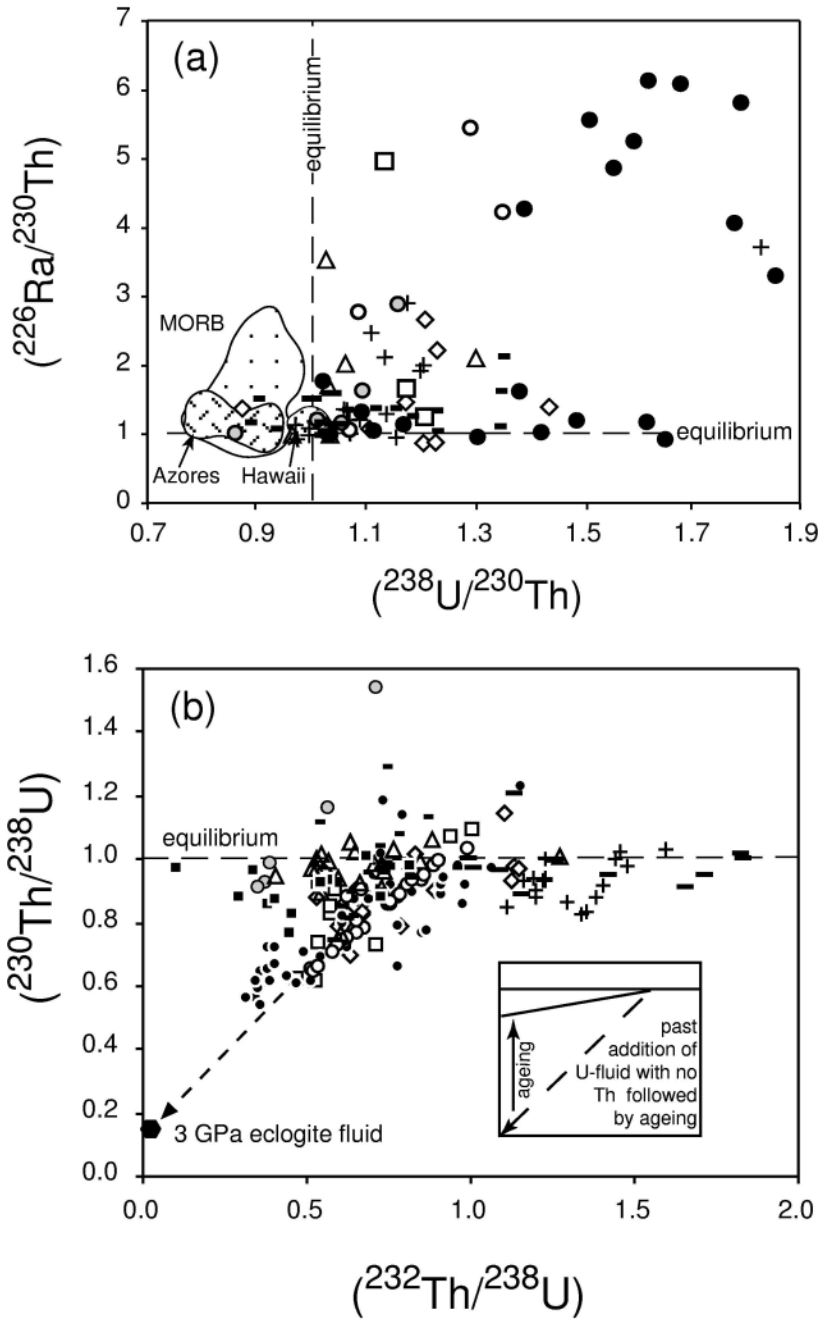

Figure 11. (a) Ra-Th versus U-Th isotopes for arc lavas. (b) ($^{230}Th/^{238}U$) versus ($^{232}Th/^{238}U$) after Bourdon et al. (2003) with composition of 3 GPa eclogite fluid from Table 3 also plotted. Inset shows interpretation for lava arrays not directed towards the fluid (see text for explanation and discussion). Symbols and data sources as in Figure 1.

and Pacific mantle, suggesting that the slope of those arrays does faithfully reflect the time since U addition (see discussion in Turner et al. 1999).

A second possibility is that the inclined U-Th arrays reflect addition of fluids containing some Th (Fig. 8c) and Pa from a source with higher U/Th than the mantle wedge (e.g., Yokoyama et al. 2002). As discussed earlier, U is significantly more fluid-mobile than Pa or Th, but the absolute magnitude remains to be confirmed. Bourdon et al. (2003) used a plot of ($^{231}Pa/^{235}U$) versus Nb/U ratios for the Tonga lavas to show that a

Nb-free fluid (at Nb/U=0) would have a ($^{231}Pa/^{235}U$) ratio of 0.7 if the Pa-U data were to reflect mixing with a fluid containing Pa. This contrasts with our estimate of a ($^{231}Pa/^{235}U$) ratio in the fluid of 0.13 (Table 3) and would require that Pa is almost as mobile as U, which is inconsistent with inferences based on the mobility of Nb (Table 2). Therefore, the high ($^{231}Pa/^{235}U$) intercept is more likely due to time than fluid-mobility of Pa, but the relative roles remain to be determined. Bourdon et al. (2003) also used an analogous plot of ($^{230}Th/^{238}U$) versus ($^{232}Th/^{238}U$) to explore the same relationship for the U-Th isotope system (Fig. 11b). Addition of U only results in mixing lines through the origin which are not observed. The high ($^{230}Th/^{238}U$) intercept must result from either addition of Th as well as U, or in-growth over time subsequent to U addition. The observed trajectories for some arc data can be explained with our estimate of a ($^{230}Th/^{238}U$) ratio in the fluid of 0.14, but others can only be explained if the ($^{230}Th/^{238}U$) ratio of the putative fluid is ~0.5 and thus D_{Th}/D_U is <2 and this seems unlikely on the basis of the experimental data unless there are large fractions of rutile in the subducting plate (Tables 2,3). For other arc data, such as Kamchatka, the discrepancy with experimental data is even larger. Moreover, the largest U-excesses occur above the coldest subducting plates where full transformation to eclogite beneath the arc volcanoes is least likely to have occurred. Therefore, it is highly likely that a reasonable proportion of the ^{230}Th in arc lavas reflects in-growth from excess ^{238}U and, therefore, time.

In conclusion, the inclined U-Pa and U-Th arrays appear to have some time significance because their interpretation as simply the result of recent mixing with a fluid containing Th and Pa as well as U requires fluid partition coefficients for Th and Pa well in excess of those observed experimentally. The corollary is that that there must be a decoupling between Ra-Th and Th-U disequilibria. A further possibility is a combination of the two end-member models discussed above into one in which some Th and Pa addition by fluids is followed by some in-growth due to ageing. In this case (discussed further below) the age inferred from the U-Th and U-Pa arrays is necessarily less straight forward to interpret.

6.5. Two-stage fluid addition

Models in which the fluid does not contain appreciable Th or Pa, require a decoupling between Ra-Th and U-Th-Pa disequilibria in order to reconcile the different implied ages of fluid addition. However, unlike U, ^{226}Ra lost to the mantle wedge during initial dehydration continues to be replenished in the subducting altered oceanic crust by decay from residual ^{230}Th (Fig. 12a) on timescales of 10's kyr until all of the residual ^{230}Th has decayed away (350 kyr after removal of the last U). Thus, if dehydration reactions and fluid addition occur step-wise or as a continuum (Schmidt and Poli 1998), the ^{226}Ra-excesses will largely reflect the last increments of fluid addition whereas U-Th (and U-Pa in the case of Tonga) isotopes reflect the integrated time elapsed since the onset of U addition. As a simple approximation to this, two-stage fluid addition was modeled quantitatively by Turner et al. (2000a) and these results are reproduced in Figure 12b (see Section A2 of the Appendix for details) which shows the evolution of ($^{226}Ra/^{230}Th$) and ($^{238}U/^{230}Th$) over time in the mantle wedge. ^{226}Ra-excesses resulting from the initial fluid addition decay away, but new ^{226}Ra-excesses result from the second fluid addition. If little U remains to be added by the second fluid addition, U/Th isotopes can remain effectively undisturbed by this event and record the integrated time elapsed since the onset of fluid addition. The results of this modeling provided a reasonable approximation of the Tonga-Kermadec ^{238}U-^{230}Th and ^{226}Ra-^{230}Th versus Ba/Th data (see Turner et al. 2000a).

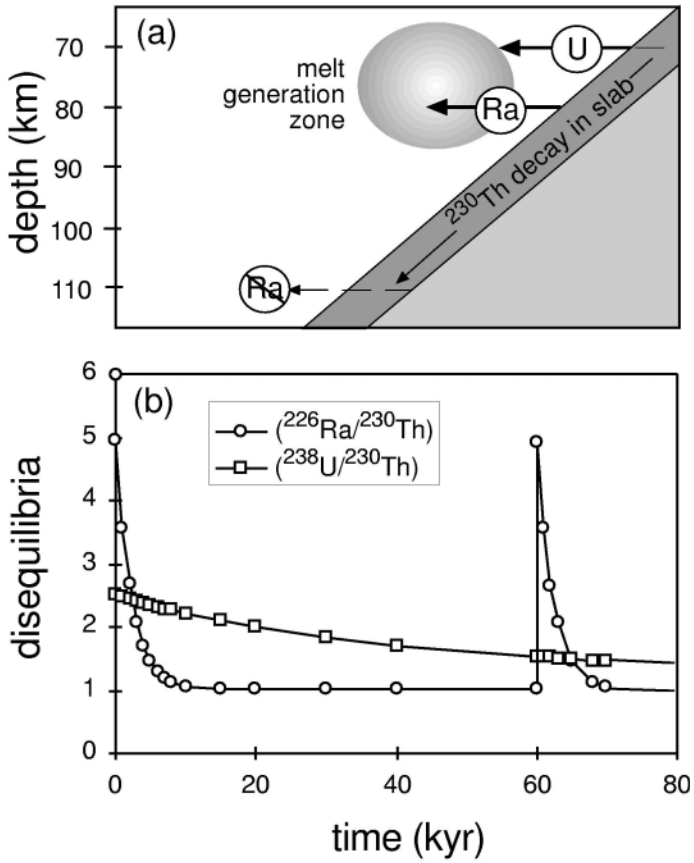

Figure 12. (a) Illustration of the spatial distribution of progressive distillation of fluid mobile elements from the subducting slab. Labeled arrows indicate the locations of U addition, Ra addition, and the point after which no further ^{226}Ra is produced in the plate. (b) Numerical simulation of two-stage fluid addition for the Tonga-Kermadec arc assuming that the degree of previous depletion was 5%(see Section A2 in the Appendix for details). Modified from Turner et al. (2000a).

6.6. Continuous fluid addition

The succession of dehydration reactions in the subducting plate could result in a nearly continuous release of aqueous fluids into the mantle wedge (Schmidt and Poli 1998) and an intuitively more satisfying solution to the two-stage fluid addition approximation, involves continuous fluid addition. This has been modeled by Dosseto et al. (2003) and Yokoyama et al. (2002) and the results of Dosseto et al. (2003) are summarized in Figure 13. In this approach it is assumed that the fluid dehydrates continuously from the slab and simple first-order differential equations are used to describe the evolution of the concentrations of relevant nuclides in both the slab and the mantle wedge. A Rayleigh distillation law is used to describe the dehydration process. Dosseto et al. (2003) have attempted to reproduce data from the most mafic lavas of the Central Kamchatka Depression with this model using published experimental data and also by inverting for mineral/fluid partition coefficients with a Monte-Carlo simulation. Thomas et al. (2002) attempted something similar for data from Nicaragua and Costa Rica. The surprising result is that both groups showed that in all cases the results were unsatisfactory unless significant quantities of Th and Pa are transported in the fluid along with U. However, both efforts sought to explain an atypically large range of high ($^{230}Th/^{232}Th$) ratios and doing the same for Marianas or Tonga may be less difficult. Nevertheless, continuous fluid addition models will certainly require further reassessment before they can be thought to have any general application.

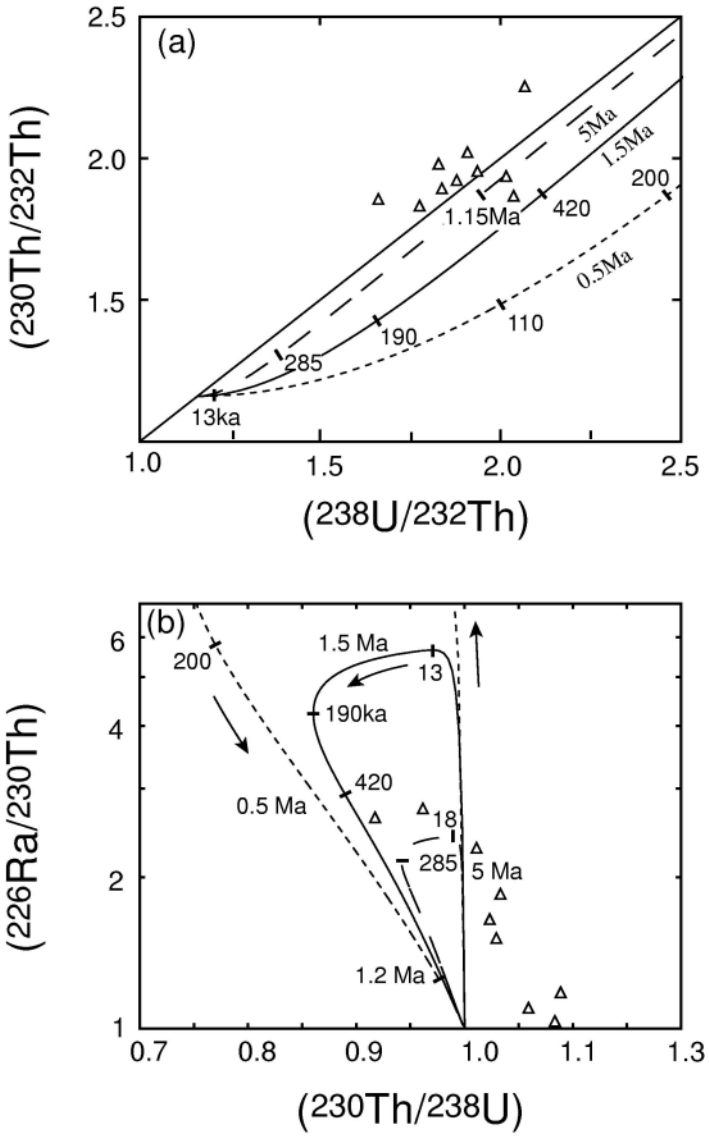

Figure 13. Model curves for continuous fluid addition to a MORB-type mantle source in (a) a ^{230}Th-^{238}U isochron diagram, and (b) a (^{226}Ra/^{230}Th) versus (^{230}Th/^{238}U) diagram. The time constant for dehydration is indicated next to the curve in Ma while the tick marks give the time since the inception of dehydration. These curves are calculated using the model described in Dosseto et al. (2003) where a fuller description is given. In this model, the fluid is released following a Rayleigh distillation process with a time constant τ such that $f = f_{max}(1\text{-}e^{-t/\tau})$ where is the total amount of fluid released (f_{max}= 0.03). The fluid is added to the source continuous and the source then undergoes batch melting with the following partition coefficients D_U = 0.0026, D_{Th} = 0.0014, D_{Pa} = 1.3×10^{-4} and D_{Ra} = 10^{-5}. The slab/fluid partition coefficients used in this calculation were determined by Montecarlo simulation (D_U= 0.16, D_{Th} = 74, D_{Ra}= 0.006) so as to fit the data for the Kamchatka arc shown as solid circles (Dosseto et al. 2003). The partition coefficient for U indicates that uranium would have to be less mobile than suggested by the experimental data in Table 2.

6.7. Mechanisms of fluid addition

One might anticipate that there should be some link between the time scales of fluid addition and some physical parameters of subduction zones (Jarrard 1986). In general such correlations have not yet been found, although there may be a weak positive correlation between the time since the inception of U addition and the rate of subduction (Turner et al. 2000b).

It has been suggested that fluid transfer could occur horizontally across the wedge by a series of hydration-dehydration reactions (Davies and Stevenson 1992). However, horizontal migration across the wedge can only occur at a velocity controlled by the rate and angle of descent of the subducting plate. This predicts fluid transfer time scales >> 350 kyr so that any ^{238}U-excess (let alone ^{226}Ra) originating from the subducting plate would have decayed away (Turner and Hawkesworth 1997; Schmidt and Poli 1998). Unlike the plethora of hydrous phases in the subducting plate, amphibole will be the main hydrous phase in the mantle wedge and the horizontal migration model could be reconciled if both the observed U- and Ra-excesses were generated by a final amphibole dehydration reaction in the wedge prior to melting (Regelous et al. 1997; Sigmarsson et al. 2002). However, whilst wedge amphibole could inherit high Ba/Th from the slab fluid and pass this trait along each time the wedge amphibole breaks down, it is unlikely that any ^{226}Ra-excess would survive. The mineral/fluid partition coefficients for Ba and Th appear to be similar in amphibole (Table 2) and so fluids produced in the presence of residual amphibole would not be predicted to have high Ba/Th yet those lavas with the largest ^{238}U- and ^{226}Ra-excesses also have the highest Ba/Th ratios (Fig. 10). Moreover, it seems more likely that the amphibole would be melt instead of dehydrate at the final stage and, at the degrees of melting inferred for arc front lavas (10-20%), it is likely to be consumed during melting. If amphibole were to be residual during melting, the high amphibole/melt partition coefficient Ba relative to Th (La Tourette et al. 1995) would predict low Ba/Th ratios. Similarly, Bourdon et al. (2003) showed that a single dehydration-reaction could not explain the presence of both ^{231}Pa-excesses and -deficits as observed in the Tonga-Kermadec arc. By implication, the major U/Th and Th/Ra fractionation is inferred to occur during fluid release from the subducting plate where redox conditions are the most strongly oxidizing (Blatter and Carmichael 1998; Parkinson and Arculus 1999). Thus, the combined U-Th-Ra isotope data would seem to require that fluid transfer occurs via a rapid mechanism. Such mechanisms may include hydraulic fracturing (Davies 1999) and experiments by Mysen et al. (1978) have indicated that H_2O will infiltrate lherzolite at 12 mm per hour at 800 ºC and 3.5 GPa. This would allow fluids from the subducting plate to traverse 20 km of mantle wedge to reach the melt generation zone in only 200 years carrying a (^{226}Ra/^{230}Th) signal largely unchanged from that of the fluid which left the subducting plate.

The U-Th time scales imply that fluid addition commences prior to the initiation of partial melting within the mantle wedge which is inferred to be more or less synchronous with ^{226}Ra addition. This is consistent with recent geophysical analysis which suggests that the onset of melting is controlled by an isotherm and thus the thermal structure within the wedge (England 2001). This contrasts with the existing paradigm that an isobaric dehydration reaction in the subducting plate or in the mantle wedge is responsible for the relatively constant depth to Benioff zone (Gill 1981; Tatsumi et al. 1986). Rapid fluid transfer also implies that fluids escape from the slab as a free phase and are not instantaneously locked in a hydrous phase such as serpentinite or Mg-rich chlorite. This may place strong constraints on the thermal structure of the wedge beneath arc volcanoes.

7. PARTIAL MELTING AND MELT ASCENT RATES

The occurrence of relatively anhydrous arc lavas, modeling of trace element behavior, tomographic imaging of the mantle wedge, and correlations between lava major element composition and thickness of the overlying lithosphere have lead several recent studies to argue for a component of decompression melting in the production of arc lavas (Plank and Langmuir 1988; Pearce and Parkinson 1993; Zhao and Hasegawa, 1993;

Sisson and Bronto 1998; Parkinson and Arculus 1999; Hochstaedter et al. 2001). We now investigate the available U-series constraints on partial melting beneath arcs.

7.1. ^{231}Pa- and ^{230}Th-excess evidence for a partial melting signature in the wedge

In MORB and OIB, ^{230}Th- and ^{231}Pa-excesses are interpreted to reflect the effects of dynamic melting or chromatographic melting during which daughter isotope in-growth is facilitated by different residence times of U and Th in the upwelling matrix and melt (see Lundstrom 2003; Bourdon and Sims 2003). Consequently, ^{230}Th-excesses are considered a hallmark of mantle partial melting and although they are uncommon in arc lavas they are not absent (see Fig. 3). Thus, in the arc setting, it is likely that ^{230}Th is controlled by in-growth resulting *both* from U added by the fluid component *and* differences in the residence times of U and Th in the melt zone during partial melting.

It is particularly notable that ^{230}Th-excesses tend to be found in those arc lavas erupted through thicker crust which, combined with the angle of subduction, will control the thickness and thermal structure of the mantle wedge. ^{230}Th-excesses are found behind the fronts of the Marianas (Gill and Williams 1990), New Britain (Gill et al. 1994) and eastern Sunda (Gill and Williams 1990; Hoogewerff et al. 1997; Turner et al. 2003) arcs and in Nicaragua (Reagan et al. 1994), Costa Rica (Reagan and Gill 1989; Clark et al. 1998; Thomas et al. 2002) and Kamchatka (Turner et al. 1998; Dosseto et al. 2003). There is also a progression from ^{238}U-excesses to ^{230}Th-excesses on passing from oceanic to continental basement in both the Kermadec-New Zealand (Turner et al. 1997) and Aleutian-Alaska arcs (George et al. 2003). These observations lend support to models in which the thickness of the overlying lithosphere influences partial melting beneath arc volcanoes either because the melting region in the wedge is upwelling, or because the thickness of the overlying lithosphere controls the thermal structure of the mantle wedge (Plank and Langmuir 1988; Kincaid and Sacks 1997; George et al. 2003).

As discussed above, addition of U by fluids will produce excesses of ^{235}U over ^{231}Pa. Therefore, an extremely important observation, shown on Figure 14, is that the great majority of arc lavas are characterized by the reverse sense of fractionation (Pickett and Murrell 1997; Bourdon et al. 1999; Thomas et al. 2002). Subsequently, Bourdon et al. (1999) showed that only lavas from the Tonga-Kermadec arc preserve both ^{231}Pa excesses and deficits (Fig. 14a). Their interpretation was that, in Tonga, fluid addition resulted in (^{231}Pa/^{235}U) < 1 and this is preserved because partial melting occurred in the absence of significant amounts of residual clinopyroxene (Fig. 14b) which minimized any subsequent fractionation of Pa/U. However, the lavas from Kermadec, like most arc lavas, have (^{231}Pa/^{235}U) ratios > 1, and this appears to provide unequivocal evidence for U/Pa fractionation during the partial melting process (Pickett and Murrell 1997; Bourdon et al. 1999; Thomas et al. 2002). Note that the displacement of the Tonga field relative to that for the Kermadec lavas on Figure 14b argues that the low HFSE concentrations in these lavas reflect prior depletion of the mantle wedge rather than just larger degrees of partial melting.

In summary, an important and exciting recent development in the application of U-series isotopes to arc lavas is the recognition that it is possible to distinguish elemental fractionation due to fluid addition from those due to partial melting, in particular using the ^{235}U-^{231}Pa system. This is a crucial point because the melting signature of arc magmas has been rather elusive in other geochemical tracers.

7.2. Ra evidence for melt ascent rates

Theoretical calculations suggest that the segregation and ascent time scales for basaltic magmas from a partially molten matrix are likely to be short (McKenzie 1985).

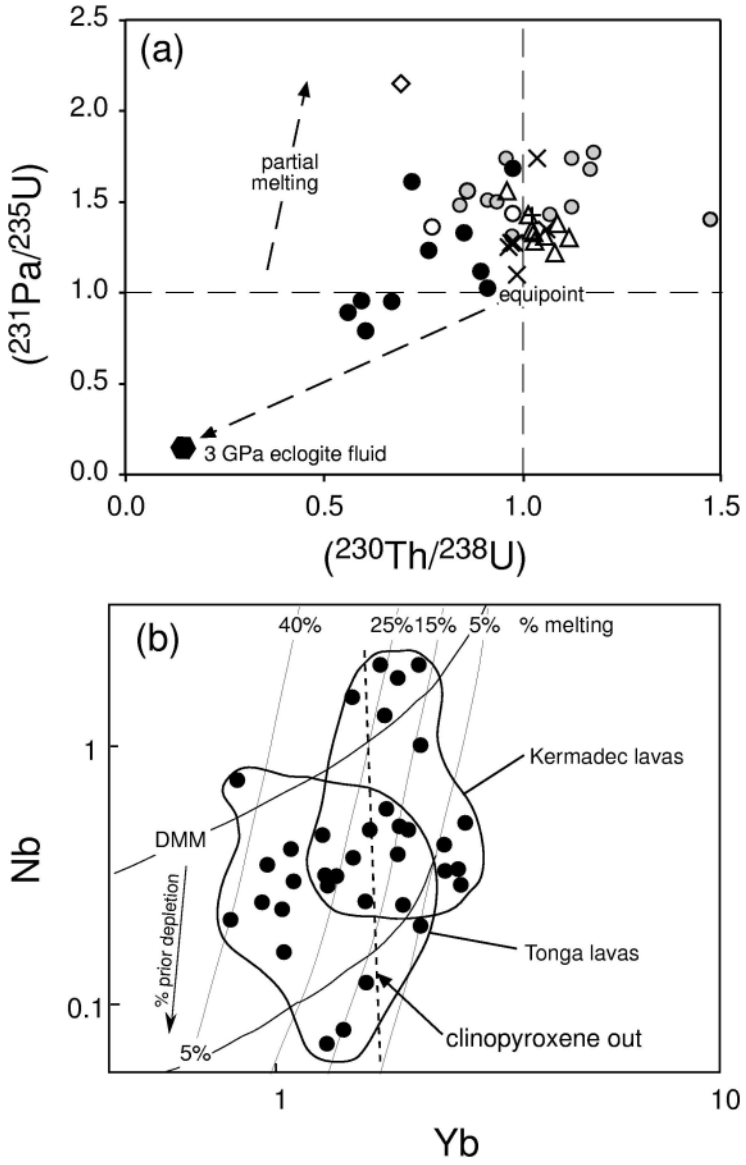

Figure 14. (a) Plot of U-Pa versus U-Th disequilibria for arc lavas. The Tonga samples are those (^{231}Pa/^{235}U) and (^{230}Th/^{238}U) < 1 as expected from U addition by subduction zone fluids. However, all other arc lavas have (^{231}Pa/^{235}U) > 1 suggesting that there was a subsequent increase in (^{231}Pa/^{235}U) due to the partial melting process, schematically illustrated by the dashed arrow, which is inferred to have a much greater effect on (^{231}Pa/^{235}U) ratios than (^{230}Th/^{238}U) ratios. Symbols and data sources as for Figure 1. Additional data for Mexico, Stomboli and the Andes from Pickett and Murrell (1997) are plotted as crosses. (b) Plot of Nb_8 versus Yb_8 (where subscripts refer to compositions regressed to 8% MgO) for Tonga-Kermadec lavas showing that the Tonga lavas are derived from a more depleted source in which clinopyroxene is likely to have been exhausted during partial melting explaining the lack of fractionation of (^{231}Pa/^{235}U) ratios during melting.

One of the seemingly inescapable conclusions from the ^{226}Ra-^{230}Th disequilibrium data, at least for Tonga and the Mariana volcanic fronts, is that significantly less than 8000 years and arguably only a few half lives (ca. 1000-3000 yrs) can have elapsed since the generation of the ^{226}Ra-excesses observed in the arc lavas plotted on Figure 10.

Porous melt flow is likely to be unstable over large distances in the mantle resulting in a transition to channeled magma flow (Aharonov et al. 1995) and this may be swift if melting rates are high and the threshold porosity is quickly exceeded. The arc ^{226}Ra-^{230}Th

disequilibria data seem to indicate that the segregation of the melt from its matrix into channeled ascent does indeed occur on a very rapid time scale. If a single-stage fluid addition model is assumed then the initial ($^{226}Ra/^{230}Th$) predicted in Table 3 is 15 for 3% fluid release (see also Yokoyama et al. 2002). In that case the largest observed ($^{226}Ra/^{230}Th$) ratios in Tonga (~ 6.1, Turner et al. 2000a) could have decayed by ~ 60% or one half life and the calculated ascent rates would be ~ 60 meters per year. However, the two-stage fluid addition model of Turner et al. (2000a) predicts maximum initial ($^{226}Ra/^{230}Th$) ratios of 6-7 and so, if partial melting occurs at 80-100 km depth beneath arc volcanoes, then the required magma ascent rates are arguably of the order of 100's to 1000's meters per year (Turner et al. 2000a, 2001). Either way, these ascent rates rule out models of melt migration in diapirs (Hall and Kincaid 2001) and even the kind of equilibrium porous flow typically invoked in other tectonic environments (cf. Lundstrom 2003; Bourdon and Sims 2003). In principle, ascent rates could be significantly faster (McKenzie 2000) and values of 1.8 km per day were estimated from seismic data in Vanuatu (Blot 1972) and 26 km per day from xenoliths in Mexico (Blatter and Carmichael 1998). As argued by Bourdon et al. (2003), the fast magma ascent rates indicated by Ra-Th disequilibria appear to be independently required in order to preserve slab-derived isotopic signatures of highly compatible elements such as Os (Woodland et al. 2002; Alves et al. 2002) which would otherwise be expected to be lost during equilibration with the wedge peridotite during melt ascent (Hauri 1997).

7.3. Models to reconcile the Pa, Th and Ra data

It is important to note that the ^{226}Ra-^{230}Th disequilibria do not preclude a partial melting origin for the ^{231}Pa-excesses. However, they do require that the residence time of Ra in the melting column was short enough, and thus that the melt velocity was fast enough, to prevent ^{226}Ra from decaying back to values solely attributable to partial melting of the mantle wedge.

7.4. Batch and equilibrium porous flow melting models

A simple batch melting model with instantaneous extraction of the melts predicts that, for degrees of melting greater than 5%, there will be little U-Th-Pa fractionation. Thus, the only models that can produce significant disequilibria involve in-growth during the melting process (see Lundstrom 2003; Bourdon and Sims 2003). Whilst equilibrium porous flow melting models involving chromatographic re-equilibration of the melts on their way to the surface (Spiegelman and Elliott 1993; Bourdon et al. 1999) can produce the observed ^{230}Th- and ^{231}Pa-excesses, they fail to preserve large $^{226}Ra/^{230}Th$ (e.g., Bourdon et al. 2003) as illustrated in Figure 15. Therefore, the most likely models to reconcile the arc Ra and Pa data will involve some variation on the theme of dynamic melting involving protracted melt production but fast melt extraction (McKenzie, 1985; Williams and Gill 1989). In these models slab components reach the surface quickly but the mantle undergoes partial melting over a time interval comparable to the half lives of ^{230}Th and ^{231}Pa. Initial attempts include dynamic melting subsequent to fluid addition (Elliott 2001; Bourdon et al. 2003; George et al. 2003) and fluxed in-growth melting (Thomas et al. 2002; Bourdon et al. 2003) as schematically illustrated on Figure 16.

7.5. Dynamic melting

For a given melting rate, dynamic melting of mantle wedge material bearing a range of ^{238}U-excesses leads to greater in-growth of ^{230}Th in those sources beginning with the largest ^{238}U-excesses. In other words, the more fluid enriched mantle undergoes the greatest ^{230}Th increase during partial melting with the net effect of rotating U-Th arrays anticlockwise (Fig. 17a). Thus, Elliott (2001) simulated the sloped U-Th array from the Marianas by dynamic melting following fluid addition of U. The model does not require,

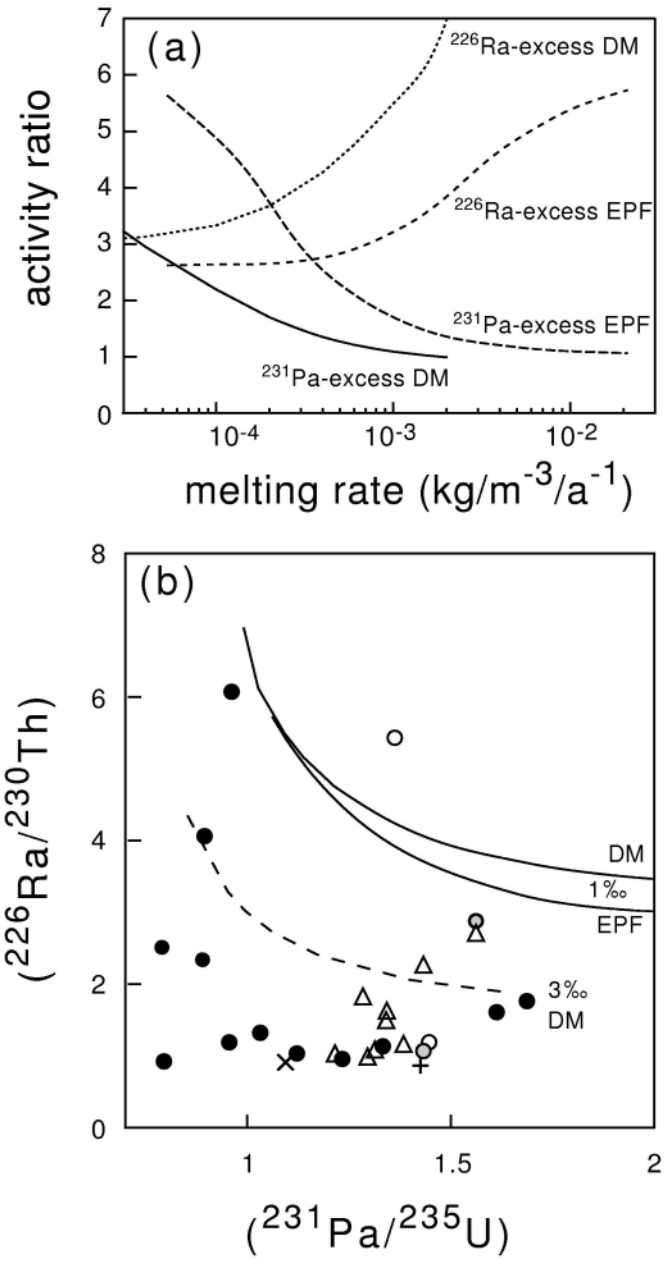

Figure 15. (a) Comparison of equilibrium porous flow (EPF; Spiegelman and Elliott 1993) and dynamic melting (DM; Williams and Gill 1989) models for ^{226}Ra-^{230}Th and ^{231}Pa-^{235}U activity ratios in the melt as a function of melting rate. Both models assume a matrix porosity of 0.001, a total extent of melting of 10% and initial (^{226}Ra/^{230}Th) = 7 and (^{231}Pa/^{235}U) = 0.8. If the melting rate is too large there is not enough time to built in-grow ^{231}Pa, whereas if it is too small, the initial ^{226}Ra-excess in the source decays rapidly and the maximum ^{226}Ra-excess is 3. In the case of the EPF model, the melting rate is scaled to an upwelling velocity assuming 1% melt produced per kbar of decompression. Total degree of melting is 10%. In order to explain the range of (^{231}Pa/^{235}U) and (^{226}Ra/^{230}Th) found in arc lavas, the melting rate needs to be of the order of 10^{-3}-10^{-4} kg.m^{-3}.a^{-1}, assuming dynamic melting and the partition coefficients used here (D_{Pa}= 0.0001, D_U= 0.003 D_{Th}= 0.002 D_{Ra}= 10^{-5}). For equilibrium porous flow to explain the data, the melting rate (and by implication the upwelling velocity) has to be extremely fast (up to 200 cm.a^{-1}) in order to preserve the large (^{226}Ra/^{230}Th) produced at the base of the melting column and the corresponding (^{231}Pa/^{235}U) ratios are low. (b) (^{226}Ra/^{230}Th) versus (^{231}Pa/^{235}U) calculated for various melting models. Melting rates were varied from 0.002-0.003 (DM) and 0.006-0.03 (EPF). The model curves are estimated based on initial (^{226}Ra/^{230}Th) =7 prior to melting. Matrix porosity in per mil is indicated next to the curves. The solid curves assume an initial (^{231}Pa/^{235}U) = 1 in the mantle wedge source whilst the dashed curve is calculated with an initial (^{231}Pa/^{235}U) = 0.8, simulating previous addition of U by fluid to the mantle wedge. The curves are compared with the published data from arcs (symbols and data sources as in Figure 1).

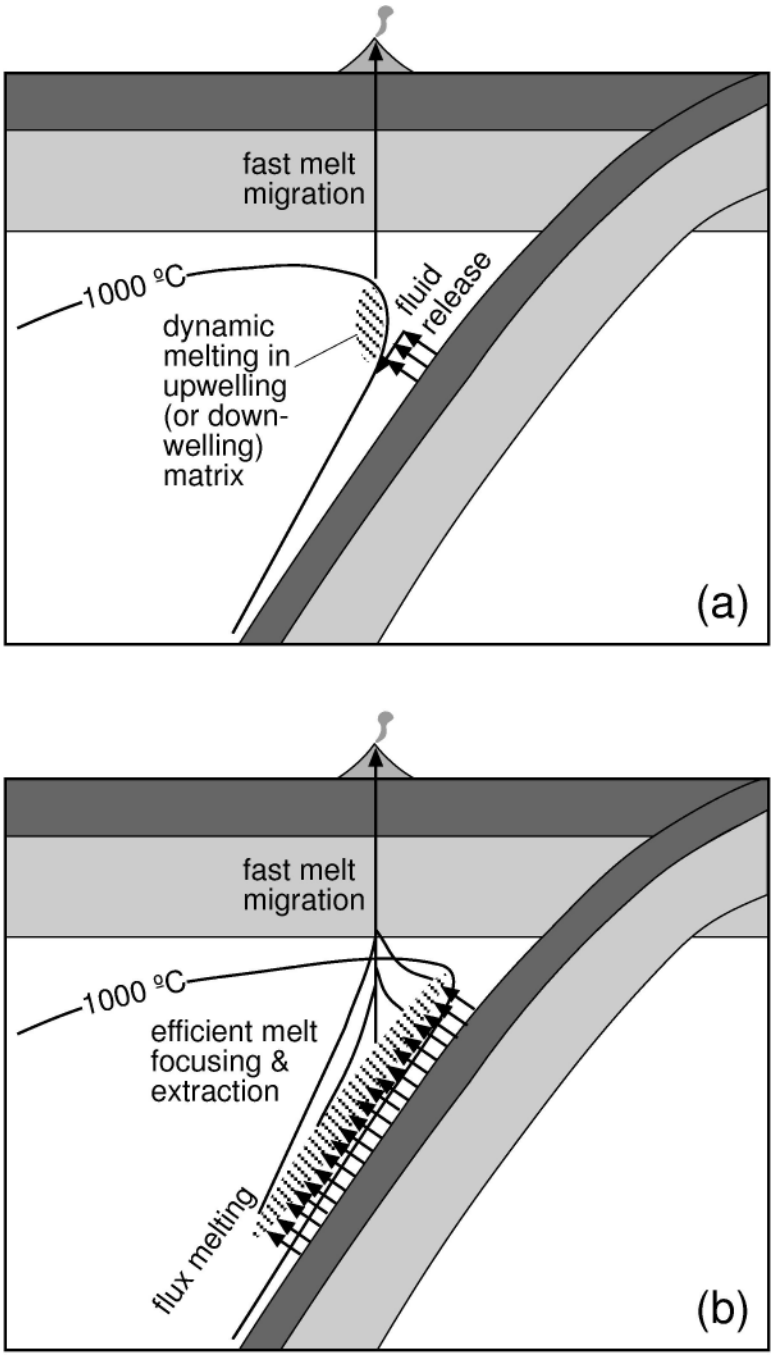

Figure 16. Cartoon cross-sections illustrating two current arc melting models. (a) Fluid release followed by dynamic melting with rapid melt extraction once the hydrated peridotite crosses its solidus. Dynamic melting can occur in either upwelling or downwelling matrix. (b) Flux in-growth melting where each fluid addition promotes a proportional amount of melting of peridotite in which in-growth is occurring in response to the preceding melt extraction increment. All melt fractions are efficiently focused and rapidly extracted.

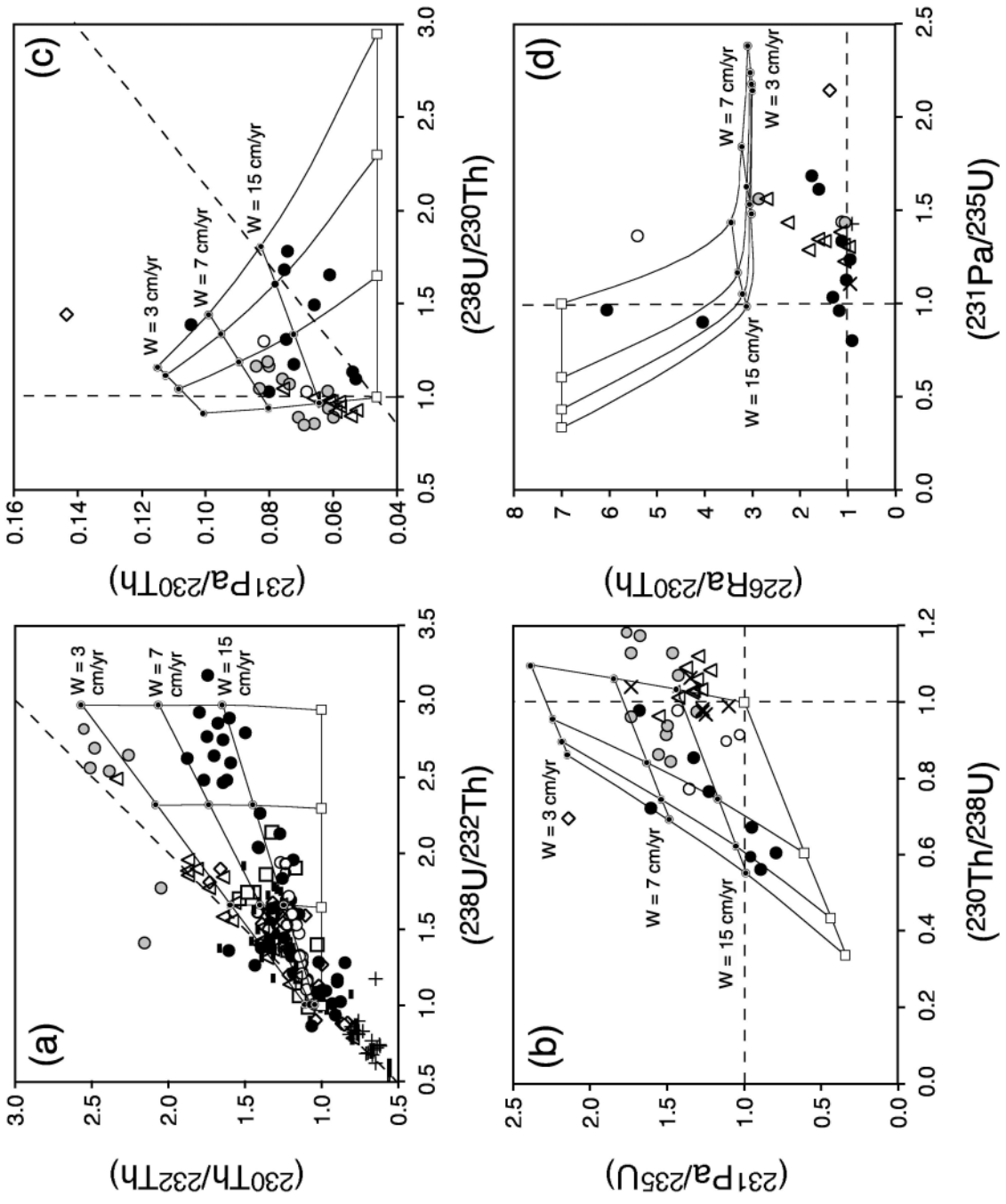

Figure 17. U-series diagrams showing the effects of in-growth produced during dynamic partial melting of an arc source region containing variable ^{238}U-excesses (cf. Figs. 8a, 14a, 15b and 19). Note in (a) that dynamic melting results in inclined arrays that resemble the effects of U addition and ^{230}Th in-growth during ageing or addition of a fluid containing some Th (George et al. 2003). The model assumes a source containing 0.15 ppm U and 0.47 ppm Th, which is initially in secular equilibrium, to which three different amounts of U (0.1, 0.2, 0.3 ppm) have been added. Dynamic melting was calculated following Williams and Gill (1989) assuming a residual porosity of 0.004 and a source mineralogy composed of 56% olivine, 22% clinopyroxene and 22% orthopyroxene. Bulk distribution coefficients for U, Th, Ra and Pa of 0.0081, 0.0066, 1.07×10^{-6} and 1.75×10^{-6}, respectively, were based on Blundy and Wood (2003). The total extent of melting was 15% and the model grid lines are labeled with the rate of matrix flow through the melting region (W) which could reflect upwelling, in a decompression model, or downwelling due to induced convection in the mantle wedge (values encompass the range of observed subduction rates).

nor does it preclude, the presence of Th or Pa in the fluid component. In these models in-growth can occur either because the matrix is mildly upwelling or because its is being progressively dragged downwards through the melting region by induced convection in the mantle wedge. Figure 17 shows that dynamic melting can replicate much of the range of the U-series observations in arc lavas but few well defined trends have been identified from the few data available for Figures 17b-d. The dynamic melting effects are inferred to occur after fluid addition when the hydrated peridotite crosses its solidus (Fig. 16a). Thus, the onset of melting in these models is assumed to be controlled by the position of an isotherm in the wedge as suggested by Tatsumi et al. (1986) and England (2001) and there is no *requirement* for a link between degree of partial melting and amount of fluid addition.

George et al. (2003) proposed model of dynamic melting in an upwelling matrix may be a viable explanation for the range of (^{230}Th/^{232}Th) ratios observed in the Alaska-Aleutian arc where ^{230}Th-excesses dominate in the continental sector of the arc and ^{226}Ra-excesses are sufficiently small to be attributable to the effects of partial melting alone. However, in this arc the horizontal base to the U-Th isotope array requires either that the fluid did not contain Th, or else that it had the same (^{230}Th/^{232}Th) ratio as the subducting sediments (George et al. 2003). In contrast, Bourdon et al. (2003) took the agreement between the U-Th and U-Pa ages in the depleted Tonga arc to indicate that U-Th systematics may be only weakly fractionated during melting beneath arcs. They used this and the pressure dependence of U/Th mineral/melt partitioning (see Blundy and Wood, 2003) to constrain the depth of the melting zone, and then developed a model of dynamic melting with fast melt extraction in a mildly upwelling wedge to reconcile the ^{226}Ra- and ^{231}Pa-excesses found in the Kermadec and other arc lavas (Fig. 15).

At first sight, upwelling may seem to be precluded by the confines of the overriding plate but, as noted earlier, upwelling of the sources of arc magmas has been inferred for a variety of reasons quite independent of the U-series disequilibria requirements (e.g., Plank and Langmuir 1988; Pearce and Parkinson, 1993; Parkinson and Arculus 1999). As noted earlier, the viscosity of the mantle wedge may be significantly lowered by the presence of volatiles (Billen and Gurnis 2001) and numerical models that incorporate a temperature-dependant viscosity also predict a component of upward flow beneath arcs (e.g., Furukawa 1993a,b; Kincaid and Sacks 1997). Small density and viscosity contrasts arising from the addition of volatiles and the presence of partial melt may be sufficient to cause gravitational instabilities leading to localized, upwelling that controls the surficial distribution and life-span of arc volcanoes (Brémond d'Ars et al. 1995). Such models might predict a positive correlation between crustal thickness and extent of melting induced disequilibria (e.g., ^{231}Pa-excess) if crustal thickness in some way relates to the overall wedge thickness (e.g., Plank and Langmuir 1988). Figure 18 shows that such a correlation may exist within the available data for oceanic arcs but that the behavior of continental arcs is more complex. Alternatively, those arcs with thicker crust may have a hotter wedge (Kincaid and Sacks 1997) and thus be characterized by larger melting rates (Bourdon et al. 2003).

7.6. Flux melting

Initial attempts at flux melting models have been made by Thomas et al. (2002) and Bourdon et al. (2003). Both assess variations on the theme of flux melting in which slab-derived fluids bearing various (including zero) amounts of U, Th, and Pa cause melting of mantle sources that have just been depleted by melt extraction in the previous melting increment. The recent depletion results in preferential in-growth of ^{231}Pa ± ^{230}Th in the matrix which is transferred to subsequent melts. In this type of model melting occurs along a lengthy zone of the wedge parallel to the subducting plate and all the melt

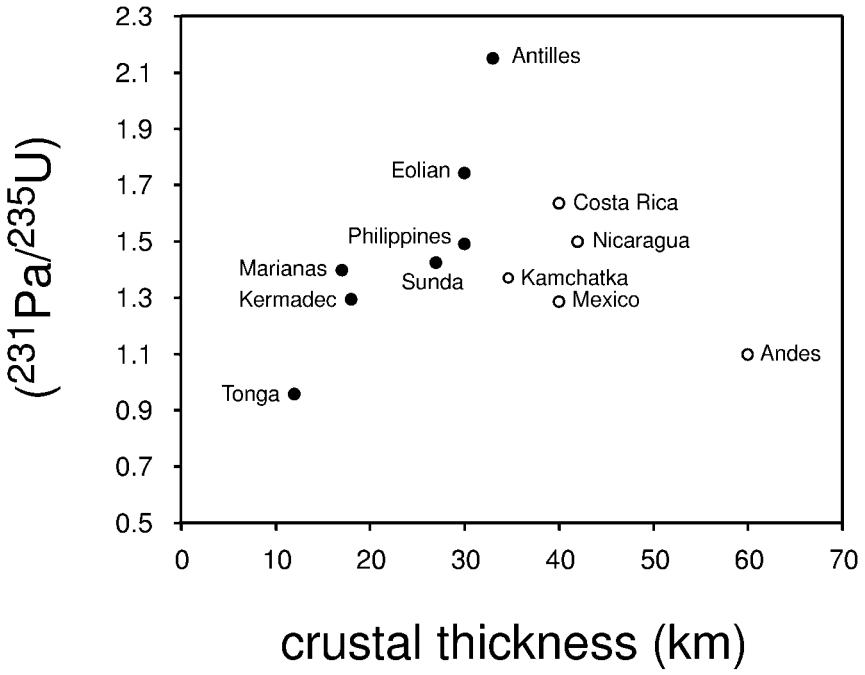

Figure 18. Plot of (^{231}Pa/^{235}U) versus crustal thickness (from Gill 1981) for each arc studied (averages are plotted where more than one analysis was available—data sources in Table 1) showing that there is a reasonable positive correlation within the oceanic arcs (filled circles).

fractions need to be efficiently extracted and focused into a zone beneath the arc front volcanoes (Fig. 16b). A link between amount of fluid addition and the degree of melting is an intrinsic and testable aspect of this type of model (e.g., Davies and Bickle 1991; Stolper and Newman 1994; Hirschmann et al. 1999; Eiler et al. 2000; Thomas et al. 2002). The chief variables (besides mantle/melt partition coefficients, porosity and permeability, total degree of melting, melting rate, and duration of chemical equilibrium that are common to all U-series melting models) are the relationship between the amount and rate of fluid addition and the degree of mantle melting and the relative solubilities of U, Th, and Pa in the fluid (see Section A3 of the Appendix for details).

Thomas et al. (2002) evaluated ^{231}Pa in-growth in downwelling mantle accompanied by continuous flux melting and instantaneous melt extraction. They note that the widespread positive correlation between ^{238}U-excess and (^{231}Pa/^{230}Th) is inconsistent with simple radioactive decay alone (Fig. 19), and implies a link between recent addition of U (via fluid) and recent in-growth of ^{231}Pa (via melting). They attribute the linkage to flux melting but Figure 17c shows that similar relationships can result from dynamic melting. The flux melting model developed is able to explain many differences between ^{230}Th-enriched lavas from Costa Rica and ^{238}U-enriched lavas from Nicaragua by greater flux melting in Nicaragua, but only when fluid addition is continuous, Th and Pa are somewhat fluid-mobile, and melt ascent is too fast to sustain chemical equilibrium. Their model also requires that (a) melts are continuously produced during continuing fluid release from the subducting plate and (b) that those fluids are derived from carbonate-rich sediments with high (^{230}Th/^{232}Th).

One aspect of the flux melting models which led Bourdon et al. (2003) to prefer a dynamic melting model is that the time scale required to in-grow ^{231}Pa (assuming that Pa is relatively fluid immobile) requires the down-dip length of the melting region to be on the order of 100 km. This is similar to the depth range over which fluid is released from

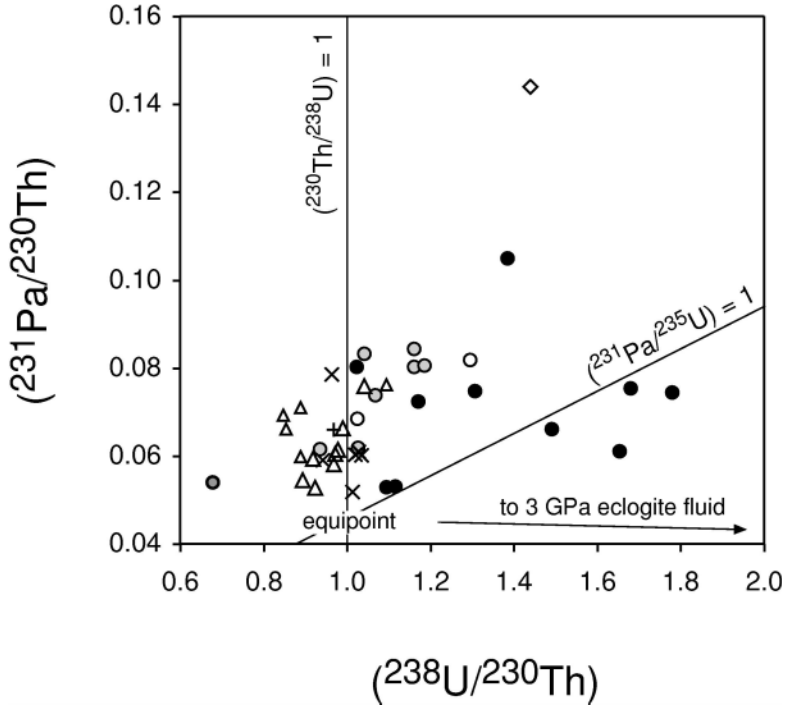

Figure 19. (^{231}Pa/^{230}Th) versus (^{238}U/^{230}Th) diagram after Thomas et al. (2002). Symbols and data sources as in Figure 1 excepting Costa Rica samples which are plotted here as open triangles so as to distinguish them from lavas from Nicaragua and samples from Mexico, Stromboli and the Andes (Pickett and Murrell 1997) which are plotted as crosses. As noted by Thomas et al. (2002) several of the arcs form trends in which (^{231}Pa/^{230}Th) increases with increasing (^{238}U/^{230}Th). Addition of the 3 GPa fluid from Table 3 forms a shallow negative trend from the equipoint. The arc lavas which form trends steeper than and lie above the (^{231}Pa/^{235}U) = 1 line arguably require a combination of fluid addition, ageing and ^{231}Pa in-growth due to partial melting in proportion to the amount of fluid added (Thomas et al. 2002).

the downgoing plate (Schmidt and Poli 1998; Thomas et al. 2002). However, assuming that wedge temperatures near the surface of the subducting plate are unlikely to be sufficient for partial melting much shallower than 80 km in any thermal model (Davies and Stevenson, 1992; Furukawa 1993a,b; Peacock, 1996), this requires that the melting zone extends up to 200 km behind the arc front and that the melts are very efficiently focused back to a predominant region beneath the arc front (e.g., Davies and Stevenson, 1992; Spiegelman and McKenzie 1987). However, this appears to significantly exceed the distance inferred from seismic data (Wyss et al. 2001).

The important conclusion from these studies is that ^{226}Ra and ^{231}Pa data add apparently robust and important, but different, insights into arc magma genesis which are less ambiguous than the ^{230}Th-^{238}U results alone. The ^{226}Ra-^{230}Th results require that melting and melt ascent are faster in subduction zones (at least for the volcanic front of some oceanic arcs) than usually inferred for mid-ocean ridges, and that at least the final fluid addition is effectively coincident with melting and rapid ascent. The entire process of slab dehydration, melt ascent, and differentiation can take less than a few thousand years. This indicates a whole new class of melt ascent mechanisms, probably made possible by the depleted nature of the mantle, the deformation style and thermal structure in the wedge corner, and the presence of water, but possibly also applicable to MORB and OIB (Turner et al. 2001). In contrast, the ^{231}Pa-^{235}U results require that melts are derived from a mantle with a recent melting history, either during upwelling or downwelling lasting scores to hundreds of thousands of years. The challenge is to

reconcile these U-series time frames with one another and to other observations. For example, some arc magmas have major element compositions that imply continual re-equilibration to shallow depths (e.g., Grove et al. 2002) whereas the Ra-Th systematics seem to preclude that.

It is also important to note that none of these models are yet without their difficulties. For example, in any model it is difficult to explain the very large range in (^{230}Th/^{232}Th) found in the Kamchatka arc (Turner et al. 1998). If the flux melting models are adopted then, whilst the linear arrays on U-Th isotope diagrams may broadly reflect the duration of fluid fluxing, they may not provide a direct indication of the time since U addition (see further discussion in Section 8). Tonga may be an exception: if the fluid contains Th and Pa then none of the models predict the deficits of ^{231}Pa relative to ^{235}U in the Tonga arc or the similarity between the time scales derived from U-Th and U-Pa systematics in that arc. Fully reconciling the constraints from the Ra-Th and Pa-U data remains an important challenge to be further addressed by future arc studies and clearly holds great promise for unraveling further the physics of the partial melting process in this tectonic environment.

7.7. Partial melting of the subducting oceanic crust

The subducting basaltic oceanic crust is generally thought not hot enough to undergo partial melting except when the plate is very young (Peacock et al. 1994). Under atypical circumstances, however, it may be hot enough for the subducting basaltic crust to melt sufficiently that the resulting melts can reach the surface with some of the elemental and isotopic features of their MORB source intact. Partial melting versus dehydration of subducted basaltic crust produces distinctive, adakitic lavas due to the already fractionated nature of the protolith and the presence of significant amounts of residual garnet (Defant and Drummond 1990). In the Austral Andean zone of southern Chile, south of the point of subduction of the Chili ridge, very young (< 20 Ma) oceanic crust is presently being subducted. Lavas erupted above this zone were analyzed by Sigmarsson et al. (1998) who showed that they are characterized by ^{230}Th-excesses and high La/Yb and Sr/Y ratios which they ascribed to melting in the presence of residual garnet. A slab-melt signature has also been recognized in the Central Kamchatka Depression located above a zone of plate-tearing. Here Dosseto et al. (2003) have shown that the lavas with higher La/Yb and ^{230}Th-excesses (inferred to have a slab melt component) also have lower (^{226}Ra/^{230}Th) and (^{231}Pa/^{235}U) which they ascribed to residual phengite and rutile which should retain Ra and Pa respectively. However, it would be erroneous to make the assumption that all arc lavas that have ^{230}Th-excesses were formed in this way (Bourdon et al. 2000a; George et al. 2003). Even other "adakitic" arc lavas with ^{230}Th- and ^{226}Ra-excesses (e.g., Shasta in the Cascades: Volpe 1992) can be interpreted as mostly mantle-derived melts through processes similar to those described in the section above (Grove et al. 2002).

8. DISCUSSION OF U-SERIES TIME SCALE IMPLICATIONS FOR ARC LAVAS

The preceding sections have established that the U-series information from arc lavas is a complex end-product of several different processes and this is especially true for U-Th isotopes. The two observations that seem to be most robust are (1) the need to transfer the ^{226}Ra-excess signal from the subducting plate into the melting zone and to the surface in less than a few 1000 years, and (2) the need for a partial melting process which allows for ^{231}Pa in-growth. There are a number of different models which can take account of these two requirements but which have different implications for the U-Th isotope arrays.

In an extreme end-member case where both Th and Pa are considered very mobile, the U-Th arrays (and U-Pa in the case of Tonga) would simply point to the U-Th-Pa composition of the fluid (e.g., Chabaux et al. 1999; Sigmarsson et al. 2002; Yokoyama et al. 2002). However, our calculations of likely fluid compositions (Table 3) make this seem unlikely (note the position of the calculated fluid on Figs. 8, 9, 11, 14, 19). Note that such models also generally *require* that the fluid is derived from the altered oceanic crust. If the fluid was derived from pelagic sediment it would have a much lower ($^{230}Th/^{232}Th$) ratio (~ 0.5 in the case of Tonga) such that fluid addition would result in a negative array on the U-Th equiline diagram and the U-Th array would underestimate the integrated time of U addition (see Fig. 9). This is not true for those margins where the subducting sediment is rich in hemi-pelagic components characterized by high U/Th (and therefore high ($^{230}Th/^{232}Th$) ratios), such as central America (Herrstrom et al. 1995; Thomas et al. 2002) but they are exceptional. Conversely, this model would fail to explain the high ($^{230}Th/^{232}Th$) ratios of the Kamchatka lavas (Turner et al. 1998; Dosseto et al. 2003) since there is no carbonate sediment input beneath this arc.

Perhaps the simplest model, most applicable to Tonga-Kermadec, involves a two-stage addition of a fluid containing no Th or Pa followed by dynamic melting in an upwelling matrix (e.g., Bourdon et al. 2003). In this model, the slope of the U-Th arrays reflects the integrated time of U addition and, in Tonga, the absence of significant residual clinopyroxene during partial melting leads to minimal ^{235}U-^{231}Pa fractionation (thus U-Pa isotopes record a similar U addition time scale). In Kermadec, partial melting results in ^{231}Pa-excesses which can be used to constrain the rate of matrix flow through the melting region. In this case it is assumed that the U-Th systematics are not affected by partial melting due to the similarity of the U and Th mineral/melt partition coefficients at the pressure of the melt generation zone (Bourdon et al. 2003).

An important question in this model is to what extent are the derived time scales compromised if there is a small amount of Th and Pa in the fluid as predicted by the data in Table 2. In Table 3 we calculate the apparent U-Th and Nb-normalized U-Pa ages of the fluid composition derived earlier. The U-Th apparent age is 14-16 kyr, so that the 50-60 kyr time scale inferred in Tonga would overestimate the true integrated U addition time scale by 14-16 kyr (Fig. 9a). However, the U-Pa apparent age is only 40-45 years due to the minimal mobilization of Pa in the fluid. This implies that the U-Pa age is the more robust estimate (Fig. 9b). These results contrast with those of Yokoyama et al. (2002) who suggested that subduction fluids could have a very large effect on the U-Th equiline diagram. Firstly, their results were based on calculations using a high eclogite/fluid partition coefficient for U largely because they did not take into account the effects of fO_2 on U partitioning into garnet. Secondly, they allowed ^{230}Th to in-grow in the accumulating fluid in the subducting plate prior to its release and during it's transport through the wedge to the melting zone. However, all ^{226}Ra-excess would have decayed in such fluids. In reality, this model is effectively indistinguishable from the Tonga-Kermadec two-stage fluid addition interpretation; in both cases, it is the time elapsed since U-Th fractionation that is constrained. The relative amounts of time spent during fluid accumulation, passage through the wedge or in the melting zone remain unknown. In this respect it is interesting that Bourdon et al. (2003) speculated that the time required for fluid build-up prior to hydrofracturing may be on the order of 10's kyr.

In the model advocated by Elliott et al. (2001) and George et al. (2003) the U-Th systematics *are* affected by partial melting leading to increases in ($^{230}Th/^{232}Th$). If the fluid does not contain appreciable Th (or Pa), then the slope of the U-Th array is simply a function of the matrix flow rate through the melting zone (Fig. 17a), rather than the time since U addition, and this bears similarities with the approach used to derive upwelling

(and melting) rates in MORB and OIB (see Lundstrom 2003; Bourdon and Sims 2003). In principle the U-Th arrays in this model could be produced by ^{230}Th in-growth in a downwelling matrix and the rate of matrix flow controls the extent of in-growth rather than any link to the amount of fluid addition and extent of melting (i.e., the amount of in-growth should be constant for a given subduction rate).

Thomas et al. (2002) have explored the flux melting models both with and without the presence of significant Th and Pa in the fluid. If the fluid contains only U, then the slopes of the U-Th and U-Pa arrays reflect the composite effects of ageing since U addition and ^{230}Th and ^{231}Pa in-growth during the partial melting process. Since the mineral/melt distribution coefficients are very similar for U and Th but very different for Pa (Blundy and Wood 2003), U-Th and U-Pa isotopes will contain information about the melting rate (which is a function of the amount of fluid addition in these models) whereas U-Pa isotopes will be more sensitive to the residual porosity in the melt region due to the very small partition coefficients for Pa. If the fluid also contains appreciable Th and Pa, then extracting information on a specific process (composition of the fluid, time since U addition, rate of melting) will necessarily be more difficult. However, there is no reason this should be impossible, especially if our knowledge of mineral-fluid partition coefficients and melting processes can be improved.

In conclusion, the significance and interpretation of the information derived from U-series isotopes in arc lavas is critically dependant on the fluid addition and melting model assumed. However, we stress that useful information is always contained in the U-series isotopes which ever model is ultimately adopted. It is incorrect (and misleading) to say, for instance, that the slopes of U-Th arrays have no time significance if there is Th in the fluid or if ^{230}Th in-growth occurs during the melting process. Rather, they contain important, albeit integrated, information about the composition of the fluid, the timing of its addition and the nature of the melting process which careful modeling should allow us to de-convolve.

9. REAR ARC LAVAS

Rear lavas provide a unique opportunity to investigate models for the progressive distillation of elements from the subducting plate and changes in magma composition in response to changes in melt fraction and residual mineralogy with increasing depth. Ryan et al. (1995), Woodhead et al. (1998), Hochsteadter et al. (2001) and others have documented that fluid-sensitive indexes like U/Th, Ba/La and Sr/Nd often decrease behind the volcanic front of most arcs suggesting a decrease in the relative fluid contribution and/or progressive depletion of these elements in the subducting plate which results in changes in the composition of the fluids released. Stolper and Newman (1994) showed that H_2O played an important role in the genesis of the Marianas back arc lavas but also suggested that the aqueous fluids became progressively stripped of all but the most fluid mobile elements with increasing passage through the mantle.

U-series data from across arc traverses are available from the New Britain (Gill et al. 1993), Kamchatka (Turner et al. 1998) and eastern Sunda (Hoogewerff et al. 1997; Turner and Foden 2001) arcs as well as from individual rear-arc volcanoes such as Bogoslof in the Aleutians (Newman et al. 1984; Turner et al. 1998; George et al. 2003) and Merelava in Vanuatu (Turner et al. 1999). Additionally, lavas from back arc spreading centres in the Lau Basin behind the Tonga arc have been analyzed by Gill and Williams (1990) and Peate et al. (2001). These data are plotted on diagrams of (^{230}Th/^{238}U) and (^{226}Ra/^{230}Th) against depth to Benioff zone in Figure 20. Although there is much scatter, Figure 20a shows that whilst in general arc front lavas are characterized

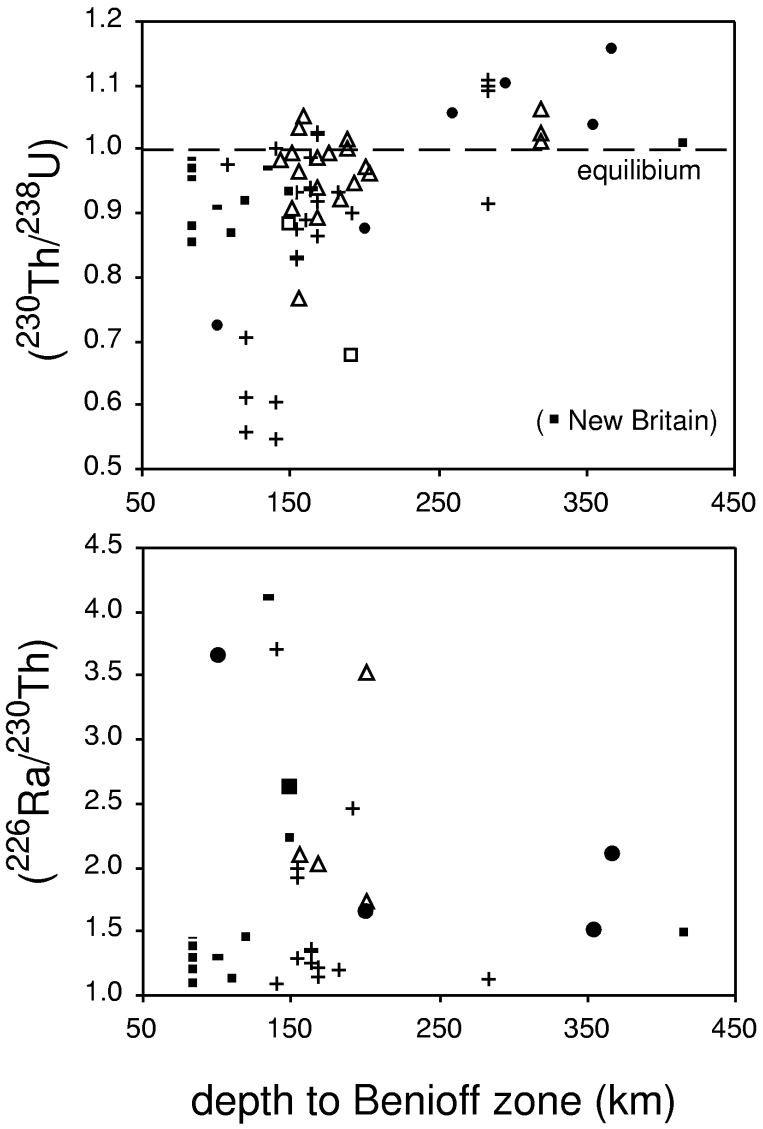

Figure 20. (a) (^{230}Th/^{238}U) and (b) (^{226}Ra/^{230}Th) versus depth to Benioff zone. Note that the age of the Lau Basin glasses (plotted as filled circles) is unknown and so the (^{226}Ra/^{230}Th) ratios should be treated as minimum values. Data are from New Britain (Gill et al. 1993), Kamchatka (Turner et al. 1998) and Sunda (Hoogewerff et al. 1997; Turner et al. 2001) arcs. Also plotted are average values for the volcanic front and several rear-arc volcanoes from the following arcs: Bogoslof - Aleutians (Turner et al. 1998, 2001; George et al. 2003), Lau Basin and Niuafo'ou - Tonga (Regelous et al. 1997; Turner et al. 1997, 2000a; Peate et al. 2001), Merelava in Vanuatu (Turner et al. 1999). Symbols and data sources as in Figure 1 unless specified differently.

by ^{238}U-excesses, these tend to decrease with increasing distance behind the arc. In principle, this could be consistent with decreasing U in the fluids, decreasing amount of fluid added to the wedge behind the volcanic front, increasing depth of melting, or any combination thereof. In contrast, there is some evidence that ^{226}Ra-excesses reach a maximum slightly behind the arc front (Fig. 20b, Gill et al. 1993; George et al. 2003) which may lend support to the model in which ^{226}Ra continues to in-grow in the subducted plate and be released beyond the point of maximum U flux. ^{226}Ra-excesses are also found far beyond the arc but these are associated with ^{230}Th-excesses suggesting that both disequilibria reflect partial melting effects more than fluid flux (Regelous et al. 1997; Turner et al. 1997, 1998, 2000a; Peate et al. 2001).

In detail, some of the trends within individual across-arc traverses are complicated. For example, within Kamchatka U/Th ratio increases with depth to the Benioff zone (Turner et al. 1998), although there is no simple correlation with (^{230}Th/^{238}U) (Fig. 20a). In Tonga, there is a relatively abrupt switch from ^{238}U-excesses to ^{230}Th-excesses some 250 km behind the arc front (Peate et al. 2001). H_2O/Ce ratios are still higher than MORB in the central and eastern Lau Basin and degree of melting is correlated with H_2O content, so H_2O demonstrably still plays an important role in back arc magma genesis (Stolper and Newman 1994; Peate et al. 2001). However, there is evidence that the composition of the fluids changes with distance from the arc in Tonga (Pearce et al. 1995; Peate et al. 2001) and, amongst the eastern Lau Basin lavas, the more H_2O-rich lavas have the larger ^{230}Th-excesses rather than ^{238}U-excesses (Peate et al. 2001). Finally, neither the dynamic or flux melting models readily explain rear-arc volcanism.

10. MODIFYING PROCESSES

This chapter is primarily concerned with the interpretation of U-series isotope disequilibria originating from arc lava sources and those created during partial melting. However, it is important to summarize the types of processes that could modify this signal and therefore potentially lead to erroneous interpretations.

10.1. Time since eruption

Sample age is clearly important, especially for ^{226}Ra-^{230}Th disequilibria. Ideally, only samples of known age should be analyzed or else U-series investigations should be combined with a geochronological study. Unfortunately, this is not always possible and samples ages have often only been estimated to be "< 10 ka," so as to imply that an age correction is unnecessary for Th isotopes, or as "this century" or, worst of all, "historic" for the purposes of ^{226}Ra. The appropriate decay equations can be used to investigate the magnitude of error introduced by a given age uncertainty. This issue is particularly important for the interpretation of ^{226}Ra-^{230}Th disequilibria in pre-historical samples. Note that the Ra data in Figures 10, 11a and 21 have been corrected to the date of eruption. In some cases, especially for Tonga, this involves assuming that the uppermost unvegetated lavas are from one of the most recent magmatic eruptions of the volcano, and correcting to the mean age of possible eruption ages. Assuming too old an eruption age increases apparent (^{226}Ra/^{230}Th) at the time of eruption. However, most samples in those figures are from eruptions this century with no major ambiguity about sample age.

10.2. Alteration and seawater interaction

Alteration is always a cause for concern in geochemical investigations and the best approach will always be to avoid samples with visual or chemical evidence for alteration. The differential fluid mobility of U, Th, Pa and Ra undoubtedly provides the potential for weathering or hydrothermal circulation to disturb the U-series signatures of arc lavas. In a study of lavas from Mt. Pelée on Martinique, Villemant et al. (1996) found that dome-forming lavas were in U-Th equilibrium whereas plinian deposits from the same eruptions had small ^{238}U-excesses which they interpreted to reflect hydrothermal alteration. However, whilst the addition of U could be due to hydrothermal alteration, the plinian deposits were also displaced to lower ^{230}Th/^{232}Th ratios which cannot. Instead, the two rock types may just be from separate magma batches.

Seawater interaction is a potential source of several U-series nuclides, and is strongly enriched in B, Cl and Sr. Thus, abundances of these elements and/or their isotopes can often be used to test for seawater contamination (e.g., Turner et al. 2000a). Because ^{234}U will be located in mineral sites that have been damaged by recoil effects, ^{234}U is likely to

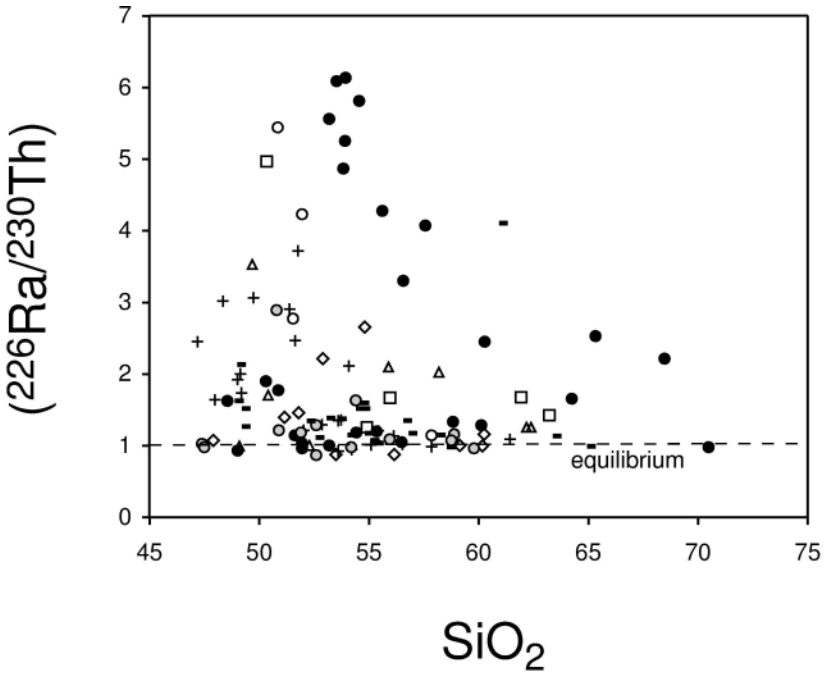

Figure 21. ($^{226}Ra/^{230}Th$) disequilibria versus SiO_2 as an index of differentiation (on this diagram lavas with SiO_2 > 60% been plotted). The general decrease in ($^{226}Ra/^{230}Th$) with increasing SiO_2 within most individual arc datasets suggests that basalts evolve to andesites and dacites within millennia.

be preferentially mobilized relative to ^{238}U (Chabaux et al. 2003). Seawater is enriched in ^{234}U and so ^{234}U-excesses may indicate recent seawater interaction in arc lavas. As shown by Yokoyama et al. (2002), seawater contamination can have a dramatic effect: a ($^{234}U/^{238}U$) only 3% higher than equilibrium (1.03) equates to 20% seawater contamination, which will shift ($^{232}Th/^{238}U$) from 0.6 to 0.45! Note that the revised decay constant for ^{234}U (Cheng et al. 2000) results in some published data giving equilibrium ($^{234}U/^{238}U$) more faithfully. Similarly, Bourdon et al. (2000b) showed that a ($^{234}U/^{238}U$) ratio only 1.5% higher than equilibrium can shift ($^{231}Pa/^{235}U$) from 2.5 to 3.4. Careful selection and leaching of submarine samples eliminates contamination by Mn-oxides which are enriched in ^{231}Pa and ^{230}Th (Bourdon et al. 2000b).

10.3. Magma chambers processes

Plutons provide undeniable evidence that rising magmas can stall in magma chambers and many magmatic processes can fractionate U-series nuclides and also potentially last for times long relative to their half-lives allowing for nuclide in-growth or decay. The encouraging thing is that the correlations described above are as good as they are because it means that such modification has been minor. Nonetheless, we now review several processes that seem to have demonstrable effects.

10.4. Radioactive decay

Radioactive decay during residence in magma chambers is critical for interpretation of the shorter lived isotopes such as ^{226}Ra. Several studies have shown negative correlations between ($^{226}Ra/^{230}Th$) and indices of fractionation (e.g., Gill and Williams 1990; Vigier et al. 2000; Turner et al. 2000a, 2001). In oceanic arcs, there is a fairly reproducible negative correlation between ($^{226}Ra/^{230}Th$) and SiO_2 (Fig. 21) suggesting that andesites and dacites may take a few millennia to evolve from basaltic parental magmas. Less commonly, some studies have suggested that magma residence times in

oceanic arcs can be significant even relative to the half-life of ^{230}Th (Heath et al. 1998; Hawkesworth et al. 2000). In continental arcs, residence times also appear to be longer and fractionation combined with assimilation of pre-existing crystal mushes has been argued to produce rhyolites on time scales of 10^4-10^5 years (Reagan et al. 2003). However, since the subsurface residence times of magmas is specifically addressed elsewhere by Condomines et al. (2003), here we will restrict ourselves to briefly considering some of the processes which could occur during this residence to modify the deep level U-series isotope signals.

10.5. Crystal fractionation or accumulation

Crystal fractionation is the most obvious but since U, Th, Pa and Ra are all highly incompatible elements in gabbroic phases (Blundy and Wood 2003), U-series nuclides in arc basalts and andesites will be remarkably robust to the effects of crystal fractionation until the saturation of K-feldspar or accessory phases is attained. The same does not hold for evolved dacites and rhyolites because zircon, apatite and sphene all have the ability to strongly fractionate U-Th-Pa-Ra (Blundy and Wood 2003). Conversely, the bulk entrainment of gabbroic phases is also likely to have minimal effect upon U-series isotopes because of the orders of magnitude higher concentrations in the magma. As noted in Section 6.2, the very low D_{Plag} for Ra (Bundy and Wood 2003), means that Ra concentrations in plagioclase are 10's fg/g compared with 100's fg/g in the groundmass and so ^{226}Ra-excesses cannot reflect plagioclase accumulation. An exception is the behavior of the short-lived nuclide ^{222}Rn which is efficiently extracted by degassing in shallow-level magma chambers. Its longer lived daughter product ^{210}Pb may also be sensitive to extraction in a volatile phase (Condomines et al. 2003). Moreover, Pb can be moderately compatible in plagioclase (Blundy and Wood 2003). However, these properties have the exciting potential to be exploited to investigate the time scales of magma degassing (Gauthier and Condomines 1999).

10.6. Magma recharge

Recharge of a magma chamber with fresh inputs may trigger eruption (Sparks et al. 1977) and can significantly alter the U-series disequilibria of the resident magma either because the new input has not undergone decay or because the new input has a different source signal to the resident magma. The former case has been investigated numerically for a fixed volume system by Hughes and Hawkesworth (1999) who showed that magmas can be maintained out of secular equilibrium over residence times that are significant relative to the half-lives of ^{226}Ra and ^{230}Th by periodic mixing with influxes of new magma. This buffering effect is sensitive to the periodicity of the replenishment events, relative to the half-lives of ^{226}Ra and ^{230}Th, and to the ratio of input to chamber volume. These two parameters also control the size of oscillations in activity ratios and the time scale over which steady state conditions can be reached. If replenishment occurs on a time scale that is short relative to the half-life of ^{226}Ra then ^{230}Th-^{238}U disequilibria will be maintained close to its starting value and ^{226}Ra-^{230}Th will approach equilibrium as the replenishment time scale increases (Hughes and Hawkesworth 1999). In the case of a chamber with variable size, similar results were obtained by Vigier et al. (1999), who showed that the actual residence time of the magma could be longer than that calculated assuming simple closed-system decay.

10.7. Crustal contamination

The passage of magma through the crust and any storage time in magma chambers provides the opportunity for crustal interaction. As with any geochemical study of igneous rocks, the possible effects of crustal contamination have to be considered when attempting to interpret U-series disequilibria in terms of source processes. However, U-

Th isotopes have the advantage of being sensitive to contamination even by very young materials and thus can be usefully employed to investigate both the time scales of assimilation and the nature of the contaminant. We illustrate this latter potential with reference to selected case studies and the U-Th equiline diagram in Figure 22 recalling that mixing lines are linear on this diagram.

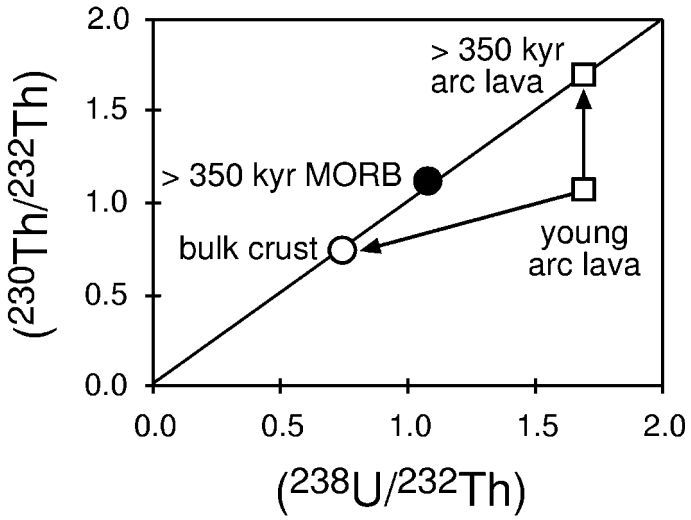

Figure 22. U-Th equiline diagram showing U-Th isotopes may be sensitive to the effects of assimilation of pre-existing (>350 kyr) arc basalts or continental crust. This is much more complicated using long-lived isotopic systems (e.g., $^{87}Sr/^{86}Sr$ or $^{143}Nd/^{144}Nd$) because in these systems pre-existing arc basalts will be indistinguishable from new magmas and crustal assimilation will be hard to distinguish from subducted sediment addition unless assimilation is coupled to differentiation.

In oceanic arcs, likely contaminants include the oceanic crust upon which the arc is built and the older arc lavas and sediments that comprise the upper arc crust. The long-lived radiogenic isotopes Sr, Nd and Pb are very poor tracers of the first two materials because they are too young to have evolved diagnostic isotope ratios and older arc lavas are likely to have similar long-lived isotope and trace element ratios to the younger ones of interest to U-series investigations. Equally, distinguishing contamination by ancient crustal materials from subducted sediment input is difficult. These features mean that contamination in oceanic arc lavas is usually a subtle feature that is hard to detect. However, the same is not necessarily true of Th isotopes because these change and reach equilibrium on a time scale of 350 kyr. Sediments and ancient continental crust have low U/Th and thus low ($^{230}Th/^{232}Th$), whereas since most arc lavas begin with ^{238}U-excesses, their $^{230}Th/^{232}Th$ evolution is conveniently in the opposite direction towards high ($^{230}Th/^{232}Th$). As illustrated on Figure 22, this may facilitate detection of contamination by such materials. Similarly, pre-existing arc lavas that are > 350 kyr old will have decayed up to the equiline and will have higher ($^{230}Th/^{232}Th$) ratios than the incoming arc lavas, although contamination with this material may be hard to distinguish from ageing of the incoming arc lavas during residence in magma chambers.

A further means by which U-series isotopes can be used to identify mixing or contamination processes is when the disequilibria in two parent-daughter systems with very different half-lives both decrease with increasing fractionation. For example, lavas from Galunggung in the Sunda arc trend towards both ($^{238}U/^{230}Th$) and ($^{226}Ra/^{230}Th$) = 1 with increasing SiO_2 (Turner and Foden 2001). Given the difference between the half-lives of these two isotope systems, these arrays cannot record the time taken for differentiation and the simplest explanation is that they reflect mixing between mantle derived magmas and silicic crustal melts or more evolved magmas in which U-Th-Ra isotopes have returned to secular equilibrium. These lavas show no change in $^{143}Nd/^{144}Nd$ with increasing SiO_2 (Turner and Foden 2001), and so the most likely candidate for the

contaminant is small degree partial melts of pre-existing basalts. An important implication is that these crustal melts were not significantly out of ^{238}U-^{230}Th or ^{226}Ra-^{230}Th equilibrium and therefore that this type of crustal contamination does not mask the mantle source component signatures.

Continental arcs provide maximum potential for crustal assimilation especially where the crustal column is thick. Ancient continental crust has high time-integrated Th/U ratios and consequently much lower ($^{230}Th/^{232}Th$) ratios (~0.4-0.7) than the MORB source (~1.2). Therefore, Th isotopes are very sensitive to even small additions of ancient crustal material which will lead to a mixing trajectory toward low ($^{230}Th/^{232}Th$) ratios. If the wedge-sediment mix has a higher ($^{230}Th/^{232}Th$) ratio than the local crustal basement then contamination will result in displacement below this value. Thus, George et al. (2003) found in the Alaska-Aleutian arc that lavas erupted in the oceanic sector had ($^{230}Th/^{232}Th$) ratios equal to or higher than the subducting sediment whereas some lavas erupted through the continent on the northeastern Alaskan peninsula were significantly displaced to lower ($^{230}Th/^{232}Th$).

The Andes is the area for which Hildreth and Moorbath (1988) originally developed their MASH model (Melting, Assimilation, Storage and Homogenization) for crustal interaction. Here, lavas from the southern volcanic zone of Chile lie on continental crust of average thickness (35-40 km) and their O and Sr isotope signatures can generally be explained by sediment addition consistent with the presence of a ^{10}Be signal (Sigmarsson et al. 1990). The U-Th-Ra systematics of these lavas appear to be unaffected by crustal contamination (Sigmarsson et al. 1990, 2002). The preservation of ^{226}Ra-excesses in most of the southern volcanic zone lavas requires sufficiently rapid transit through the crust that there may have been no time for the formation of large magma chambers in which major contamination could take place. One exception to this is a lava from San Jose which lies on significantly thicker crust (55-60 km) and has elevated $^{87}Sr/^{86}Sr$ and ^{18}O isotopes indicative of crustal contamination. This lava is also characterized by ^{226}Ra-^{230}Th equilibrium and lies slightly above the U-Th isotope array for the remainder of the lavas (Sigmarsson et al. 1990, 2002) suggesting that it may have had a greater crustal residence time during which contamination occurred.

In contrast to the southern volcanic zone, Parinacota volcano lies on very thick continental crust (> 70 km) in the central volcanic zone of Chile. Bourdon et al. (2000a) showed that young Parinacota lavas encompass a wide range of U-Th disequilibria. ^{238}U-excesses were attributed to fluid addition to the mantle wedge but ^{230}Th-excesses in lavas from the same volcano are more difficult to explain. The lavas with ^{230}Th-excesses also have low ($^{230}Th/^{232}Th$) (< 0.6) characteristic of lower continental crust characterized by low Th/U and in their preferred model, Bourdon et al. (2000a) attributed the ^{230}Th-excesses to contamination by partial melts, formed in the presence of residual garnet, of old lower crustal materials.

11. TIME-INTEGRATED U-Th-Pb EVOLUTION OF THE CRUST-MANTLE

Convergent margins are generally considered to be the principle present-day tectonic setting where new continental crust is formed (~ 1.1 km^3/yr, Reymer and Schubert 1984). As illustrated on Figure 23, this new crustal material is characterized by Th/U ratios that are even lower than the Th/U ratio of the MORB mantle (2.6, Sun and McDonough 1989) yet the Th/U ratio of the bulk continental crust (3.9, Rudnick and Fountain 1995) is close to the Th/U ratio of the bulk silicate earth (see Bourdon and Sims 2003). There are several possible explanations for this paradox. Firstly, it is possible that the processes that formed the continental crust in the past were different to those in operation today. Since

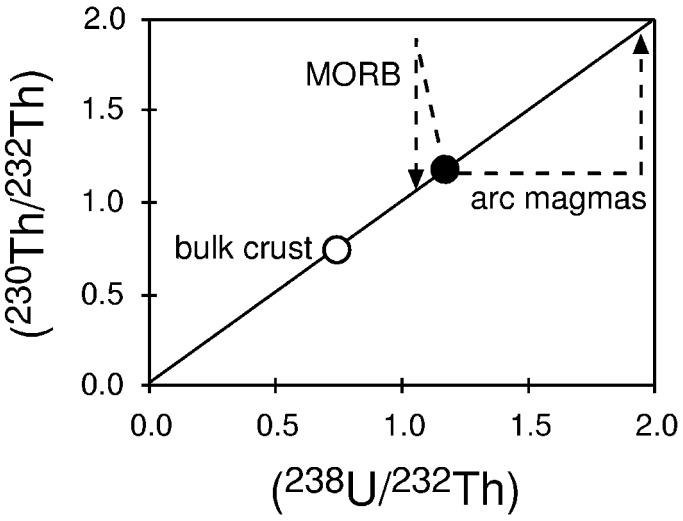

Figure 23. U-Th equiline diagram illustrating trajectories for present day MORB production (^{230}Th in-growth due to dynamic melting in the presence of aluminous clinopyroxene or garnet followed by ^{230}Th decay back to the equiline) and arc magma production (U addition followed by ^{230}Th in-growth back to the equiline due to ageing ± melting processes). Neither process seems to be able to be account for the present day composition of bulk crust.

the mantle was some 200°C hotter, melting of the subducting oceanic curst is likely to have been more prevalent (Peacock et al. 1994) and this is the process that is thought to have produced TTG (tondjhemite-tonalite-granite) series in the Archaean crust (Defant and Drummond 1990). As discussed above, during slab melting, residual garnet retains U relative to Th and this is consistent both with the observation of ^{230}Th-excess in putative slab melts from the Austral Andean zone in southern Chile (Sigmarsson et al. 1998), and the need for residual garnet to explain the Sm/Nd ratio of the crust (O'Nions and McKenzie 1988). Secondly, it is likely that the surface of the Earth was less oxidizing in the Archaean such that U was less preferentially transported to oceans and recycled (Hawkesworth et al. 1997a,b).

Alternatively, it can be argued that U and Th are both highly incompatible during melting and that there is only minor fractionation between U and Th during the formation of *most* arc lavas which lie close to U-Th equilibrium (see Fig. 3). In that case, the higher Th/U ratio of the bulk continental crust would reflect a higher Th/U ratio of the mantle in the past when the bulk of the continental crust was formed. In this model, the present day low Th/U ratio of the upper mantle would be the result of more recent evolution of the mantle. The long-term evolution of Th/U ratios in mantle rocks can be tracked with both ^{208}Pb-^{206}Pb and ^{230}Th/^{232}Th systematics (Bourdon and Sims 2003). Pb is also preferentially removed to the crust at subduction zones leading to long term secular depletion of the mantle in Pb (Miller et al. 1994). Thus, Galer and O'Nions (1985) showed that MORB and OIB are characterized by present-day Th/U ratios that are lower than their time-integrated Th/U ratios inferred from Pb isotopes (the so-called kappa conundrum) and called upon a steady-state model for exchange between the lower and upper mantle to explain this observation. However, the operation of the mantle at steady-state for long-lived isotope systems has been questioned by Albarède (2001) and alternative explanations have been suggested by Zartmann and Haines (1988), McCulloch (1993) and Elliott et al. (1999). As shown by Elliott et al. (1999), an alternative explanation to explain the lower Th/U ratio of the upper mantle relative to the time-integrated Th/U ratio from Pb isotopes, is to recycle preferentially U relative to Th in subduction zones. Estimates of recycling fluxes based on Th-U disequilibrium data for the Marianas (Elliott et al. 1997, 1999) have shown that U is preferentially recycled in the mantle compared with Th. However, this will only happen when U is in its fluid-mobile U^{6+} form and this would have commenced only when the atmosphere and hydrosphere became sufficiently oxidizing some time in the Post-Archaean Earth (Holland 1984). The

actual reasons for build up of oxygen in the atmosphere are still a hotly debated issue (e.g., Kasting 2001) but it is important to note how the chemistry of the deep-earth might be fundamentally affected by the chemistry of the atmosphere and how the fractionation of elements such as U and Th is only enhanced in the hydrosphere and shallow Earth where they have largely different behavior compared with the reducing conditions of the deep mantle.

12. FUTURE WORK

The use of U-series disequilibria in unraveling the physical processes of fluid transfer, partial melting, melt migration and modification at convergent margins is still a new and rapidly expanding field of research. Indeed, some of the full implications of the available data are only just beginning to be appreciated and many have barely been explored. In tandem with this, advances in analytical techniques are allowing for more rapid and precise analysis of ever smaller amounts of materials. These will inevitably lead to new data sets which can only help improve our understanding of convergent margin processes. It must be stressed that these need to be undertaken upon fully characterized and well dated, ideally primitive lavas. Studies of fore-arc and back-arc seamounts would help to map fluid release and melting effects along the slab. However, these data will need to be combined with better numerical models if their full significance is to be realized and an outstanding need in this regard is for a testable melting model for arcs. This will need to be evolved with geophysical constraints and independent information about the P, T and H_2O conditions of melting beneath arcs. For example, the flux melting models imply a testable link between melting rate and subduction velocity. While the current 1-D models seem to explain many of the U-series observations in arcs, they certainly do not capture some of the complexity that should arise in 2- or 3-D models. Thus, there are many potential rewards available from future melt and fluid inclusion studies on primitive arc lavas. Finally, additional experiments on fluid-mineral partition coefficients at the appropriate conditions and mantle melting under hydrous conditions also need to be conducted to allow for better forward modeling of the U-series data.

ACKNOWLEDGMENTS

Our present understanding of U-series disequilibria in arc lavas has benefited from interaction with too many people to acknowledge them all individually. We are especially grateful to Claude Allègre, Jon Davidson, Tony Dosseto, Tim Elliott, Chris Hawkesworth, Terry Plank, Mark Reagan, and the participants of the State Of The Arc meetings for many lively discussions over the years. For Simon Turner this represents the culmination of an 8 year research fellowship from the Royal Society which he gratefully acknowledges. Simon Turner also thanks IPGP for funding a one month visit during which the initial version of this chapter was written. Mark Reagan, Marc Hirschmann and Olgeir Sigmarsson provided careful reviews which helped to improve the final version.

REFERENCES

Albarède F (2001) Radiogenic ingrowth in systems with multiple reservoirs: applications to the differentiation of the mantle-crust system. Earth Planet Sci Lett 189:59-73

Aharonov E, Whitehead JA, Kelemen PB, Spiegelman M (1995) Channeling instability of upwelling melt in the mantle. J Geophys Res 100:20433-20450

Allègre CJ, Condomines M (1982) Basalt genesis and mantle structure studied through Th-isotopic geochemistry. Nature 299:21-24

Allègre CJ, Dupré B, Lewin E (1986) Thorium/uranium ratio of the Earth. Chem Geol 56:219-227

Alves S, Schiano P, Capmas F, Allègre CJ (2002) Osmium isotope binary mixing arrays in arc volcanism. Earth Planet Sci Lett 198:355-369

Ayers JC, Dittmer SK, Layne GD (1997) Partitioning of elements between peridotite and H_2O at 2.0-3.0 GPa and 900-1000˚C, and application to models of subduction zone processes. Earth Planet Sci Lett 150:381-398

Bebout GE, Barton MD (2002) Tectonic and metasomatic mixing in a high-T subduction zone melange - insights into the geochemical evolution of the slab-mantle interface. Chem Geol 187:79-106

Becker H, Jochum KP, Carlson RW (1999) Constraints from high-pressure veins in eclogites on the composition of hydrous fluid in subduction zones. Chem Geol 160:291-308

Bennett JT, Krishnaswami S, Turekian KK, Melson WG, Hopson CA (1982) The uranium and thorium decay series nuclides in Mt. St. Helens effusives. Earth Planet Sci Lett 60:61-69

Billen MI, Gurnis M (2001) A low viscosity wedge in subduction zones. Earth Planet Sci Lett 193:227-236

Black S, Macdonald R, DeViro B, Kilburn CRJ, Rolandi G (1998) U-series disequilibria in young (A.D. 1944) Vesuvius rocks: Preliminary implications for magma residence times and volatile addition. J Volcanol Geotherm Res 82:97-111

Blatter DL, Carmichael ISE (1998) Hornblende peridotite xenoliths from central Mexico reveal the highly oxidized nature of subarc upper mantle. Geology 26:1035-1038

Blundy J, Wood B (2003) Mineral-melt partitioning of uranium, thorium and their daughters. Rev Mineral Geochem 52:59-123

Bourdon B, Turner S, Allègre C (1999) Melting dynamics beneath the Tonga-Kermadec island arc inferred from ^{231}Pa-^{235}U systematics. Science 286:2491-2493

Bourdon B, Wörner G, Zindler A (2000a) U-series evidence for crustal involvement and magma residence times in the petrogenesis of Parinacota volcano, Chile. Contrib Mineral Petrol 139:458-469

Bourdon B, Bourlès D, Goldstein SJ, Murrell MT, Langmuir CH, Allègre CJ (2000b) Evidence from ^{10}Be and U-series disequilibria on the possible contamination of MORB glasses by sedimentary material. Geochem Geophys Geosyst 2000GC000047

Bourdon B, Turner S, Dosseto A (2003) Dehydration and partial melting in subduction zones: constraints from U-series disequilibria. J Geophys Res (in press).

Bourdon B, Sims KWW (2003) U-series constraints on intraplate basaltic magmatism. Rev Mineral Geochem 52:215-254

Blot C (1972) Volcanisme et séismes du manteau supérieur dans l'Archipel des Nouvelles-Hebrides. Bull Volcanol 36:446-461

Brémond d'Ars J, Jaupart C, Sparks RSJ (1995) Distribution of volcanoes in active margins. J Geophys Res 100:20421-20432

Brenan JM, Shaw HF, Phinney DL, Ryerson FJ, (1994) Rutile-aqueous fluid partitioning of Nb, Ta, Hf, Zr, U and Th: implications for high field strength element depletions in island-arc basalts. Earth Planet Sci Lett 128:327-339

Brenan JM, Shaw HF, Ryerson FJ, Phinney DL (1995) Mineral-aqueous fluid partitioning of trace elements at 900 ˚C and 2.0 GPa: constraints on the trace element chemistry of mantle and deep crustal fluids. Geochim Cosmochim Acta 59:3331-3350

Brophy JG, Whittington CS, Park Y-R (1999) Sector-zoned augite megacrysts in Aleutian high alumina basalts: implications for the conditions of basalt crystallization and the generation of calc-alkaline series magmas. Contrib Mineral Petrol 135:277-290

Capaldi G, Del Pezzo E, Ghiara MR, Guerra I, La Volpe L, Lirer L, Lo Basico A, Luongo G, Martini M, Munno R, Pece R, Rapolla A, Scarpa R (1978) Stromboli and its 1977 eruption. Bull Volcanol 41:259-285

Capaldi G, Cortini M, Pece R (1982) Th isotopes at Vesuvius: evidence for open-system behavior of magma-forming processes. J Volcanol Geotherm Res 14:247-260

Capaldi G, Cortini M, Pece R (1983) U and Th decay-series disequilibria in historical lavas from the Eolian islands, Tyrrhenian Sea. Isot Geosci 1:39-55

Chabaux F, Hémond C, Allègre CJ (1999) ^{238}U-^{230}Th-^{226}Ra disequilibria in the Lesser Antilles arc: implications for mantle metasomatism. Chem Geol 153:171-185

Cheng H, Edwards RL, Hoff J, Gallup CD, Richards DA, Asmerom Y (2000) The half-lives of uranium-234 and thorium-230. Chem Geol 169:17-33

Clark SK, Reagan MK, Plank T (1998) Trace element and U-series systematics for 1963-1965 tephras from Irazú volcano, Costa Rica: implications for magma generation processes and transit times. Geochim Cosmochim Acta 62:2689-2699

Class C, Miller DM, Goldstein SL, Langmuir CH (2000) Distinguishing melt and fluid subduction components in Umnak volcanics. Aleutian arc. Geochem Geophys Geosys 1: paper number 1999GC000010

Condomines M, Sigmarsson O (1993) Why are so many arc magmas close to ^{238}U-^{230}Th radioactive equilibrium? Geochim Cosmochim Acta 57:4491-4497

Crisp JA (1984) Rates of magma emplacement and volcanic output. J Volcanol Geotherm Res 20:177-211

Davies JH (1999) The role of hydraulic fractures and intermediate-depth earthquakes in generating subduction-zone magmatism. Nature 398:142-145

Davies JH, Bickle MJ (1991) A physical model for the volume and composition of melt produced by hydrous fluxing above subduction zones. Phil Trans R Soc Lond 335:355-364

Davies JH, Stevenson DJ (1992) Physical model of source region of subduction zone volcanics. J Geophys Res 97:2037-2070

Defant MJ, Drummond MS (1990) Derivation of some modern arc magmas by melting of young subducted lithosphere. Nature 347:662-665

Dosseto A, Bourdon B, Joron JL, Dupré B (2003) U-Th-Pa-Ra study of the Kamchatka arc: new constraints on the genesis of arc lavas. Geochim Cosmochim Acta (submitted)

Druitt TH, Edwards L, Mellors RM, Pyle DM, Sparks RSJ, Lanphere M, Davies M, Barriero B (1999) Santorini Volcano. Geol Soc Lond Mem 19

Eiler, JM, Crawford A, Elliott T, Farley KA, Valley JW, Stolper EM (2000) Oxygen isotope geochemistry of oceanic-arc lavas. J Petrol 41:229-256

Ellam RM, Hawkesworth CJ (1988) Elemental and isotopic variations in subduction related basalts: evidence for a three component model. Contrib Mineral Petrol 98:72-80

Elkins Tanton LT, Grove TL, Donnelly-Nolan J (2001) Hot, shallow mantle melting under the Cascades volcanoc arc. Geology 29:631-634

Elliott T, Plank T, Zindler A, White W, Bourdon B (1997) Element transport from slab to volcanic front at the Mariana arc. J Geophys Res 102:14991-15019

Elliott T, Zindler A, Bourdon B (1999) Exploring the Kappa conundrum: the role of recycling in the lead isotope evolution of the mantle. Earth Planet Sci Lett 169:129-145

Elliott T, Heumann A, Koetsier G (2001) U-series constraints on melting beneath the Marianas. *In*: Intra-oceanic subduction systems: Tectonic and Magmatic Processes. Geol Soc Lond Abstr

England PC (2001) Why are the arc volcanoes where they are? EOS Trans, Amer Geophys Union 82:F1156

Ewart A, Hawkesworth CJ (1987) The Pleistocene-Recent Tonga-Kermadec arc lavas: Interpretation of new isotopic and rare earth data in terms of a depleted mantle source model. J Petrol 28:495-530

Furukawa F (1993a) Magmatic processes under arcs and formation of the volcanic front. J Geophys Res 98:8309-8319

Furukawa F (1993b) Depth of the decoupling plate interface and thermal structure under arcs. J Geophys Res 98:20,005-20,013

Galer SJG, O'Nions RK (1985) Residence time of thorium, uranium and lead in the mantle with implications for mantle convection. Nature 316:778-782.

Gauthier P-J, Condomines M (1999) ^{210}Pa-^{226}Ra radioactive disequilibria in recent lavas and radon degassing: inferences on the magma chamber dynamics at Stromboli and Merapi volcanoes. Earth Planet Sci Lett 172:111-126

George R, Turner S, Hawkesworth C, Morris J, Nye C, Ryan J, Zheng S-H (2003) Melting processes and fluid and sediment transport rates along the Alaska-Aleutian arc from an integrated U-Th-Ra-Be isotope study. J Geophys Res (in press).

Gill JB (1981) Orogenic Andesites and Plate Tectonics. Springer-Verlag , New York

Gill JB, Williams RW (1990) Th isotope and U-series studies of subduction-related volcanic rocks. Geochim Cosmochim Acta 54:1427-1442

Gill JB, Pyle DM, Williams RW (1992) Igneous rocks. *In*: Uranium-series disequilibrium. Ivanovich M, Harmon RS (eds) Oxford University Press, Oxford, p 207-258.

Gill JB, Morris JD, Johnson RW (1993) Timescale for producing the geochemical signature of island arc magmas: U-Th-Po and Be-B systematics in Recent Papua New Guinea lavas. Geochim Cosmochim Acta 57:4269-4283

Goldstein SJ, Stirling CH (2003) Techniques for measuring uranium-series nuclides: 1992-2002. Rev Mineral Geochem 52:23-57

Grove TL, Parman SW, Bowring SA, Price RC, Baker MB (2002) The role of an H_2O-rich fluid component in the generation of primitive basaltic andesites and andesites from the Mt. Shasta region, N. California. Contrib Mineral Petrol 142:375-396

Guillaumont R, Bouissières G, Muxart Y (1968) Protactinium chemistry. 1. Aqueous solutions for penta and tetravalent protactinium. Actinid Rev 1:135

Hall PS, Kincaid C (2001) Diapiric Flow at Subduction Zones: A Recipe for Rapid Transport. Science 292:2472-2475

Harris DM, Anderson AT (1984) Volatiles H_2O, CO_2, and Cl in a subduction related basalt. Contrib Mineral Petrol 87:120-128

Hauri EH (1997) Melt migration and mantle chromatography, 1:simplified theory and conditions for chemical and isotopic decoupling. Earth Planet Sci Lett 153:1-19

Hawkesworth CJ, Gallagher K, Hergt JM, McDermott F (1993) Mantle and slab contributions in arc magmas. Ann Rev Earth Planet Sci 21:175-204

Hawkesworth C, Turner S, Peate D, McDermott F, van Calsteren P (1997a) Elemental U and Th variations in island arc rocks: implications for U-series isotopes. Chem Geol 139:207-222

Hawkesworth CJ, Turner SP, McDermott F, Peate DW, van Calsteren P (1997b) U-Th isotopes in arc magmas: implications for element transfer from the subducted crust. Science 276:551-555

Hawkesworth C, Blake S, Evans P, Hughes R, Macdonald R, Thomas L, Turner S, Zellmer G (2000) The time scales of crystal fractionation in magma chambers - integrating physical, isotopic and geochemical perspectives. J Petrol 41:991-1006

Heath E, Turner SP, Macdonald R, Hawkesworth CJ, van Calsteren P (1997) Long magma residence times at an island arc volcano (Soufriere, St. Vincent) in the Lesser Antilles: evidence from ^{238}U-^{230}Th isochron dating. Earth Planet Sci Lett 160:49-63

Herrstrom EA, Reagan MK, Morris JD (1995) Variations in lava composition associated with flow of asthenosphere beneath southern Central America. Geology 23:617-620

Hildreth W, Moorbath S (1988) Crustal contributions to arc magmatism in the Andes of Central Chile. Contrib Mineral Petrol 98:455-489

Hirschmann MM, Asimow PD, Ghiorso MS, Stolper EM (1999) Calculation of peridotite partial melting from thermodynamic models of minerals and melts. III Controls on isobaric melt production and the effect of water on melt production. J Petrol 40:831-851

Hochstaedter A, Gill J, Peters R, Broughton P, Holden P, Taylor B (2001) Across-arc geochemical trends in the Izu-Bonin arc: contributions from the subducting slab. Geochem Geophys Geosys 2:paper number 2000GC000105

Hole MJ, Saunders AD, Marriner GF, Tarney J (1984) Subduction of pelagic sediments: implications for the origin of Ce-anomalous basalts from the Mariana islands. J Geol Soc London 141:453-472

Holland HD (1984) The Chemical Evolution of the Atmosphere and Oceans. Princeton University Press, Princeton

Hoogewerff JA, van Bergen MJ, Vroon PZ, Hertogen J, Wordel R, Sneyers A, Nasution A, Varekamp JC, Moens HLE, Mouchel D (1997) U-series, Sr-Nd-Pb isotope and trace-element systematics across an active island arc-continent collision zone: implications for element transfer at the slab-wedge interface. Geochim Cosmochim Acta 61:1057-1072

Hughes RD, Hawkesworth CJ (1999) The effects of magma replenishment processes on ^{238}U-^{230}Th disequilibrium. Geochim Cosmochim Acta 63:4101-4110

Ivanovich M, Harmon RS (1992) Uranium-series disequilibrium. Oxford University Press, Oxford

Jarrard RD (1986) Relations among subduction parameters. Rev Geophys 24:217-284

Johnson MC, Plank T (1999) Dehydration and melting experiments constrain the fate of subducted sediments. Geochem Geophys Geosys 1:paper number 1999GC000014

Kasting JF (2001) The rise of atmospheric oxygen. Science 293:819-820

Kay RW (1980) Volcanic arc magmas: implications of a melting-mixing model for element recycling in the crust-upper mantle system. J Geol 88:497-522

Kelemen PB, Johnson KTM, Kinzler RJ, Irving AI (1990) High-field strength element depletions in arc basalts due to mantle-magma interaction. Nature 345:521-524

Kelemen PB, Yogodinsky GM, Scholl DW (2003) Along strike variation in lavas of the Aleutian island arc: implications for the genesis of high Mg# andesite and the continental crust. *In*: The Subduction Factory. Eiler JM (ed) AGU Geophys Monogr Ser (in press)

Keppler H, Wyllie P (1990) Role of fluids in transport and fractionation of uranium and thorium in magmatic processes. Nature 348:531-533

Keppler H (1996) Constraints from partitioning experiments on the composition of subduction-zone fluids. Nature 380:237-240

Kincaid C, Sacks IS (1997) Thermal and dynamic evolution of the upper mantle in subduction zones. J Geophys Res 102:12,295-12,315

Kirby S, Engdahl ER, Denlinger R (1996) Intermediate-depth intraslab earthquakes and arc volcanism as physical expressions of crustal and uppermost mantle metamorphism in subducting slabs. *In*: Subduction Top to Bottom. Bebout GE et al. (eds) AGU Geophys Monogr Ser 96:195-214

La Tourette T, Hervig RL, Holloway JR (1995) Trace element partitioning between amphibole, phlogopite and basanite melt. Earth Planet Sci Lett 135:13-30

Lundstrom CC, Shaw H, Ryerson F, Phinney D, Gill J, Williams Q (1994) Compositional controls on on the partitioning of U, Th, Ba, Pb, Sr and Zr between clinopyroxene and haplobasaltic melts; implications for uranium series disequilibria in basalts. Earth Planet Sci Lett 128:407-423

Lundstrom CC (2003) Uranium-series disequilibria in mid-ocean ridge basalts: observations and models of basalt genesis. Rev Mineral Geochem 52:175-214

Marsh BD (1987) Petrology and evolution of the N.E. Pacific including the Aleutians. Pacific Rim Congress 87:309-315

Maury RE, Defant MJ, Joron J-L (1992) Metasomatism of the sub-arc mantle inferred from trace elements in Philippine xenoliths. Nature 360:661-663

McCulloch MT (1993) The role of subducted slabs in an evolving earth. Earth Planet Sci Lett 115:89-100

McCulloch MT, Gamble JA (1991) Geochemical and geodynamical constraints on subduction zone magmatism. Earth Planet Sci Lett 102:358-374

McDermott F, Hawkesworth C (1991) Th, Pb, and Sr isotope variations in young island arc volcanics and oceanic sediments. Earth Planet Sci Lett 104:1-15

McDermott F, Defant MJ, Hawkesworth CJ, Maury RC, Joron JL (1993) Isotope and trace element evidence for three component mixing in the genesis of the North Luzon arc lavas (Philippines). Contrib Mineral Petrol 113:9-23

McKenzie D (1985) The extraction of magma from the crust and mantle. Earth Planet Sci Lett 74:81-91

McKenzie D (1985) ^{230}Th-^{238}U disequilibrium and the melting process beneath ridge axes. Earth Planet Sci Lett 72:149-157

McKenzie D (2000) Constraints on melt generation and transport from U-series activity ratios. Chem Geol 162:81-94

Miller DM, Goldstein SL, Langmuir CH (1994) Cerium/lead and lead isotope ratios in arc magmas and the enrichment of lead in the continents. Nature 368:514-520

Morris JD, Hart SR (1983) Isotopic and incompatible element constraints on the genesis of island arc volcanics from Cold Bay and Amak Island, Aleutians, and implications for mantle structure. Geochim Cosmochim Acta 47:2015-2030

Morris JD, Leeman BW, Tera F (1990) The subducted component in island arc lavas: constraints from Be isotopes and B-Be systematics. Nature 344:31-36

Mysen BO, Kushiro I, Fujii T, (1978) Preliminary experimental data bearing on the mobility of H_2O in crystalline upper mantle. Carnegie Inst Washington Yearbook 77:793-797

Navon O, Stolper E (1987) Geochemical consequences of melt percolation: the upper mantle as a chromatographic column. J Geol 95:285-307

Newman S, Macdougall JD, Finkel RC (1984) ^{230}Th-^{238}U disequilibrium in island arc lavas: evidence from the Aleutians and the Marianas. Nature 308:266-270

Newman S, Macdougall JD, Finkel RC (1986) Petrogenesis and ^{230}Th-^{238}U disequilibrium at Mt. Shasta, California, and in the Cascades. Contrib Mineral Petrol 93:195-206

Nichols GT, Wyllie PJ Stern CR (1994) Subduction zone melting of pelagic sediments constrained by melting experiments. Nature 371:785-788

O'Nions RK, McKenzie DP (1988) Melting and continent generation. Earth Planet Sci Lett 90:449-456

Parkinson IJ, Arculus RJ (1999) The redox state of subduction zones: insights from arc-peridotites. Chem Geol 160:409-423

Peacock SM (1996) Thermal and petrologic structure of subduction zones. *In*: Subduction Top to Bottom. Bebout GE et al. (eds) AGU Geophys Monogr Ser 96:119-133

Peacock SM, Rushmer T, Thompson AB (1994) Partial melting of subducting oceanic crust. Earth Planet Sci Lett 121:227-244

Pearce JA, Parkinson IJ (1993) Trace element models for mantle melting: application to volcanic arc petrogenesis. J Geol Soc Lond 76:373-403

Pearce JA, Ernewein M, Bloomer SH, Parson LM, Murton BJ, Johnson LE (1995) Geochemistry of Lau Basin volcanic rocks: influence of ridge segmentation and arc proximity. *In*: Volcanism associated with extension at consuming plate margins. Smellie JL (ed) Geol Soc Lond Spec Publ 81:53-75

Peate DW, Kokfelt TF, Hawkesworth CJ, van Calsteren PW, Hergt JM, Pearce JA (2001) U-series isotope data on Lau Basin glasses: the role of subduction-related fluids during melt generation in back-arc basins. J Petrol 42:1449-1470

Pickett DA, Murrell MT (1997) Observations of ^{231}Pa/^{235}U disequilibrium in volcanic rocks. Earth Planet Sci Lett 148:259-271

Plank T (1993) Mantle melting and crustal recycling in subduction zones. PhD Dissertation, Columbia University, New York City, New York

Plank T, Langmuir CH (1988) An evaluation of the global variations in the major element chemistry of arc basalts. Earth Planet Sci Lett 90:349-370

Plank T, Langmuir CH (1993) Tracing trace elements from sediment input to volcanic output at subduction zones. Nature 362:739-743

Plank T, Langmuir CH (1998) The chemical composition of subducting sediment and its consequences for the crust and mantle. Chem Geol 145:325-394

Poli S, Schmidt MW (1995) H_2O transport and release in subduction zones: experimental constraints on basaltic and andesitic systems. J Geophys Res 100:22,299-22,314

Pyle DM, Ivanovich M, Sparks RSJ (1988) Magma-cumulate mixing identified by U-Th disequilibrium dating. Nature 331:157-159

Reagan MK, Gill JB (1989) Coexisting calkalkaline and high-Nb basalts from Turrialba volcano, Costa Rica: implications for residual titanites in arc magma sources. J Geophys Res 94:4619-4633

Reagan MK, Morris JD, Herrstrom EA, Murrell MT (1994) Uranium series and beryllium isotope evidence for an extended history of subduction modification of the mantle below Nicaragua. Geochim Cosmochim Acta 58:4199-4212

Reagan MK, Sims KW, Erich J, Thomas RB, Cheng H, Edwards RL, Layne G, Ball L (2003) Timescales of differentiation from mafic parents to rhyolite in North American continental arcs. J Petrol (in press)

Regelous M, Collerson KD, Ewart A, Wendt JI (1997) Trace element transport rates in subduction zones: evidence from Th, Sr and Pb isotope data for Tonga-Kermadec arc lavas. Earth Planet Sci Lett 150:291-302

Reymer A, Schubert G (1984) Phanerozoic addition rates to the continental crust and crustal growth. Tectonics 3:63-77

Rubin KH, Wheller GE, Tanzer MO, MacDougall JD, Varne R, Finkel R (1989) ^{238}U decay series systematics of young lavas from Batur volcano, Sunda arc. J Volcanol Geotherm Res 38:215-226

Rudnick RL, Fountain DM (1995) Nature and composition of the continental crust: a lower crustal perspective. Rev Geophys 33:267-309

Ryan JG, Morris JD, Tera F, Leeman WP, Tsvetkov A (1995) Cross-arc geochemical variations in the Kurile arc as a function of slab depth. Science 270:625-627

Ryerson FJ, Watson EB (1987) Rutile saturation in magmas: implications for Ti-Nb-Ta depletion in island-arc basalts. Earth Planet Sci Lett 86:225-239

Schaefer SJ, Sturchio NC, Murrell MT, Williams SN (1993) Internal ^{238}U-series systematics of pumice from the November 13, 1985, eruption of Nevado del Ruiz, Columbia. Geochim Cosmochim Acta 57:1215-1219

Schmidt MW, Poli S (1998) Experimentally based water budgets for dehydrating slabs and consequences for arc magma generation. Earth Planet Sci Lett 163:361-379

Sigmarsson O, Condomines M, Morris JD, Harmon RS (1990) Uranium and ^{10}Be enrichments by fluids in Andean arc magmas. Nature 346:163-165

Sigmarsson O, Martin H, Knowles J (1998) Melting of a subducting oceanic crust from U-Th disequilibria in austral Andean lavas. Nature 394:566-569

Sigmarsson O, Chmeleff J, Morris J, Lopez-Escobar L (2002) Origin of ^{226}Ra-^{230}Th disequilibria in arc lavas from southern Chile and magma transfer time. Earth Planet Sci Lett 196:189-196

Sisson TW, Layne GD (1993) H_2O in basalt and basaltic andesite inclusions from four subduction-related volcanoes. Earth Planet Sci Lett 117:619-635

Sisson TW, Bronto S (1998) Evidence for pressure-release melting beneath magmatic arcs from basalt at Galunggung, Indonesia. Nature 391:883-886

Smith GP, Weins DA, Fischer KM, Dorman LM, Webb SC, Hildebrand JA (2001) A complex pattern of mantle flow in the Lau backarc. Science 292:713-716

Sparks RSJ, Sigurdsson H, Wilson L (1977) Magma mixing: a mechanism of triggering acid explosive eruptions. Nature 267:315-318

Spiegelman M, McKenzie D (1987) Simple 2-D models for melt extraction at mid-ocean ridges and island arcs. Earth Planet Sci Lett 83:137-152

Staudigel H, Plank T, White W, Schminke H-U (1996) Geochemical fluxes driving seafloor alteration of the basaltic upper oceanic crust: DSDP sites 417 and 418. *In*: Subduction: top to bottom. Bebout GE, Scholl DW, Kirby SH, Platt JP (eds) Am Geophys Union Geophys Monogr 96:19-38

Stolper E, Newman S (1994) The role of water in the petrogenesis of Mariana trough magmas. Earth Planet Sci Lett 121:293-325

Sun SS, McDonough WF (1989) Chemical and isotopic systematics of oceanic basalts: implications for mantle composition and processes. *In*: Magmatism in ocean basins. Saunders AD, Norry MJ (eds) Geol Soc Lond Spec Publ 42:313-345

Tatsumi Y, Hamilton DL, Nesbitt RW, (1986) Chemical characteristics of fluid phase released from a subducted lithosphere and origin of arc magmas: evidence from high-pressure experiments and natural rocks. J Volcanol Geotherm Res 29:293-309

Taylor RS, McLennan SM (1981) The composition and evolution of the continental crust: rare earth element evidence from sedimentary rocks. Phil Trans R Soc Lond 301:381-399

Thomas RB, Hirschmann MM, Cheng H, Reagan MK, Edwards RL (2002) (^{231}Pa/^{235}U)-(^{230}Th/^{238}U) of young mafic volcanic rocks from Nicaragua and Costa Rica and the influence of flux melting on U-series systematics of arc lavas. Geochim Cosmochim Acta 66:4287-4309

Turner S, Hawkesworth C, van Calsteren P, Heath E, Macdonald R, Black S (1996) U-series isotopes and destructive plate margin magma genesis in the Lesser Antilles. Earth Planet Sci Lett 142:191-207

Turner S, Hawkesworth C (1997) Constraints on flux rates and mantle dynamics beneath island arcs from Tonga-Kermadec. Nature 389:568-573

Turner S, Hawkesworth C, Rogers N, Bartlett J, Worthington T, Hergt J, Pearce J, Smith I (1997) ^{238}U-^{230}Th disequilibria, magma petrogenesis and flux rates beneath the depleted Tonga-Kermadec island arc. Geochim Cosmochim Acta 61:4855-4884

Turner S, Hawkesworth C (1998) Using geochemistry to map mantle flow beneath the Lau Basin. Geology 26:1019-1022

Turner S, McDermott F, Hawkesworth C, Kepezhinskas P (1998) A U-series study of lavas from Kamchatka and the Aleutians: constraints on source composition and melting processes. Contrib Mineral Petrol 133:217-234

Turner SP, Peate DW, Hawkesworth CJ, Eggins SM, Crawford AJ (1999) Two mantle domains and the time scales of fluid transfer beneath the Vanuatu arc. Geology 27:963-966

Turner S, Bourdon B, Hawkesworth C, Evans P, (2000a) ^{226}Ra-^{230}Th evidence for multiple dehydration events, rapid melt ascent and the time scales of differentiation beneath the Tonga-Kermadec island arc. Earth Planet Sci Lett 179:581-593

Turner SP, George RMM, Evans PE, Hawkesworth CJ, Zellmer GF (2000b) Time-scales of magma formation, ascent and storage beneath subduction-zone volcanoes. Phil Trans R Soc Lond 358:1443-1464

Turner S, Foden J (2001) U, Th and Ra disequilibria, Sr, Nd and Pb isotope and trace element variations in Sunda arc lavas: predominance of a subducted sediment component. Contrib Mineral Petrol 142:43-57

Turner S, Evans P, Hawkesworth C, (2001) Ultra-fast source-to-surface movement of melt at island arcs from ^{226}Ra-^{230}Th systematics. Science 292:1363-1366

Turner S, Foden J, George R, Evans P, Varne R, Elburg M, Jenner G (2003) Rates and processes of potassic magma evolution beneath Sangeang Api volcano, east Sunda arc, Indonesia. J Petrol (in press)

Vigier N, Bourdon B, Joron JL, Allègre CJ (1999) U-decay series and trace element systematics in the 1978 eruption of Ardoukoba, Asal rift: timescale of magma crystallisation. Earth Planet Sci Lett 174:81-97

Villemant B, Flehoc C (1989) U-Th fractionation by fluids in K-rich magma genesis: the Vico volcano, central Italy. Earth Planet Sci Lett 91:312-326

Villemant B, Boudon G, Komorowski JC (1996) U-series disequilibrium in arc magmas induced by water-magma interaction. Earth Planet Sci Lett 140:259-267

Volpe AM, Hammond PE (1991) ^{238}U-^{230}Th-^{226}Ra disequilibrium in young Mt. St. Helens rocks: time constraint for magma formation and crystallization. Earth Planet Sci Lett 107:475-486

Volpe A M (1992) ^{238}U-^{230}Th-^{226}Ra disequilibrium in young Mt. Shasta andesites and dacites. J Volcanol Geotherm Res 53:227-238

Wendt JI, Regelous M, Collerson KD, Ewart A (1997) Evidence for a contribution from two mantle plumes to island arc lavas from northern Tonga. Geology 25:611-614

Williams RW, Gill JB (1989) Effects of partial melting on the uranium decay series. Geochim Cosmochim Acta 53:1607-1619

Woodhead J, Eggins S, Gamble J (1993) High field strength and transition element systematics in island arc and back-arc basin basalts: evidence for multi-phase melt extraction and a depleted mantle wedge. Earth Planet Sci Lett 114:491-504

Woodhead JD, Eggins SM, Johnson RW (1998) Magma genesis in the New Britain arc: further insights into melting and mass transfer processes. J Petrol 39:1641-1668

Woodland SJ, Pearson DG, Thirlwall MF (2002) A Platinum Group Element and Re–Os Isotope Investigation of Siderophile Element Recycling in Subduction Zones: Comparison of Grenada, Lesser Antilles Arc, and the Izu–Bonin Arc. J Petrol 43:171-198

Wood BJ, Bryndzia LT, Robinson JAC (1990) Mantle oxidation state and its relationship to tectonic environment and fluid speciation. Science 248:337-345

Wood BJ, Blundy JD, Robinson JAC (1999) The role of clinopyroxene in generating U-series disequilibrium during mantle melting. Geochim Cosmochim Acta 63:1613-1620

Wyss M, Hasegawa A, Nakajima J (2001) Source and path of magma for volcanoes in the subduction zone of northeastern Japan. Geophys Res Lett 28:1819-1822

Yokoyama T, Kobayashi K, Kuritani T, Nakamura E (2002) Mantle metasomatism and rapid ascent of slab components beneath island arcs: evidence from ^{238}U-^{230}Th-^{226}Ra disequilibria of Miyakejima volcano, Izu arc, Japan. J Geophys Res (in press)

Zartman RE, Haines SM (1988) The plumbotectonic model for Pb isotopic systematics among major terrestrial reservoirs – a case for bi-directional transport. Geochim. Cosmochim Acta 52:1327-1339

Zellmer G, Turner S, Hawkesworth C (2000) Timescales of destructive plate margin magmatism: new insights from Santorini, Aegean volcanic arc. Earth Planet Sci Lett 174:265-281

Zhao D, Hasegawa A. (1993) P-wave tomographic imaging of the crust and upper mantle beneath the Japan Islands. J Geophys Res 98:4333-4353

APPENDIX: EQUATIONS FOR SIMULATING MELTING AND DEHYDRATION MODELS IN ARCS

A1. Single-stage model

The fluid compositions given in Table 3 and plotted on various figures were calculated assuming Rayleigh distillation of altered oceanic crust using the partition coefficients for rutile-free eclogite at 3 Gpa from Table 2. However, the composition of the mantle wedge prior to melting reflects a mass balance of this fluid plus wedge peridotite and sediment. Here we present a simple mass balance calculation which indicates how the U-Th or Th-Ra composition can be estimated in the composite mantle wedge source prior to melting. In this model, the fluid release by dehydration occurs as a single event releasing both U and Ra (and small amounts of Th or Pa based on the partition coefficients estimated for Th or Pa in Table 2). This dehydration can be thought of as either a "batch" or a "Rayleigh" process, the latter being more efficient in stripping the elements from the altered oceanic crust. The mineral fluid partition coefficients compiled in Table 2 and/or A1 can be used to calculate the fluid concentration. If C_f is the concentration in the fluid, then the composition of the metasomatized mantle wedge prior to melting is:

$$C_w = C_{dw}X_{dw} + X_{sed}C_{sed} + \left(1 - X_{sed} - X_{dw}\right)C_f$$

where the sum of all the fractions (X_i) from the depleted wedge (dw), sediment (sed) and slab fluid (f) equals 1. The concentration of a given element in the depleted mantle wedge can be estimated, as follows, assuming that the wedge has become variably depleted during a back-arc melt extraction event:

$$C_{dw} = \frac{DC_{MORB}}{D + F(1 - D)}$$

where C_{MORB} represents the composition of the MORB source, D is a partition coefficient during melting and F the degree of melting in the back-arc. Using the partition coefficients given in Table 2, this model produces almost horizontal arrays on the ^{238}U-^{230}Th isochron diagram for a constant amount of fluid addition. As argued in the text, inclined arrays can then be produced by dynamic melting (George et al. 2003; Lundstrom 2003; Bourdon and Sims 2003). If we allow for greater amounts of Th in the slab fluid, then inclined arrays can also be produced with a single stage fluid addition without the need for ^{230}Th in-growth during melting or ageing.

A2. Two stage-model for fluid addition

This model assumes that fluid dehydration takes place in two distinct stages (Fig. 12). The first stage produces most of the ^{238}U-^{230}Th signature while the second stage adds mainly ^{226}Ra. The model assumes that Th is not fluid mobile and that no Th is lost from the altered oceanic crust (slab) during either dehydration stage. Dehydration transport of U from the altered oceanic crust during the first stage is assumed to occur via a Rayleigh distillation process according to the following equation describing the activity of residual uranium in the slab:

$$^{238}U_1 = {}^{238}U_0\left(1 - F_1\right)^{\frac{1}{D_U} - 1}$$

where F_1 is the fraction of fluid released during the first stage, U_0 is the activity of U in the slab, U_1 is the activity of residual U in the slab and D_U is the fluid/solid partition coefficient. Note that here the elemental symbols U, Th and Ra represent activities of the nuclides considered (^{238}U, ^{230}Th and ^{226}Ra) rather than concentration. In this calculation, we assume that the initial U concentration in the slab is 0.1-0.3 ppm and F_1 is 0.02-0.03. This first step efficiently removes U from the slab. Had we chosen batch dehydration, the amount of U left in the slab would be greater and there could be some U in the second stage fluid addition.

The time between the two dehydration stages is Δt and is taken to match the slope of array on the U-Th diagram. The activity of ^{230}Th in the wedge after this time is:

$$^{230}\mathrm{Th}_2 = {}^{230}\mathrm{Th}_1 e^{-\lambda\Delta t} + {}^{238}\mathrm{U}_1(1-e^{-\lambda\Delta t})$$

where

$$^{230}\mathrm{Th}_1 = \frac{^{230}\mathrm{Th}_0}{1-F_1}$$

where λ is the decay constant of ^{230}Th. After Δt, ^{226}Ra added to the mantle wedge during the first dehydration stage will have decayed back to secular equilibrium with the ^{230}Th in the wedge ($^{230}Th_2$) such that:

$$^{226}\mathrm{Ra}_2 = {}^{230}\mathrm{Th}_2$$

The activity of ^{226}Ra available to be added by the second stage dehydration is that which has in-grown from ^{230}Th left behind in the slab. Thus, we can calculate the ^{226}Ra and U activities in the second step dehydration fluid:

$$\mathrm{Ra}_2^f = \frac{\mathrm{Ra}_2}{F_1}\left(1-\left(1-F_2\right)^{1/D_{Ra}}\right)$$

$$\mathrm{U}_2^f = \frac{\mathrm{U}_1}{F_2}\left(1-\left(1-F_2\right)^{1/D_{U}}\right)$$

where Ra_2^f and U_2^f are the integrated Ra and U activities during fractional dehydration of the slab, F_2 is the fraction of fluid released in the second stage (up to 0.02) and U_1 is the residual U content in the slab before the second fractional dehydration (first equation). An outcome of the Rayleigh distillation process is that the amount of U in the second-stage fluid is negligible compared with the first stage.

In the second step, we calculate the mass balance for all the components present in the mantle wedge: (1) depleted peridotite (dw), (2) sediment (sed), (3) first fluid (mass fraction F_1) and (4) second fluid (mass fraction F_2). The depleted peridotite is assumed to be a depleted peridotite (8 ppb) that is further depleted during batch extraction of melt in a back-arc (F = 0-10%). In the case of Tonga-Kermadec the mantle wedge appears to be variably depleted (e.g., Turner et al. 1997) and so it is appropriate to use a range of previous depletion in the modeling discussed here. The fraction of sediment can be estimated from Pb or Nd isotopes (e.g., 5‰ for Tonga-Kermadec). For ^{230}Th, there is no input from the second fluid because Th is again assumed to be fluid-immobile and the only contribution of ^{230}Th comes from decay from U_1^f. To a first approximation, we assume that the ratio of slab mass to mantle mass is equal to 1. This parameter could of course be tuned and incorporated in the mass balance equation given below. For U, the first dehydration stage removed all the U from the slab. Thus the budget of ^{230}Th in the mantle wedge is given by:

$$^{230}\mathrm{Th}_{\mathrm{mix}} = {}^{230}\mathrm{Th}_{\mathrm{w}}\mathrm{X}_{\mathrm{w}} + (1-\mathrm{X}_{\mathrm{w}})\,{}^{230}\mathrm{Th}_{1}^{\mathrm{f}}$$

$$^{230}\mathrm{Th}_{1}^{\mathrm{f}} = \overline{^{238}\mathrm{U}_{1}^{\mathrm{f}}}\left(1-\mathrm{e}^{-\lambda\Delta\mathrm{t}}\right)$$

$$\overline{^{238}\mathrm{U}_{1}^{\mathrm{f}}} = {}^{238}\mathrm{U}_{0}\left(1-\left(1-\mathrm{F}_{1}\right)\right)^{\frac{1}{\mathrm{D}_{\mathrm{U}}}}$$

Finally, the ^{226}Ra content in the mixture wedge + fluid 1+ fluid 2 is:

$$^{226}\mathrm{Ra}_{\mathrm{mix}} = {}^{226}\mathrm{Ra}_{\mathrm{w}}(1-\mathrm{F}_{1}-\mathrm{F}_{2}) + \mathrm{F}_{1}\,{}^{230}\mathrm{Th}_{1}^{\mathrm{f}} + \mathrm{F}_{2}\,{}^{226}\mathrm{Ra}_{2}^{\mathrm{f}}$$

$$^{226}\mathrm{Ra}_{\mathrm{w}} = {}^{230}\mathrm{Th}_{\mathrm{w}}$$

$$^{230}\mathrm{Th}_{\mathrm{w}} = {}^{230}\mathrm{Th}_{\mathrm{dw}}\mathrm{X}_{\mathrm{dw}} + (1-\mathrm{X}_{\mathrm{dw}})\,{}^{230}\mathrm{Th}_{\mathrm{sed}}$$

Where w denotes the mantle wedge (w). The total fraction of fluid added is inferred to be close to 0.03, a reasonable estimate for the fraction of fluid contained in the oceanic crust; for example, $F_1 = 0.01$ and $F_2 = 0.02$. A sediment component (sed) is also added to the variably depleted mantle wedge (dw). The sediment composition can be based on values for the composition of the sediment entering the trench using, for example, the compilation of Plank and Langmuir (1998). Figure 12 illustrates an example of the two-stage model used to simulate the Tonga-Kermadec arc whilst matching the 30-50 ka timescale from the U-Th array.

A3. Continuous dehydration and melting

This section describes the continuous flux melting model used in Bourdon et al. (2003) and has many similarities with the model of Thomas et al. (2002). A significant difference is that the model described here keeps track of the composition of the slab as it dehydrates. This model is based on mass balance equations for both the mantle wedge and the slab. We assume secular equilibrium in the U-series decay chain initially:

$$\left(^{238}\mathrm{U}_{\mathrm{oc}}^{\mathrm{o}}\right) = \left(^{230}\mathrm{Th}_{\mathrm{oc}}^{\mathrm{o}}\right) = \left(^{226}\mathrm{Ra}_{\mathrm{oc}}^{\mathrm{o}}\right)$$

In this equation, the parentheses denote activities. The model operates with a series of time-steps. Between two time steps, a fraction of fluid (df) is added to the mantle wedge. The activity of Ra in the fluid is calculated from the composition of the slab at the preceding step (similar equations for U, Th, Ra, Pa) :

$$\left(^{226}\mathrm{Ra}_{\mathrm{i}}^{\mathrm{f}}\right) = \frac{\left(^{226}\mathrm{Ra}_{\mathrm{oc}}^{\mathrm{i-1}}\right)}{\mathrm{D}^{\mathrm{s/f}} + \mathrm{f}\left(1-\mathrm{D}^{\mathrm{s/f}}\right)}$$

At each step, a fraction of fluid f is added to the mantle wedge from the slab. The bulk partition coefficients used for fluid dehydration can be derived from published mineral/fluid partition coefficients (see Tables A1 and A2). The composition of the residual slab is estimated as follows after Δt which is the time step between two melt extractions (similar equation for Th and Pa):

$$\left(^{230}\mathrm{Th}_{\mathrm{oc}}^{\mathrm{i}}\right) = \mathrm{D}_{\mathrm{Th}}^{\mathrm{s/f}}\left(^{230}\mathrm{Th}_{\mathrm{f}}^{\mathrm{i-1}}\right)\mathrm{e}^{-\lambda_{230}\Delta\mathrm{t}} + \mathrm{D}_{\mathrm{U}}^{\mathrm{s/f}}\left(^{238}\mathrm{U}_{\mathrm{f}}^{\mathrm{i-1}}\right)\left(1-\mathrm{e}^{-\lambda_{230}\Delta\mathrm{t}}\right)$$

A similar but more complex equation is derived for Ra:

$$\left(^{226}\mathrm{Ra}_{\mathrm{oc}}^{\mathrm{i}}\right) = \mathrm{D}_{\mathrm{s/f}}^{\mathrm{Ra}}\left(^{226}\mathrm{Ra}_{\mathrm{f}}^{\mathrm{i}}\right)\mathrm{e}^{-\lambda_{226}\mathrm{t}} + \frac{\lambda_{226}\mathrm{D}_{\mathrm{s/f}}^{\mathrm{Th}}}{\lambda_{226}-\lambda_{230}}\left(^{230}\mathrm{Th}_{\mathrm{f}}^{\mathrm{i}}\right)\left(\mathrm{e}^{-\lambda_{230}\mathrm{t}} - \mathrm{e}^{-\lambda_{226}\mathrm{t}}\right) +$$

$$\lambda_{226}\lambda_{230}\mathrm{D}_{\mathrm{U}}^{\mathrm{s/f}}\left(^{238}\mathrm{U}_{\mathrm{f}}^{\mathrm{i-1}}\right)\left[\alpha\mathrm{e}^{-\lambda_{226}\mathrm{t}} + \beta\mathrm{e}^{-\lambda_{230}\mathrm{t}} + \gamma\mathrm{e}^{-\lambda_{238}\mathrm{t}}\right]$$

Table A1. Partition coefficients used in dehydration and melting models

	U	*Th*	*Ra*	*Pa*
$D^{solid/fluid}$	0.02	0.2	0.002	0-1
$D^{solid/melt}$	0.003	0.0014	1×10^{-5}	1×10^{-5}

D's were calculated assuming 60% cpx, 40% garnet and no rutile using values from Keppler (1996) and garnet/melt cpx/melt partition coefficients to estimate garnet/fluid partitioning.

Table A2. Parameters used in melting and dehydration models

Parameters	*Notation*	*Units*	*Range*
Degree of melting	F	none	0-0.2
Upwelling rate	W	m a^{-1}	0-1
Melting rate	Γ	kg m^{-3} a^{-1}	10^{-3}-10^{-5}
Solidus temperature	T	K	1000-1400
Length of melting column	Z	km	0-50
Matrix porosity	ϕ	none	0-0.005
Solid density	ρ_s	kg m^{-3}	3350
Melt density	ρ_m	kg m^{-3}	2700

where

$$\alpha = \frac{1}{\left(\lambda_{238} - \lambda_{226}\right)\left(\lambda_{230} - \lambda_{226}\right)}$$

$$\beta = \frac{1}{\left(\lambda_{238} - \lambda_{230}\right)\left(\lambda_{226} - \lambda_{230}\right)}$$

$$\gamma = \frac{1}{\left(\lambda_{230} - \lambda_{230}\right)\left(\lambda_{226} - \lambda_{238}\right)}$$

The initial U activity in the mantle wedge (U_w) is set to an arbitrary value of 1 and all the other nuclides are scaled relative to U_w. The initial U activity in the oceanic crust is twice the activity in the mantle wedge. The Th/U ratios of the mantle wedge and the slab are both equal to 2.5. This value is relevant for modeling the higher ($^{230}Th/^{232}Th$) observed in some arc lavas. Fluid is added to a portion of mantle wedge, and the mass fraction of fluid (f) and the composition of the mixture at time step i is given by (same equation for all the nuclides):

$$\left(^{230}\mathrm{Th}_w^i\right) = \left(^{230}\mathrm{Th}_w^{i-1}\right)(1-f) + \left(^{230}\mathrm{Th}_f^i\right)f$$

The composition of the melt is then estimated with a batch melting model as follows assuming that there is a total porosity of dfm+f_r, where f_r is the mass fraction of melt prior to this new melting event:

$$\left(^{230}\mathrm{Th}_{m}^{i}\right)=\frac{\left(^{230}\mathrm{Th}_{w}^{i}\right)}{D_{Th}^{s/m}+\left(dfm+f_{r}\right)\left(1-D_{Th}^{s/m}\right)}$$

We assume that a constant mass fraction f_r remains in the mantle wedge after melt extraction. As in Section A2 of the Appendix, the ratio of slab mass to wedge mass is assumed to be equal to 1 but more complex models are also possible. The bulk composition of the mantle wedge after melt extraction is calculated with the following equation after each extraction increment:

$$C_{R}^{T}=\left(D\left(1-f_{r}\right)+f_{r}\right)C_{m}$$

where C_R^T and C_m represent the activity in the matrix after melt extraction and in the melt respectively. Before the subsequent dehydration/melting event, the metasomatized mantle wedge behaves as closed system and the decay equations (which are similar to the equations given for the slab) are used to track the abundances of U-series nuclides.